Log-Periodic Loop Antennas

by

Jeong Il Kim

Thesis submitted to the Faculty of the
Virginia Polytechnic Institute and State University
in partial fulfillment of the requirements for the degree of

Master of Science
in
Electrical Engineering

Ahmad Safaai-Jazi, Chairman
Ting-Chung Poon
Warren L. Stutzman

July, 1999
Blacksburg, Virginia

Keywords : Frequency Independent Antenna, Log-Periodic Loop Antenna, Log-Periodic Dipole Antenna, Ground Reflector, ESP

Log-Periodic Loop Antennas

Jeong Il Kim

ABSTRACT

The Log-Periodic Loop Antenna with Ground Reflector (LPLA-GR) is investigated as a new type of antenna, which provides wide bandwidth, broad beamwidth, and high gain. This antenna has smaller transverse dimensions (by a factor of $2/\pi$) than a log-periodic dipole antenna with comparable radiation characteristics. Several geometries with different parameters are analyzed numerically using ESP code, which is based on the method of moments. A LPLA-GR with 6 turns and a cone angle of 30° offers the most promising radiation characteristics. This antenna yields 47.6 % gain bandwidth and 12 dB gain according to the numerical analysis. The LPLA-GR also provides linear polarization and unidirectional patterns.

Three prototype antennas were constructed and measured in the Virginia Tech Antenna Laboratory. Far-field patterns and input impedance were measured over a wide range of frequencies. The measured results agree well with the calculated results. Because of its wide bandwidth, high gain, and small size, the LPLA is expected to find applications as feeds for reflector antennas, as detectors in EMC scattering range, and as mobile communication antennas.

Acknowledgements

I would like to sincerely thank my advisor, Dr. Ahmad Safaai-Jazi, for an interesting topic and continuing advice. Without his encouragement and suggestions, this work could not have been completed. I would also like to thank the members of my graduate committee, Dr. Warren L. Stutzman and Dr. Ting-Chung Poon, for their helpful advice. Especially, Dr. Stutzman's classes during the research for my thesis were invaluable.

I would like to express special thanks to Mr. Randall Nealy in the Virginia Tech Antenna Group for the help with the pattern and input impedance measurements. I can not forget to thank Mr. Byeong-Mun Song, Gyoo-Soo Chae, Seong-Youp Suh, Byung-Ki Kim, and Tae-Geun Kim for their sincere advice or support. Also, I would like to thank my colleagues, Eakasit Weeratumanoon and Seok-Won Song.

Finally, I wish to thank my family–mother, two brothers, two sisters-in-law, a sister and a brother-in-law for their immeasurable concern and support to me. I would like to thank my friends and all of those who offered me help. And I would like to dedicate my thesis to my father to be in Heaven. I would like to forward all thanks to God, because He makes it possible to finish this thesis.

Table of Contents

List of Figures

List of Tables

Chapter 1. Introduction

The recent explosion in information technology and wireless communications has created many opportunities for enhancing the performance of existing signal transmission and processing systems and has provided a strong motivation for developing novel devices and systems. There is a continued demand for data transmission at higher rates and over longer distances. Wireless and mobile communication systems are, nowadays, at the forefront of research activities. An indispensable element of any wireless communication system is the antenna. Transmission of data at higher rates requires wider bandwidths for the elements constituting a communication link. This requirement for the antenna, which is the subject of interest in this thesis, means wideband antennas need be designed and used.

Frequency independent antennas, as a particular class of wideband antennas, were first studied by Rumsey [1]. His simple but significant theory has become the foundation for studying many wideband antennas, such as log-periodic dipole antenna (LPDA). The LPDA, whose properties vary periodically with the logarithm of frequency, consists of linear dipoles as basic constituent elements, as illustrated in Figure 1-1. The elements are fed from a balanced transmission line, each element being placed in an alternating configuration that leads to 180° phase change from the adjacent elements.

A limitation of the LPDA is that the dipole element for the lowest operation frequency in the HF range may become too long to be conveniently handled in the environment of application. This fact has led to numerous modifications to the original structure in order to reduce the transverse dimension. In pursuit of reducing the LPDA size, Berry and Ore [2] changed the dipole element to a monopole element over a ground plane, which allows half the transverse dimension. Roy and Chatterjee [3] also proposed log-periodic antennas with helical elements, because the log-periodic helical antenna has a smaller transverse dimension if the helices are designed to operate in the normal mode.

Using the LPDA concept, in this thesis, a new type of log-periodic antenna, as shown in Figure 1-2, is designed, simulated and tested. Since this antenna has a loop as the constituting element and has ground reflector, it is referred to as log-periodic loop antenna with ground reflector (LPLA-GR). Using the circular loop element instead of the dipole agrees with the attempt to reduce the transverse dimension of the LPDA. In addition, the log-periodic loop antennas with ground reflector are expected to have higher gain than LPDAs, because the loop element generally provides a higher gain than the dipole and the ground plane further increases the gain due to the image effect.

Because the proposed antenna has a complicated geometry, its analysis is nearly impossible without making some constraining approximations or using numerical methods. Fortunately, there are quite a few software programs available, which allow us to analyze wire antennas numerically. For example, NEC (Numerical Electromagnetic Code), WIPL (electromagnetic modeling of composite WIre and PLate structures), ESP (Electromagnetic Surface Patch code), etc. can be used for the analysis of antennas. Especially, ESP has proved useful in many antenna analyses [4, 5]. ESP is a code based on the method of moments (MoM) to treat geometries consisting of interconnections of thin wires and perfectly conducting polygonal plates [6]. The code can compute most of the useful quantities of interest such as current distribution, antenna input impedance, radiation efficiency, and far-zone gain patterns.

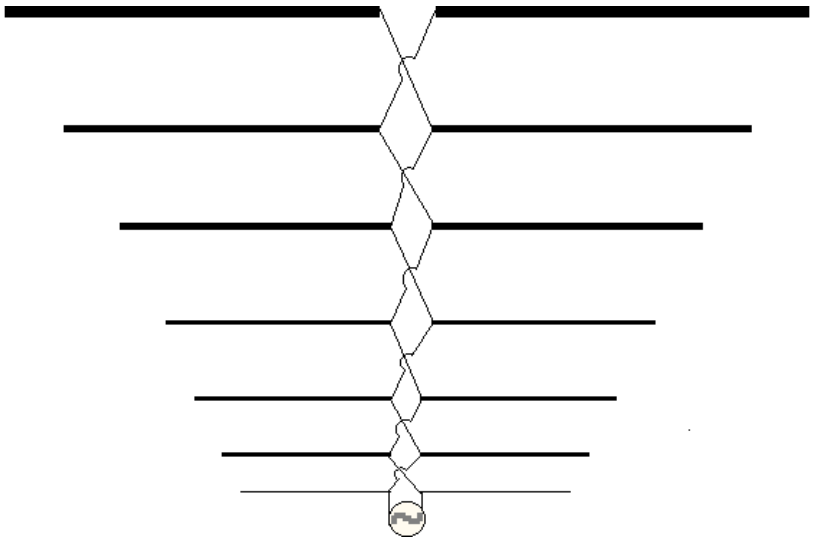

Figure 1-1 Log-periodic dipole antenna without ground reflector

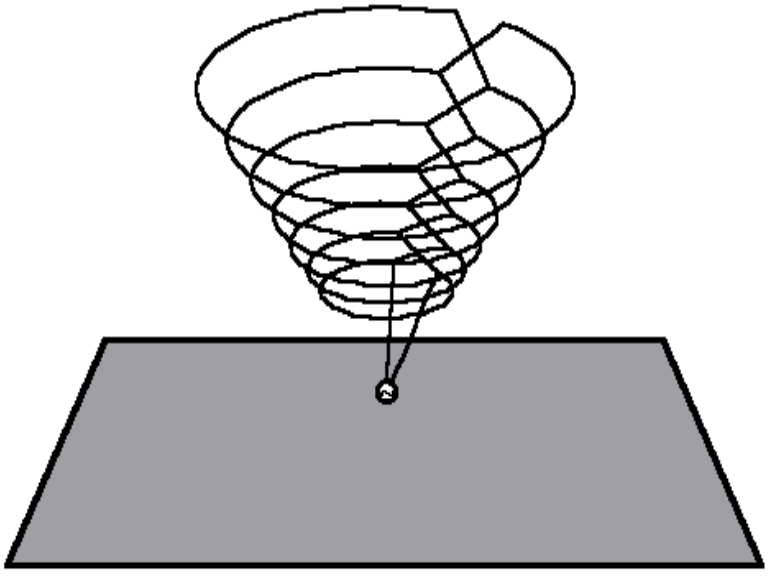

Figure 1-2 Proposed log-periodic loop antenna with ground reflector

The results of this research indicate that, like LPDA, the log-periodic loop antenna with ground reflector provides unidirectional radiation pattern and linear polarization over a wide bandwidth. In order to confirm predicted radiation properties, several prototype LPLAs are constructed and measured at the Virginia Tech Antenna Laboratory. The measured results are compared with numerical data obtained from ESP. The agreement between experimental and theoretical results is remarkably good.

Chapter 2 describes the theoretical and historical background that can be applied to designing the proposed new antenna. Chapter 3 analyzes a single circular loop antenna to provide a basic understanding and discusses the log-periodic loop antenna without ground reflector. This chapter also includes a comparison of ESP-generated results with those by other researchers in order to ascertain the accuracy of ESP and make sure that it is used properly. Chapter 4 introduces the log-periodic loop antenna with ground reflector and presents numerical results for far-field patterns, gain, input impedance, and phase difference between orthogonal field components. Chapter 5 addresses the construction and measurement of three prototype antennas. The measured radiation characteristics of these antennas are compared with those produced by ESP in Chapter 4. Chapter 6 concludes this research and offers suggestions for future directions. The appendices contain the computer code to generate input data for the different geometries as well as the numerically-generated and measured far-field patterns for cases not covered in the main chapters.

Chapter 2. Evolution of Log-Periodic Dipole Antenna

The LPDA, with linear diploes as constituent elements, is well known for its wide bandwidth and moderate gain. As far as the broadband characteristic is concerned, this antenna evolved from the concept of frequency independent antennas whose theoretical foundation was laid down by Rumsey at the University of Illinois. Rumsey's work became the motive for the development of log-periodic antennas by DuHamel [7] which then led to the introduction of the LPDA by IsBell [8]. Later, Carrel analyzed the LPDA mathematically and computed its radiation pattern, input impedance, etc., using a digital computer [9].

2.1 Principles of Frequency Independent Antennas

Since their dimensions, when expressed in terms of wavelength, vary with frequency, antennas usually exhibit different radiation properties at different frequencies. For example, a center-fed half-wave dipole at its resonant frequency has an input resistance of about 73 ohms while at twice this frequency the input resistance is much larger. Moreover,

a one-wavelength dipole has more directive radiation pattern than the half-wave dipole [10]. Variations of radiation characteristics with frequency limit the bandwidth of the antenna and thus the information carrying capacity of the communication link to which the antenna belongs. The issue of frequency independent antennas, which ideally provide an infinite bandwidth, was first addressed by Rumsey, who explained the following basic requirements for these antennas.

2.1.1 Angle-Specified Antennas

Rumsey proposed that if the shape of a lossless antenna is such that it can be specified entirely by angles, its performance such as pattern and input impedance would remain unchanged with frequency. In other words, the dimensions of this class of antennas, when expressed in terms of wavelength, are the same at every frequency. The implication is that electrical characteristics of the antenna do not change with frequency [11]. This is a very simple and powerful idea for the design of broadband antennas, which are referred to as frequency independent antennas for the ideal case.

The general equation for angle-only specified antenna geometries, assuming that both of the antenna's terminals are infinitely close to the origin of a spherical coordinate system, is expressed as

$$r = F(\theta, \phi) = e^{a\phi} f(\theta) \qquad (2.1.1\text{-}1)$$

where $f(\theta)$ is an arbitrary function and $a = \frac{1}{K}\frac{dK}{dC}$ is a parameter, in which K depends neither on θ nor ϕ but on angle C for congruence [12]. Typical examples of antennas described by (2.1.1-1) are the planar equiangular spiral antenna and conical spiral antenna.

2.1.2 Self-Complementary Configuration

In addition to the angle dependence, a second principle was used in the early development of frequency independent antennas. This principle states that if an antenna has the same shape as its complement empty part, its impedance is constant at all frequencies. Figure 2.1.2-1 (a) shows an example of complementary antenna. The relationship between input impedances, Z_1 and Z_2 , for the complementary planar structures is expressed as [13]

$$Z_1 Z_2 = (60\pi)^2 \qquad (2.1.2\text{-}1)$$

If the complementary parts of the empty space and the shaded metal plate, which are extended to infinity, are self-complementary as illustrated in Figure 2.1.2-1 (b), the shaded plate antenna has the input impedance of constant 60π ohms, because, intuitively, Z_1 of the shaded antenna should be equal to Z_2 of its complement. That is

$$Z_1 = Z_2 = 60\pi \qquad (2.1.2\text{-}2)$$

Since a truly frequency-independent antenna would have constant input impedance, it seems promising to design antennas that resemble their complements, in order to achieve frequency independence. It should be noted that log-periodic loop antennas, however, do not adhere to this principle.

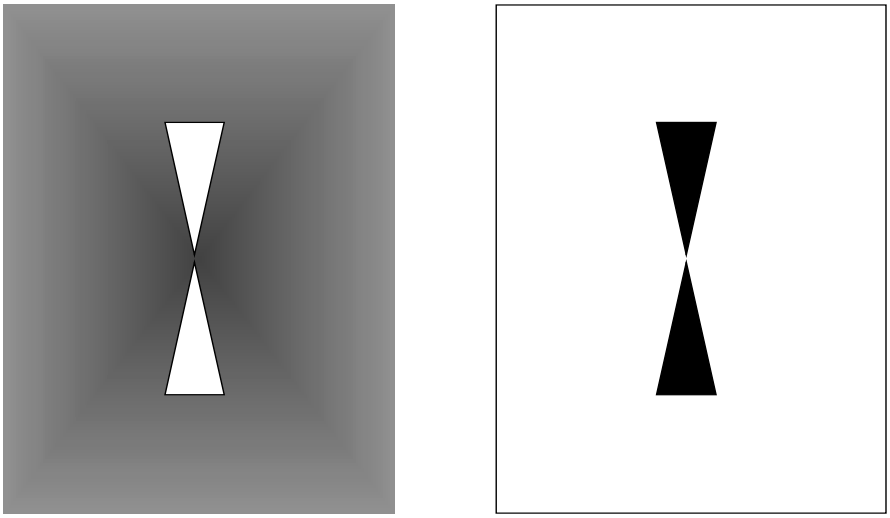

(a)

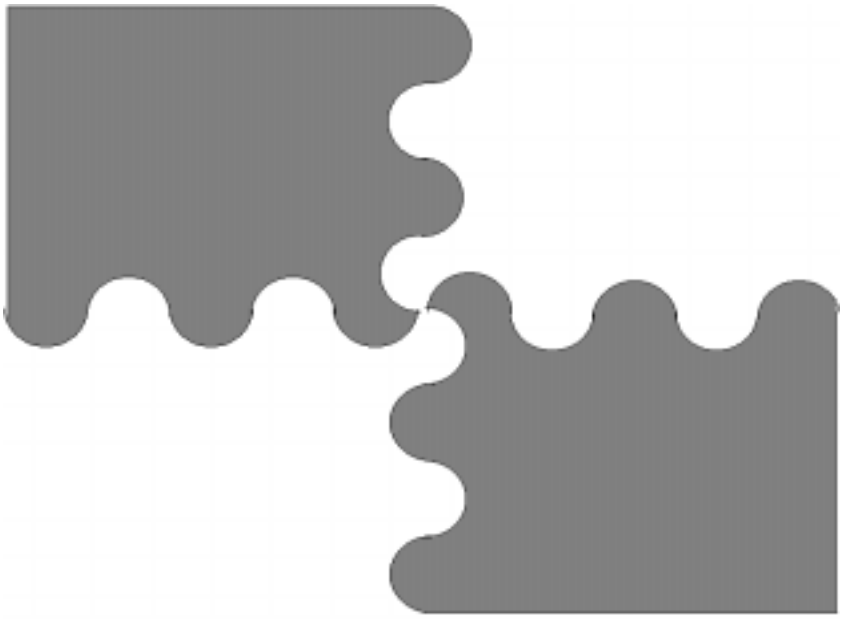

(b)

Figure 2.1.2-1 Examples for (a) Complementary pair and
(b) Self-complementary configuration

2.2 Log-Periodic Antennas

A development, which closely paralleled the concept of frequency-independent antennas, was the log-periodic structures introduced by DuHamel and IsBell in 1957 [7]. Because their entire shapes cannot be solely specified by angles in the spherical coordinate system, log-periodic antennas are not truly frequency independent. However, before the change in the performance can become significant one element of the structures repeats itself with a logarithmic periodicity. Thus, small variations are allowed.

Since in practice the antenna must be of finite length, radiation characteristics vary considerably below the lower frequency limit. This phenomenon is termed as "truncation effect" (or the effect of finite length). In contrast to the truncation effect, the input impedance can be maintained at a constant value at higher frequencies, because the antenna structure can be regarded locally as mutual complement.

2.2.1 Log-Periodic Toothed Planar Antenna

The initial design based on the concept of the log-periodic structure was the log-periodic toothed planar antenna (LPTPA), as shown in Figure 2.2-1 (a). Following the angle concept, if one tooth has a width W_0 the next smaller one is τW_0 wide, the third is $\tau^2 W_0$, and so on [10].

Let the width of the widest tooth be W_1, which is approximately one quarter wavelength corresponding to the lower frequency limit. Then, the width of n^{th} tooth, W_n, is

$$W_n = W_1 \tau^n \qquad (2.2.1\text{-}1)$$

where τ is a constant representing the ratio of width of $(n+1)^{th}$ tooth to width of n^{th} tooth.

Taking the logarithm of both sides of (2.2.1-1) yields:

$$\log W_n = \log W_1 + n \log \tau \quad . \qquad (2.2.1\text{-}2)$$

For a given antenna, log W_1 and log τ are constant. Consequently, the logarithm of W_n increases in equal steps with n. That is, log W_n increases periodically–hence the name "log periodic". It is also implied that whatever electrical properties the antenna may have at a frequency f_0, will be repeated at all frequencies given by $\tau^n f_0$.

Combining the periodicity with the angle concept, the LPTPA has a self-complementary configuration. This results in a constant input impedance of about 60π ohms independent of frequencies within the operation range limited only by physical size.

2.2.2 Log-Periodic Toothed Trapezoidal Antenna

The LPTPA can be slightly modified to obtain a more refined geometry referred to log-periodic toothed trapezoidal antenna (LPTTA), as shown in Figure 2.2-1 (b). The LPTTA is also specified by angle in a manner similar to the LPTPA described in Section 2.2.1 and is self-complementary. The important feature of this antenna is that it represents an earlier link to the development of log-periodic dipole antenna.

By bending the triangular shape arms of the antenna, so that the angle between the two arms, ψ, is less than 180°, a non-planar log-periodic toothed wedge antenna can be made. Furthermore, the teeth could be reduced to the thicknesses of wires permitting a parallel arrangement of the elements in the two half-structures with a ψ angle equal to zero. This became the log-periodic dipole coplanar antenna as illustrated in Figure 1-1.

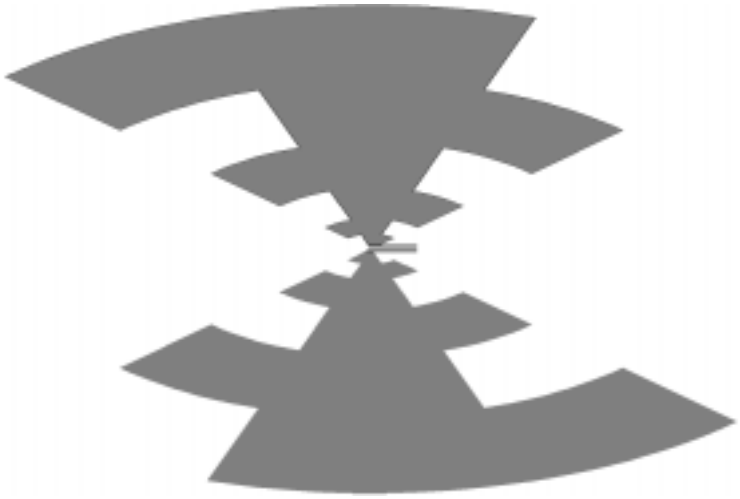

(a) Log-periodic toothed planar antenna

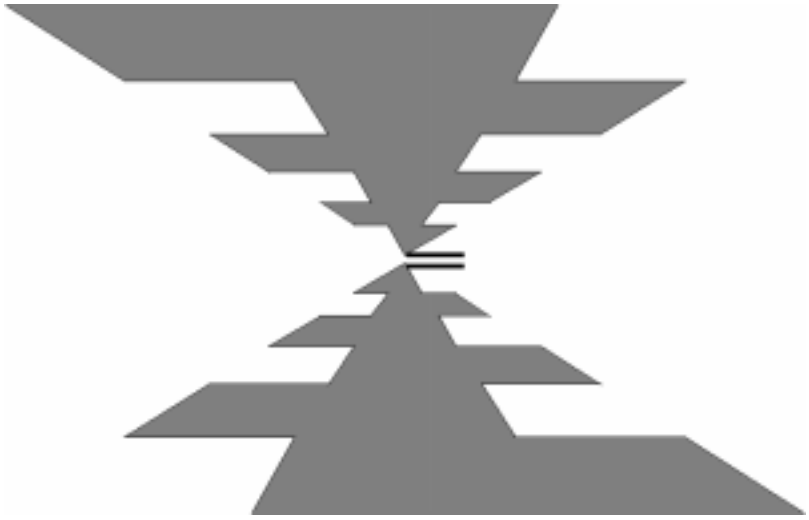

(b) Log-periodic toothed trapezoidal antenna

Figure 2.2-1 Log-periodic antennas

2.3 Log-Periodic Dipole Antenna

Folding the two arms of the LPTTA so that the included angle ψ becomes zero leads to a unidirectional form of log-periodic antenna known as LPDA. This type of log-periodic antenna was first developed by IsBell [8], and later organized by Carrel [9]. The schematic diagram of LPDA is given in Figure 2.3-1. This antenna is not completely described by angles, but still depends on angular coordinates. The LPDA seems to be a self-complementary structure, because it has the permissible characteristic of constant input impedance as will be discussed.

As shown in Figure 2.3-1, the successive dipoles are connected alternately to a balanced transmission line called feeder. That is to say these closely spaced elements are oppositely connected so that endfire radiation in the direction of the shorter elements is created and broadside radiation tends to cancel. Actually, a coaxial line running through one of the feeders from the longest element to the shortest is used. The center conductor of the coaxial cable is connected to the other feeder so that the antenna has its own balun [14].

Radiation energy, at a given frequency, travels along the feeder until it reaches a section of the structure where the electrical lengths of the elements and phase relationships are such as to produce the radiation. As frequency is varied, the position of the resonant element is moved smoothly from one element to the next. The upper and lower frequency limits will then be determined by lengths of the shortest and longest elements or conversely these lengths must be chosen to satisfy the bandwidth requirement. The longest half-element must be roughly 1/4 wavelength at the lowest frequency of the bandwidth, while the shortest half-element must be about 1/4 wavelength at the highest frequency in the desired operating bandwidth [15].

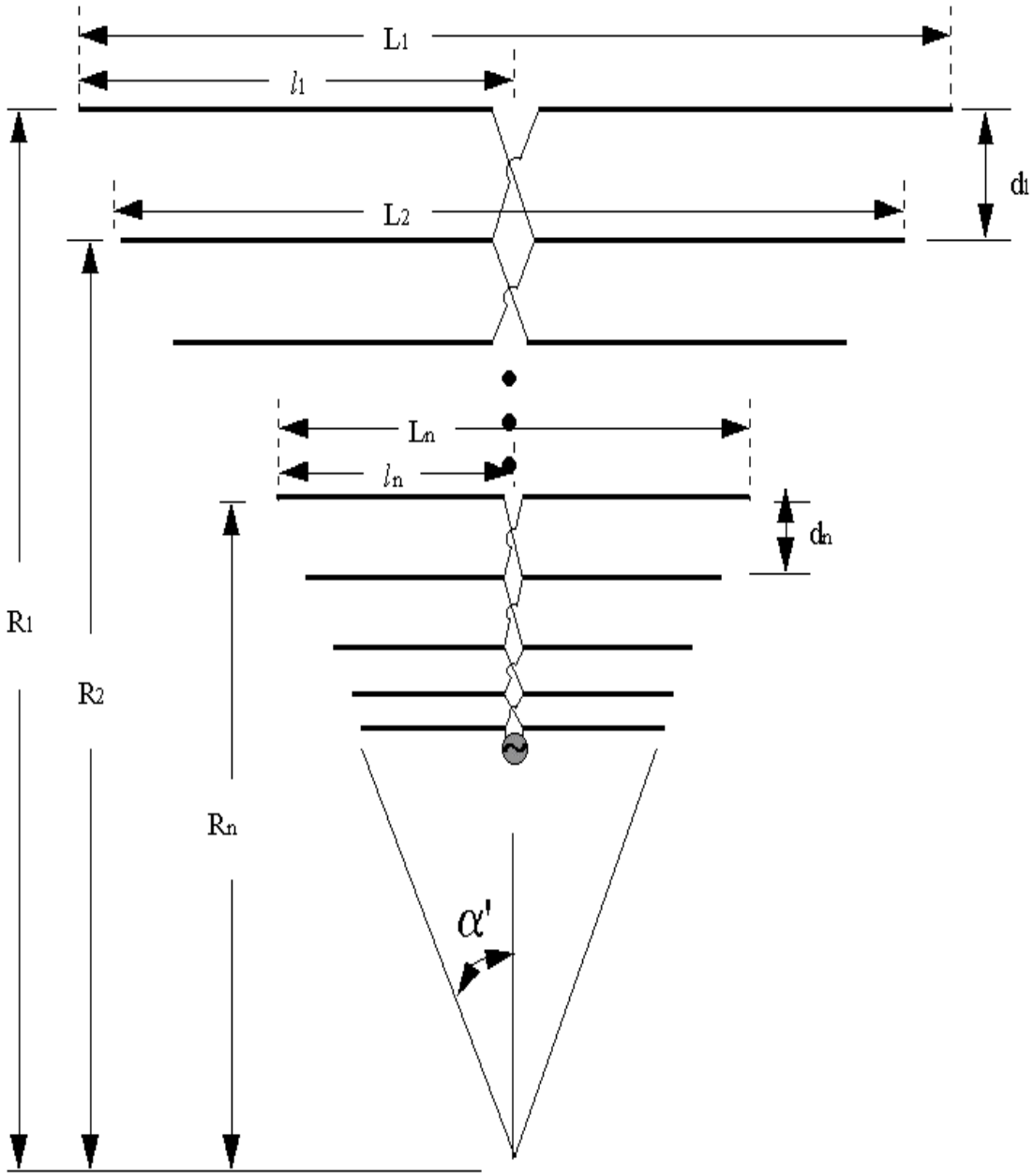

Figure 2.3-1 Schematic diagram of log-periodic dipole antenna

Now, let us define parameters, τ, α', and σ, to describe the geometry of the LPDA. The relationships between α', τ, element dipole lengths L_n, and distances R_n to the apex are determined by the geometry and expressed as

$$\frac{L_1}{R_1} = \frac{L_n}{R_n} = 2\tan\alpha' \qquad (2.3\text{-}1)$$

where R_n = distance from apex to the n^{th} element

L_n = total length of the n^{th} element

α' = half-angle subtended by the ends of radiating elements.

In addition, the ratios of d_{n+1}/d_n and R_{n+1}/R_n are equal to τ, which is usually a number less than 1.0. That is,

$$\frac{d_{n+1}}{d_n} = \frac{R_{n+1}(1-\tau)}{R_n(1-\tau)} = \frac{R_{n+1}}{R_n} = \tau \qquad (2.3\text{-}2)$$

where d_n is the distance between n^{th} and $(n+1)^{th}$ elements.

It is often convenient to think of the element spacing d_n in terms of wavelength. The free-space wavelength λ_1 of a signal that resonates the first largest element, l_1, is approximately four times l_1, thus

$$\lambda_1 \approx 4l_1 \qquad (2.3\text{-}3)$$

Similarly

$$\lambda_2 \approx 4l_2;\ \lambda_3 \approx 4l_3;\ \lambda_n \approx 4l_n \qquad (2.3\text{-}4)$$

For any value of n, the ratio $d_n/4l_n$ is a useful quantity. It is called spacing factor (σ) and can be expressed in terms of τ and α' as follows:

$$\sigma = \frac{d_1}{4l_1} = \frac{d_n}{4l_n} = \frac{R_n(1-\tau)}{4(R_n\tan\alpha')} = \frac{1-\tau}{4\tan\alpha'} \qquad (2.3\text{-}5)$$

The performance of LPDA is a function of the antenna parameters τ and α'. In particular, the input impedance depends on τ and α' [10]. For example, when the value of τ is 0.95, the unloaded feeder impedance is 104 ohms, and when α' varies from 10° to 30°, the input impedance falls between the limits of 76 and 53 ohms. Here, the unloaded feeder impedance refers to the characteristic impedance of the central transmission line without all the elements.

As the value of τ is decreased, the input impedance will increase toward the value of the unloaded feeder impedance. The reason is that fewer elements per feeder unit length are connected in parallel to the feeder. On the contrary, it is expected that for the higher values of τ the LPDA will be less dependent on frequency.

2.4 Modifications of the LPDA

Since the introduction of LPDA, many modifications with the aim of improving its performance or reducing its size have been investigated. Many different ways such as inductive or capacitive loading [16] and utilization of normal mode helical dipoles [3] have been proposed as improvements to the basic LPDA geometry. Among them, the LPLA is a noticeable departure. This antenna will be treated in the following chapter.

Chapter 3. Log-Periodic Loop Antenna

In Section 2.3 , the LPDA (log-periodic dipole antenna) was discussed. The LPDA consists of dipole elements. Based on the LPDA concept, a new type of log-periodic antenna is introduced in which dipoles are replaced with circular loop elements. Section 3.1 will present the analysis of circular loops as the constituting elements of this new antenna.

An extensive literature survey revealed that several studies were attempted on the LPLA (log-periodic loop antenna). The idea of log-periodic loop antenna was first proposed by Singh, et al. [17] in early 1970s. They presumed that the geometry gives a circular polarization. However, the possibility of achieving circular polarization does not exist as will be discussed in Section 4.3.3. Later, more theoretical and experimental studies were conducted by Rojarayanont, et al. [18] in mid 1970s. Section 3.2 focuses on their work and presents the comparison of their results with those obtained from the ESP.

3.1 Analysis of Single-Loop Antenna

Compared with the linear dipole, the analysis of loop antennas, especially circular loop antennas with arbitrary circumferences, is much more complicated and involved. Recently, however, single circular loop antennas with cosinusoidal current distributions were solved analytically by Werner [19]. He generalized loop currents by using Fourier cosine series representations and obtained exact field solutions, including near-field components.

In this section, starting from a vector magnetic potential, the solution of the electromagnetic fields in the far-zone region for a single-loop antenna is presented. Then, the radiation patterns from this analysis and from ESP simulation will be compared.

In general, the radiated fields from an antenna are solutions of Maxwell's equations. These solutions are more conveniently obtained by introducing a vector magnetic potential $\vec{A}$, which is governed by an inhomogeneous vector wave equation [20]. The solution of $\vec{A}$ for an arbitrary filamentary current on a closed loop is expressed as

$$\vec{A}(\vec{r}) = \frac{\mu}{4\pi}\oint I(\vec{r}\,')\frac{e^{-j\beta R'}}{R'}d\vec{l}' \qquad (3.1\text{-}1)$$

where $\vec{r}\,' = x'\hat{a}_x + y'\hat{a}_y + z'\hat{a}_z$ and $R' = |\vec{r} - \vec{r}\,'|$.

Figure 3.1-1 illustrates the geometry and coordinates for a circular loop antenna with radius b. Referring to this figure, R′ and $I(\vec{r}\,')d\vec{l}\,'$ are expressed as

$$R' = \sqrt{r^2 + b^2 - 2br\sin\theta\cos(\phi - \phi')} \qquad (3.1\text{-}2)$$

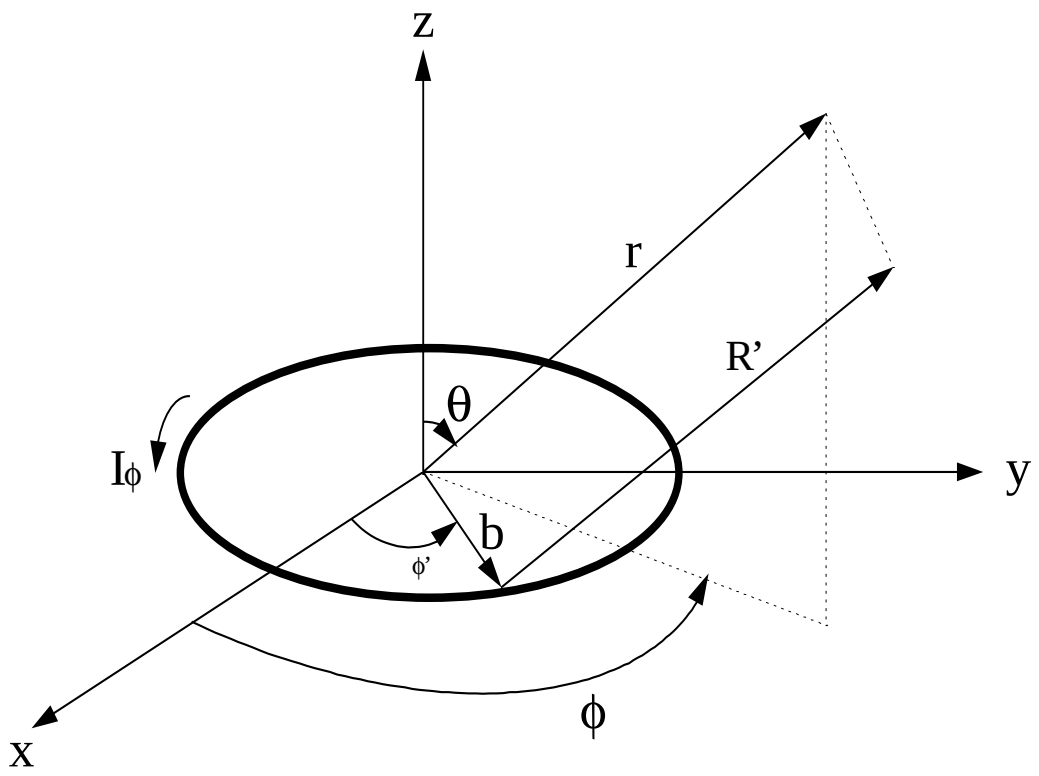

Figure 3.1-1 Geometrical arrangement of a circular loop antenna for far-field analysis

$$Id\vec{l}' = I(\phi')\left[\sin\theta\sin(\phi-\phi')bd\phi\hat{a}_r + \cos\theta\sin(\phi-\phi')bd\phi\hat{a}_\theta + \cos(\phi-\phi')bd\phi\hat{a}_\phi\right] \quad (3.1\text{-}3)$$

Here, it should be emphasized that the source is defined using primed coordinates (ρ', ϕ', z'), while the observation point is defined using unprimed coordinates (r, θ, ϕ).

Substituting (3.1-3) into (3.1-1), the spherical components of the vector magnetic potential are obtained as [19]

$$A_r(r,\theta,\phi) = \frac{\mu b\sin\theta}{4\pi}\int_0^{2\pi} I(\phi')\sin(\phi-\phi')\frac{e^{-j\beta R'}}{R'}d\phi' \quad (3.1\text{-}4)$$

$$A_\theta(r,\theta,\phi) = \frac{\mu b\cos\theta}{4\pi}\int_0^{2\pi} I(\phi')\sin(\phi-\phi')\frac{e^{-j\beta R'}}{R'}d\phi' \quad (3.1\text{-}5)$$

$$A_\phi(r,\theta,\phi) = \frac{\mu b}{4\pi}\int_0^{2\pi} I(\phi')\cos(\phi-\phi')\frac{e^{-j\beta R'}}{R'}d\phi' \quad (3.1\text{-}6)$$

To facilitate evaluation of the integral expressions in (3.1-4) to (3.1-6), a replacement integral $\Re$ is introduced, such that

$$A_r(r,\theta,\phi) = -\frac{\mu}{j2\beta r}\frac{\partial}{\partial\phi}\Re(r,\theta,\phi) \quad (3.1\text{-}7)$$

$$A_\theta(r,\theta,\phi) = -\frac{\mu}{j2\beta r\tan\theta}\frac{\partial}{\partial\phi}\Re(r,\theta,\phi) \quad (3.1\text{-}8)$$

$$A_\phi(r,\theta,\phi) = \frac{\mu}{j2\beta r\cos\theta}\frac{\partial}{\partial\theta}\Re(r,\theta,\phi) \quad (3.1\text{-}9)$$

where the replacement integral is

$$\Re(r,\theta,\phi) = \frac{1}{2\pi}\int_0^{2\pi} I(\phi')e^{-j\beta R'}d\phi' \quad (3.1\text{-}10)$$

For the analysis of loop antennas in a variety of cases, the source current on the loop wire can be represented by the following Fourier cosine series:

$$I(\phi') = \sum_{n=0}^{\infty} I_n \cos(n\phi') \qquad (3.1\text{-}11)$$

For current distributions as in (3.1-11), the integration in (3.1-10) can be performed in a straight forward manner and the vector potential can be readily obtained.

Having found the magnetic vector potential $\vec{A}$, the far-zone electric field is obtained from [15]

$$\vec{E} = -j\omega(A_\theta \hat{a}_\theta + A_\phi \hat{a}_\phi) \qquad (3.1\text{-}12)$$

Assuming a cosinusoidal current distribution for the loop antenna, $I(\phi') = I_p\cos(p\phi')$, the far-field components of $\vec{E}$ are determined as

$$E_\theta = -\frac{\eta(\beta b)\, p(j)^p I_p \sin(p\phi)\cos\theta}{2} \frac{e^{-j\beta r}}{r} \frac{J_p(w)}{w} \qquad (3.1\text{-}13)$$

$$E_\phi = -\frac{\eta(\beta b)(j)^p I_p \cos(p\phi)}{2} \frac{e^{-j\beta r}}{r} J_p'(w) \qquad (3.1\text{-}14)$$

where $w = \beta b \sin\theta$ and J_p is the Bessel function of the first kind.

A case of special interest is when the circumference of the loop is one wave length. This corresponds to a value of p equal to 1. If a source is on the x-axis, the current distribution on the loop wire will be described as $I(\phi') = I_1\cos(\phi')$.

As an example, if the frequency of operation is chosen to be 2 GHz, the corresponding loop radius is 2.3873 cm. The radiation patterns in the linear scale for this example are plotted in Figure 3.1-2. These plots were obtained using the MATLAB code in Appendix A. Figure 3.1-2 (a) shows the E_θ radiation pattern in the y-z plane, while Figure 3.1-2 (b) illustrates the E_ϕ pattern in the x-z plane. It should be noted that y-z and x-z plane patterns are E-plane and H-plane patterns, respectively. These planes contain the electric field and magnetic field vectors.

For the purpose of comparison, the above patterns were also calculated using the ESP software. Figures 3.1-3 (a) and (b) illustrate the E_θ and E_ϕ patterns, respectively. Both patterns are in good agreement with those in Figures 3.1-2 (a) and (b). The patterns also agree well with those in the Antenna Engineering Handbook [21] with half-power beamwidths of about 84° in the E-plane and 133° in the H-plane.

In addition, the ESP can also provide a very small E_ϕ component in the E-plane and small E_θ in the H-plane. The formulas by Werner, however, result in zero E_ϕ component in the E-plane and zero E_θ component in the H-plane.

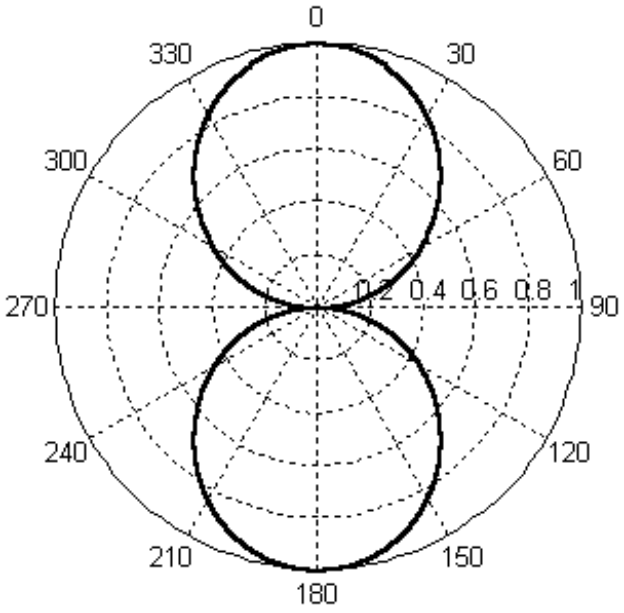

(a)

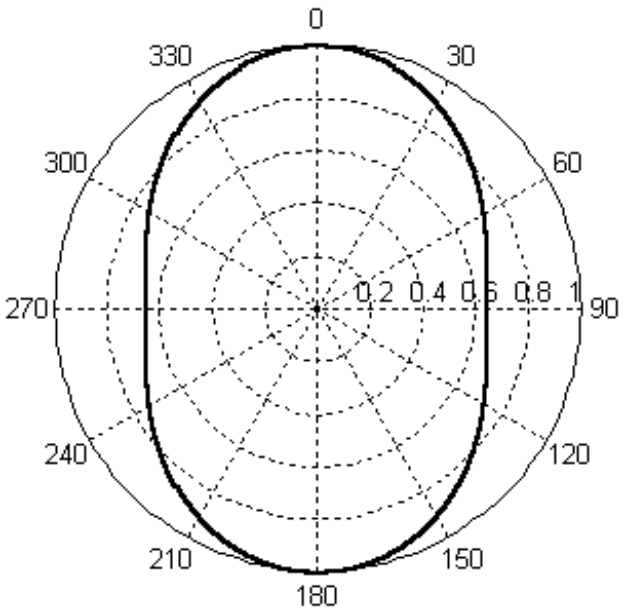

(b)

Figure 3.1-2 (a) E_θ radiation pattern in the y-z plane and (b) E_ϕ pattern in the x-z plane for a one wavelength circular loop at 2 GHz obtained from equations (3.1-13) and (3.1-14), respectively.

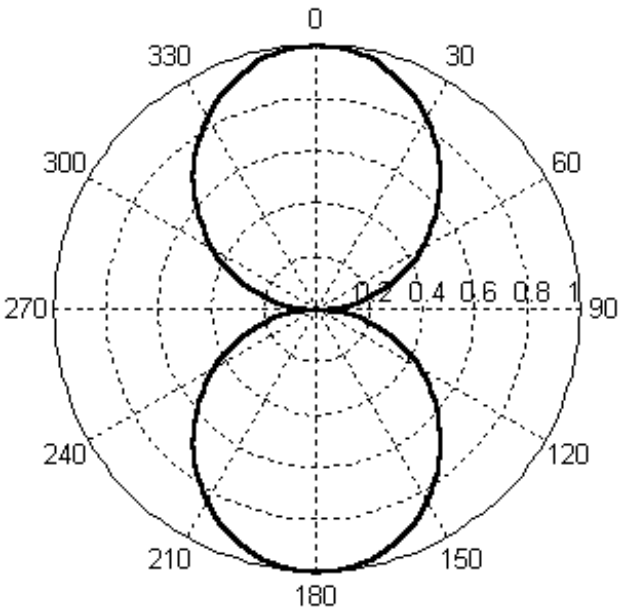

(a)

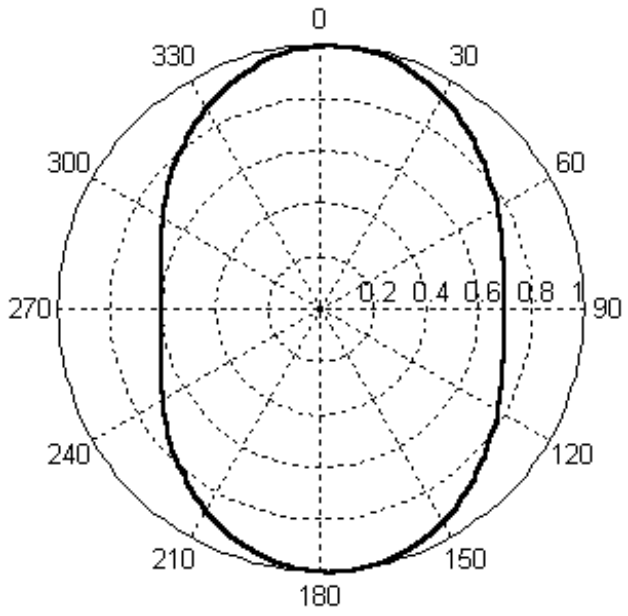

(b)

Figure 3.1-3 (a) E_θ radiation pattern in the E-plane and (b) E_ϕ pattern in the H-plane for a one wavelength circular loop at 2 GHz obtained from ESP code

3.2 Analysis of Log-Periodic Loop Antenna

With the basic properties of the circular loop antenna reviewed in the previous section, we are now ready to embark upon the analysis and design of LPLA. Figure 3.2-1 illustrates the geometry and coordinates for a log-periodic circular loop antenna. The LPLA is an array consisting of N loop elements. The parameters describing a LPLA are τ (scale factor), σ (spacing factor), and α (subtended angle). It should be noted that α is different from α' in Section 2.3. Each loop element is identified with a loop radius, a wire radius, and a feed gap, which obey a logarithm relationship as in Section 2.3. This can be expressed, using the scale factor τ, as:

$$\frac{b_i}{b_j} = \frac{a_i}{a_j} = \tau^{j-i} \tag{3.2-1}$$

where b_j, and a_j are the loop and wire radii of the j-th element, respectively.

The spacing factor, σ, used to define the distance between the adjacent elements obeys a relationship similar to (2.3-5). That is,

$$\sigma = \frac{d_i}{4b_i} = \frac{1-\tau}{4\tan\left(\alpha/2\right)} \tag{3.2-2}$$

where d_i is the spacing between the i-th and (i-1)-th elements.

Starting from the array geometry, Rojarayanont and co-workers [18] derived the far-field expressions of the LPLA. Similar to the approach used by Carrel for the analysis of the log-periodic dipole antenna, they used circuit techniques. The circuits for the analysis of the LPLA are illustrated in Figure 3.2-2.

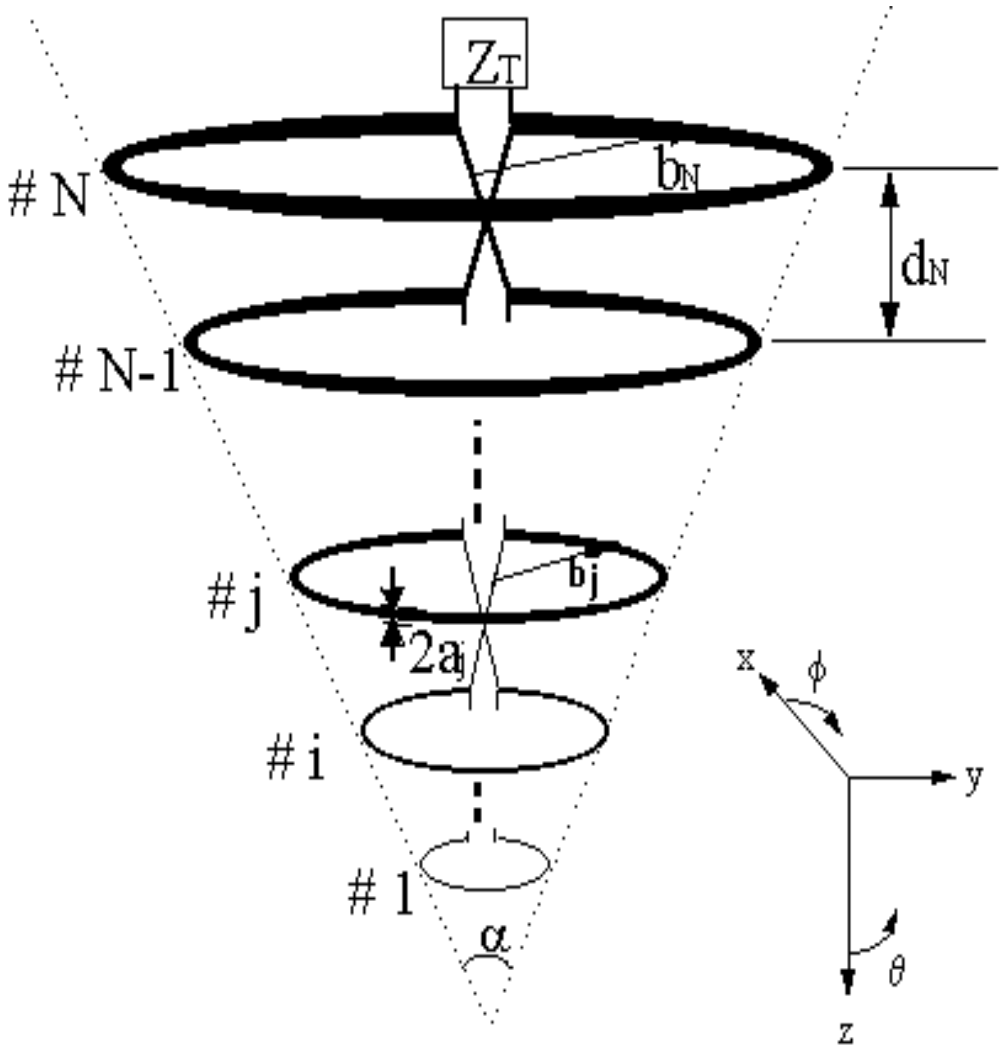

Figure 3.2-1 Geometry and coordinates for log-periodic circular loop antenna.

It has two parts; one is the feeder circuit (Figure 3.2-2 (b)) with alternating and properly spaced gaps to which the elements are actually attached, and the other is the antenna-elements part (Figure 3.2-2 (a)), from which the fields are radiated.

If the impedance matrix of the antenna element circuit is denoted as $[Z_a^n]$, the element current $[I_a^n]$ for the n-th mode loop current, which may be expanded into Fourier series as in (3.1-11), is related to the element voltage $[V_a^n]$ by

$$\begin{aligned}\left[Z_a{}^n\right]\cdot\left[I_a{}^n\right] &= \left[V_a{}^n\right] \\ &= \left[\beta^n\right]\cdot\left[V_a\right]\end{aligned} \qquad (3.2\text{-}3)$$

where $[V_a^n]$ depends on the feed gap size of each loop element, which is accounted for in $[\beta^n]$ term.

Likewise, feed current $[I_f]$ on each feed terminal pair is related to the feed voltage $[V_f]$ by

$$\left[I_f\right] = \left[Y_f\right]\cdot\left[V_f\right] \qquad (3.2\text{-}4)$$

where $[Y_f]$ is the admittance matrix of the feeder circuit. It should be noted that in (3.2-3) and (3.2-4), $[Z_a^n]$ and $[Y_f]$ are N×N matrices.

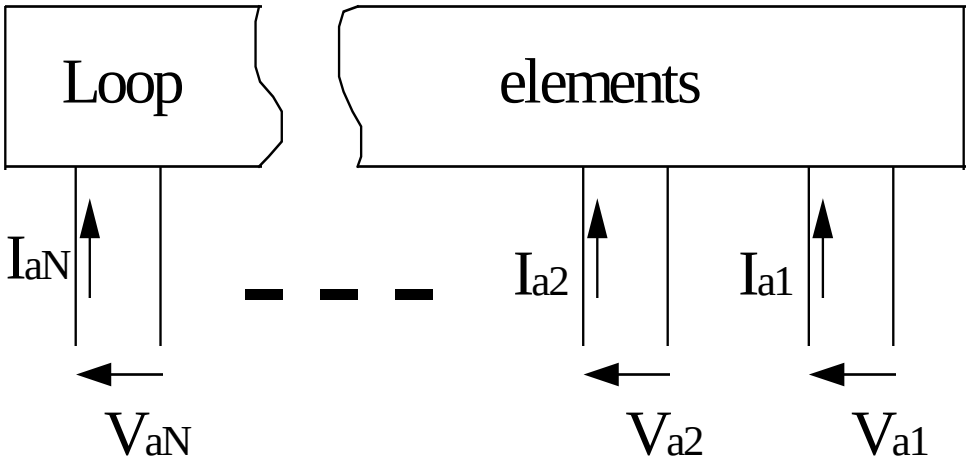

(a)

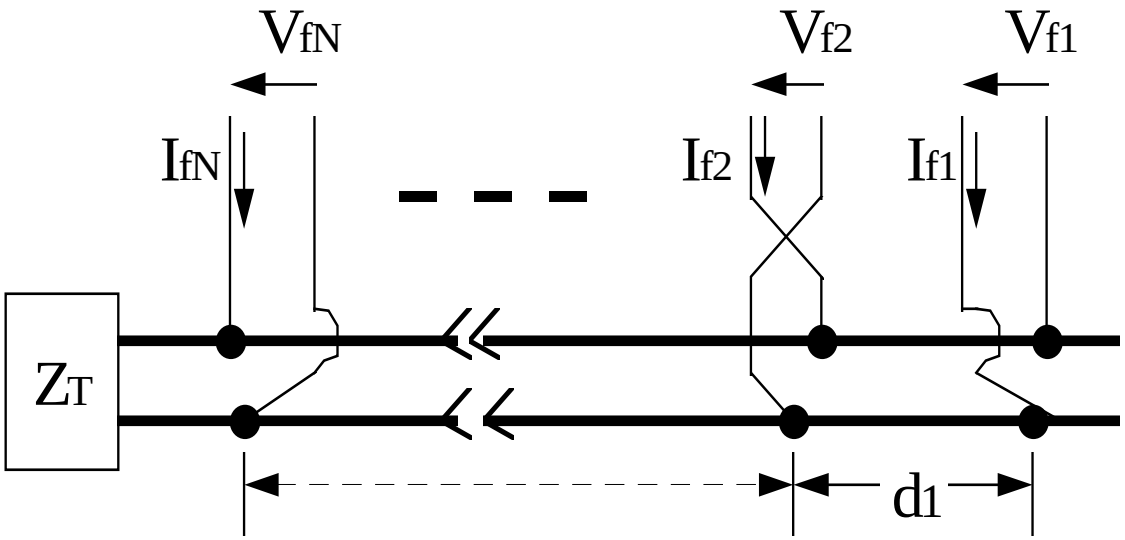

(b)

Figure 3.2-2 (a) Element circuit and (b) feeder circuit for the analysis of LPLA

Now, because the driving current matrix is the sum of $[I_a^n]$ and $[I_f]$ due to the Kirchhoff's current law, we can write

$$\begin{aligned}[I] &= [I_a] + [I_f] \\ &= \sum_{n=0}^{\infty} [Z_a{}^n]^{-1} \cdot [V_a{}^n] + [Y_f] \cdot [V_f] \\ &= \left\{ \sum_{n=0}^{\infty} [Z_a{}^n]^{-1} \cdot [\beta^n] + [Y_f] \right\} \cdot [V]\end{aligned} \tag{3.2-5}$$

where $[V] = [V_a] = [V_f]$. Therefore, once $[Z_a^n]$, $[\beta^n]$ and $[Y_f]$ are found from the array geometry [22], the driving voltage matrix can be readily calculated as

$$[V] = \left\{ \sum_{n=0}^{\infty} [Z_a{}^n]^{-1} [\beta^n] + [Y_f] \right\}^{-1} \cdot [I] \tag{3.2-6}$$

where

$$[I] = \begin{bmatrix} 1 \\ 0 \\ \vdots \\ 0 \end{bmatrix}. \tag{3.2-7}$$

Then, from (3.2-3) the antenna current on each element can be found using the Fourier series expansion and matrix form as given below,

$$[I_a] = \sum_{n=0}^{\infty} [I_a{}^n] = \sum_{n=0}^{\infty} \left\{ [Z^n]^{-1} \cdot [\beta^n] \right\} \cdot [V_a] \tag{3.2-8}$$

Once the current distribution on the antenna geometry is known, the radiation pattern can be readily obtained. Rojarayanont, et al. [18] derived and calculated expressions for the far-field E- and H-plane patterns. They also measured these patterns. Figure 3.2-3 (a)

shows their results for a 10-element LPLA with the parameter values: $\tau = 0.9$, $\sigma = 0.09\pi$, and $b_6 = 7.9577$ cm.

The patterns for the same antenna were also calculated by using the ESP code. The patterns are shown in Figure 3.2.3 (b). Comparison of Figures 3.2-3 (a) and (b) reveals that the main lobes and the overall shapes of patterns are in very good agreement. It is noted that the main beam peaks are directed toward the apex because the fields in the broadside direction are cancelled due to 180° alternating phase shift between the adjacent loop elements. The subprogram WGEOM in Appendix B was used for this simulation. In this subprogram, the terminal impedance Z_T (see Figure 3.2-1), if present, can be added.

Rojarayanont, et al [18] also compared the gains and front-to-back ratios of LPLA and LPDA, as shown in Figure 3.2-4 (a). Generally, LPLA has 1.5 to 2 dB higher gain than LPDA, which was also predicted by Singh, et al [17]. The reason is that a loop antenna at the resonant frequency has much higher gain than a dipole antenna at its resonant frequency. Figure 3.2-4 (b) shows variations of gain versus frequency calculated from the ESP with 200 Ω terminal impedance. Although gain values obtained from ESP are about 2 to 4 dB lower, the overall shape of the gain curve in Figure 3.2-4 (b) is similar to that in Figure 3.2-4 (a).

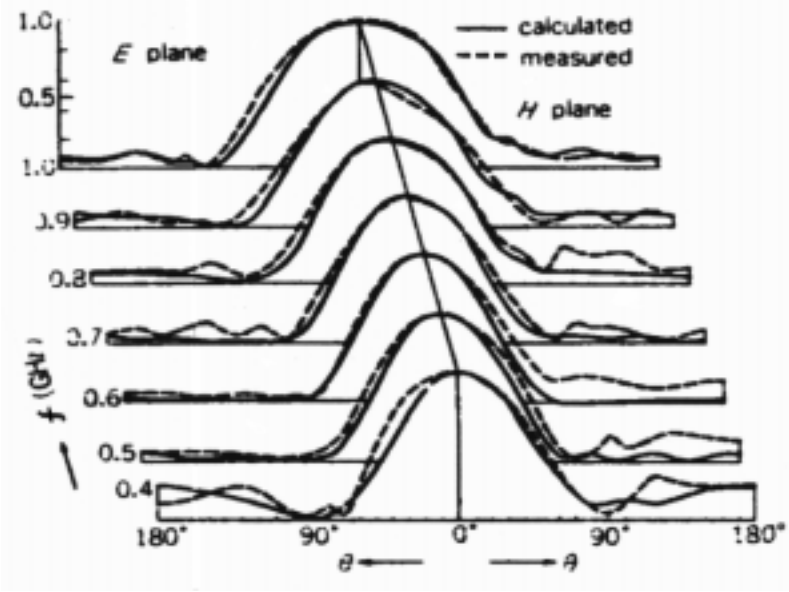

(a)

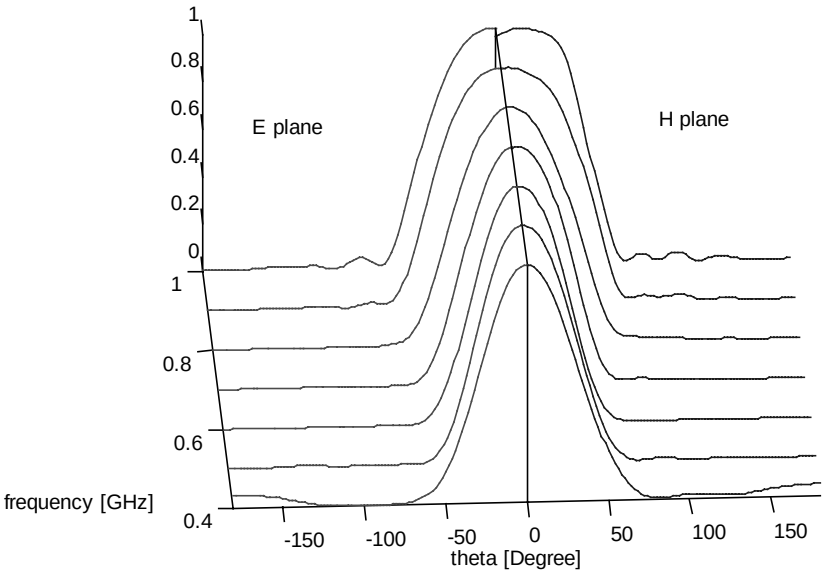

(b)

Figure 3.2-3 Far-field radiation patterns of LPLA in the E- and H-planes by (a) Rojarayanont, et al [18] and (b) ESP

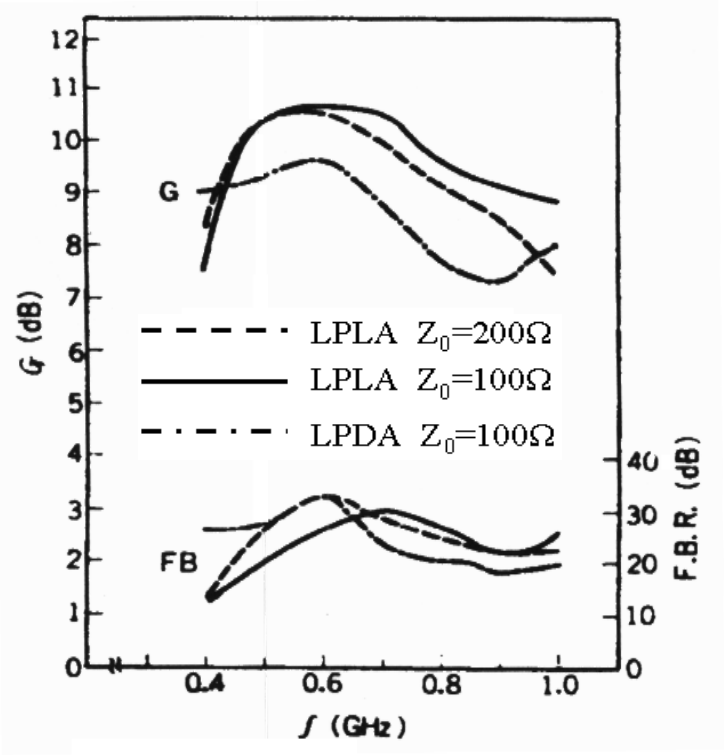

(a)

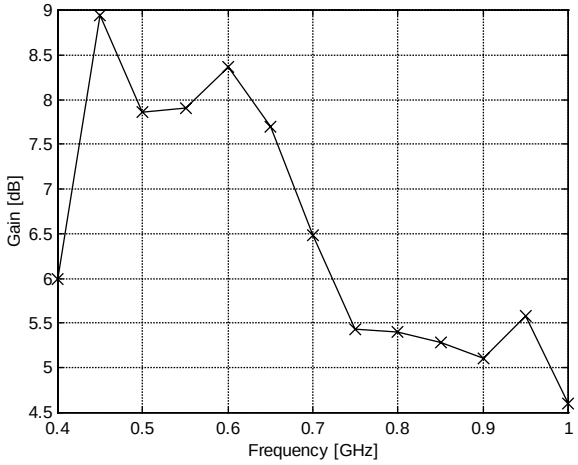

(b)

Figure 3.2-4 (a) Comparison of LPLA and LPDA gains and front-to-back ratios [18], (b) gain from ESP simulation for LPLA with 200 Ω terminal resistance.

Chapter 4. Numerical Analysis of LPLA with Ground Reflector

The investigation of the log-periodic loop antenna with ground reflector is presented with a numerical analysis of its radiation characteristics including gain, far-field pattern, polarization, and input impedance. The method of moment program ESP is used to calculate these characteristics. The goal of this research is to design and analyze a new kind of antenna, which can provide wide bandwidth, high gain, and (if possible) circular polarization for wideband wireless communication applications. Also, size reduction is an important objective of this research. The numerical analysis for the antenna is later complemented with measurements performed at the Virginia Tech Antenna Laboratory. Details of antenna construction and pattern and input impedance measurements are addressed in Chapter 5.

4.1 Geometries and Parameters

At the early stage of this investigation, a log-periodic hemispherical antenna was examined to see if the desirable characteristics might be achieved. The research was

expanded to a number of other geometries. It was found that sometimes one geometry provides high gain but not desirable polarization, whereas another geometry shows very high gain and stable linear polarization only in a narrow bandwidth. After several trials, eventually the log-periodic loop antenna with a ground reflector below the apex of the antenna emerged as a useful candidate.

Many cases of the LPLA with ground reflector were examined over a wide range of frequencies. Numerical results for LPLAs with 5 to 10 circular loops are calculated and compared. These LPLAs have a conical or inverted conical shape, as shown in Figure 4.1-1, with full angles of 30°, 45°, and 60°. The geometries can be generated by using the subroutine WGEOM, which is listed in Appendix B. Also, the subroutine would be very useful for the analysis of any variations, which have circular loop antennas as elements. All antennas are designed for operation around 2.0 GHz, because mobile communication systems like pagers, cellular and PCS phones use the frequency range of 800 MHz - 2800 MHz. Table 4-1 summarizes the range of variables used in the numerical analysis of LPLAs. The values of τ, α, and σ are chosen so that the resulting gains can be compared to the constant directivity contours for LPDAs by Carrel [14] after several trials with the aim of achieving wide bandwidth and high gain.

Table 4-1 Variables and corresponding ranges for the investigation of LPLA with ground reflector.

Parameter	Value Range
• Scale factor, τ	$\tau = 0.84$
• Subtended angle, α	$\alpha = 30°, 45°, 60°$
• Spacing factor, σ	$\sigma = 0.149, 0.097, 0.069$
• Frequency, f	$0.8 \text{ GHz} \le f \le 4.8 \text{ GHz}$
• Number of loops, N	$5 \le N \le 10$

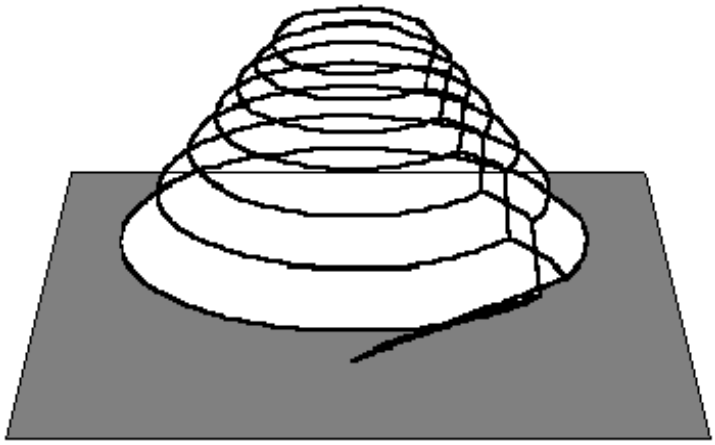

(a)

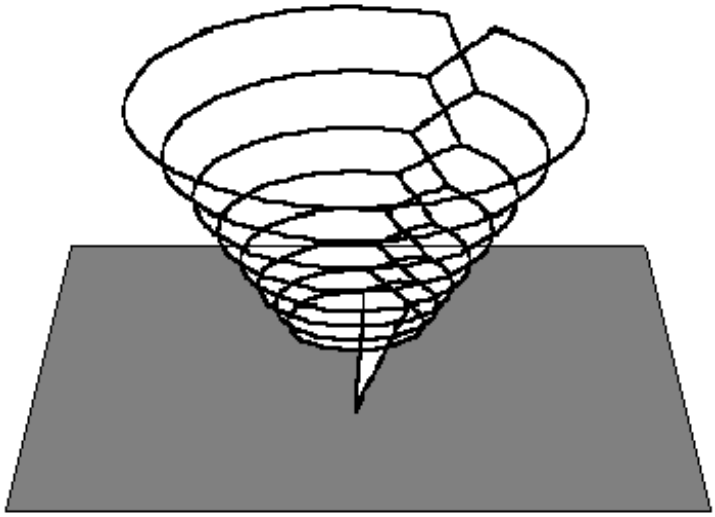

(b)

Figure 4.1-1 (a) Inverted LPLA and (b) LPLA generated by ESP.

During the numerical analysis of these antennas, it was discovered that an antenna with N=6 and $\alpha=30^\circ$ provides the best performance in terms of gain and polarization bandwidth. Also the antenna with N=7 and $\alpha=45^\circ$ exhibits good characteristics. Section 4.3 focuses on evaluation of properties of these antennas.

4.2 Simulation by ESP

The ESP code is a Fortran program of about 7,000 lines, including many subroutines such as WGEOM, which was developed at the Ohio State University. It uses delta gap source, electric field integral equation (EFIE), and piecewise sinusoidal reaction formulation. Since basis (expansion) and test (weighting) functions are both piecewise sinusoidal, the used MoM can be called Galerkin's method [15].

Four types of files are used in the ESP code. The first is an input file (.INP), through which input data are entered. The second one is an output file (.OUT), where output data such as wire geometry, far-zone patterns and input impedance are created. The third is a pattern file (.PAT), where data for far-zone pattern and phase difference are obtained. The last is referred to as plate file (.PLT), which contains plate geometry information.

Antenna geometries can be formed in two ways in the ESP; one is by using an input file (.INP) and the other is by programming the WGEOM subroutine, in which a user can create a wire antenna geometry. Once an antenna geometry consisting of wires and plates is defined in the ESP, the antenna characteristics such as gain, radiation pattern and input impedance can be analyzed easily.

In making a new wire geometry by the ESP, there are some limitations that must be observed. They are listed as follows [6]:

- FMC = frequency in megahertz
- A = the wire radius in meters. 'A' should be less than 0.01λ. The thin wire approximations will also be violated if two wire segments intersect at a small acute angle (i.e. <30°) or if two wire segments pass within a few wire diameters of each other.
- SEGM(NPL) = the maximum segment size of the surface patch monopole should not exceed 0.25λ and is typically chosen 0.25λ.
- The length of each segment should not exceed a quarter wavelength.
- No wire segment should be smaller than two times the wire radius.
- The feed locations, for mutual coupling, must be adjacent to a point on the wire which has only two segments emanating from it.
- Excitation may be either by a delta-gap voltage generator or by a plane wave.
- The frequency must be low enough that BDSK(I)=0.4 meters is no more than 0.25λ.
- Wire/plate junctions must be at least 0.1λ away from all edges of the plate to which the wire is attached.

4.3 Radiation Characteristics of LPLA with Ground Reflector

The geometry of LPLA is shown in Figure 4.1-1 (b). This antenna is based on the log-periodic antenna concept, as discussed in Sections 2.3 and 3.2. Moreover, ground reflector in the apex region of the LPLA can be included in order to obtain higher gain and reduce back radiation.

Because LPLAs are expected to be wideband, their segmentation should be

determined in terms of the corresponding wavelength. For gain calculation, presented in Section 4.3.1, 12 segments per one wavelength on loop elements and about 4 segments on feed lines between two adjacent elements of the antennas are used for faster calculation to figure out general outline. Since ESP uses piecewise sinusoidal functions as the basis and weight functions, these numbers of segments are adequate for convergence of solution with reasonable accuracy. However, 28 segments per one wavelength on both loop elements and feed lines are used to achieve more accuracy for comparison with the measured results. In all cases, a square ground reflector plane, 0.24 m on each side, is used as shown in Figure 1-2.

4.3.1 Gain and Directivity

The ESP program calculates the gain components, G_θ and G_ϕ, referenced to an isotropic linearly-polarized antenna, from the following expressions:

$$G_\theta = \frac{|E_\theta|^2 r^2}{30|I_A|^2 R_A} \qquad (4.3.1\text{-}1)$$

$$G_\phi = \frac{|E_\phi|^2 r^2}{30|I_A|^2 R_A} \qquad (4.3.1\text{-}2)$$

where I_A and R_A are the current and resistance at the antenna input terminals, and E_θ and E_ϕ are electric field components in the far-zone region [23]. In addition, G_θ and G_ϕ are dimensionless and can be expressed in dB or linear scales. ESP produces G_θ and G_ϕ in dB. Once the two gain components, G_θ and G_ϕ, are obtained, the total gain can be found as [15]:

$$G(\theta, \phi) = G_\theta + G_\phi$$
$$= \frac{\left[\left|E_\theta\right|^2 + \left|E_\phi\right|^2\right] r^2}{30\left|I_A\right|^2 R_A} \qquad (4.3.1\text{-}3)$$

If antenna radiation efficiency, e, is 100 percent, the directivity, D, becomes equal to the gain, because

$$G = eD = \frac{R_r}{R_A} D \qquad 0 \le e \le 1 \qquad (4.3.1\text{-}4)$$

where R_r is radiation resistance. The 100 % efficiency means that the antenna is lossless and all input power is accepted as radiation power. Usually, e is equal to 1 in simulations by the ESP. Thus, for all the results in this chapter and in Appendix C, e = 1 is assumed.

The LPLAs investigated, here, have full cone angles of 30°, 45°, and 60° and all have the same scale factor, τ = 0.84. The remaining specifications of the antennas are summarized below :

- σ = 0.149, 0.097, and 0.069 for LPLA with α = 30°, 45°, and 60°, respectively
- For 30° LPLA, the 5th loop is located in 7 cm from ground reflector and the circumference of the loop is 11.785 cm, which has a resonant frequency at 2545.6 MHz
- For 45° LPLA, the 6th loop is at a height of 7 cm from ground reflector and the circumference of the loop is 18.218 cm, which resonates at 1646.7 MHz
- For 60° LPLA, the 7th loop is 7 cm from ground reflector and the circumference of the loop is 25.393 cm, which corresponds to 1181.4 MHz

Figure 4.3.1-1 shows variations of G_θ and G_ϕ at θ=0° in the H-plane for a 5-turn LPLA (see Figure 4.1-1 (b)) and inverted LPLA (see Figure 4.1-1 (a)) with ground reflector over

a frequency range of 1.0 to 6.0 GHz, with 200 MHz increments. Figure 4.3.1-2 shows the gain fluctuations for 6- and 7-turn LPLA with ground reflector in the same plane, over the same frequency range as in Figure 4.3.1-1.

Examination of Figure 4.3.1-1 reveals that G_ϕ is significantly larger than G_θ in the H-plane. This characteristic is believed to originate from the element pattern of the single loop antenna discussed in Section 3.1. Thus, the total gain is approximately equal to G_ϕ.

Comparison of Figure 4.3.1-1 (a) and (b) reveals that, generally, the inverted LPLA with ground plane has less gain than the non-inverted LPLA with ground plane. This is attributed to the fact that the main beam of LPLA without ground plane, discussed in Section 3.2, is directed toward the apex. Here the ground plane plays the role of a reflector, hence the name, "Ground Reflector (GR)". Moreover, the LPLA-GR provides a wider 3-dB gain bandwidth for G_ϕ component than the inverted LPLA-GR.

It is also noticed that G_ϕ is significantly lager than G_θ for 6- and 7-turn LPLA-GR in the H-plane, as shown in Figure 4.3.1-2. More importantly, the 6-turn LPLA-GR with α=30° exhibits gain values above 10 dB from 2.0 to 3.25 GHz with less than 3-dB variation (see Figure D-1 in Appendix D for detail). This design appears to be the best among all cases studied in this research. This antenna yields a bandwidth of [15]:

$$BW = \frac{f_U - f_L}{f_C} \times 100\% = \frac{3.25 - 2.0}{2.625} \times 100\% = 47.62\% \qquad (4.3.1\text{-}5)$$

where f_c denotes the center frequency. The 7-turn 45° LPLA with GR provides 21.05% bandwidth from 1.7 to 2.1 GHz with a gain of about 9 dB.

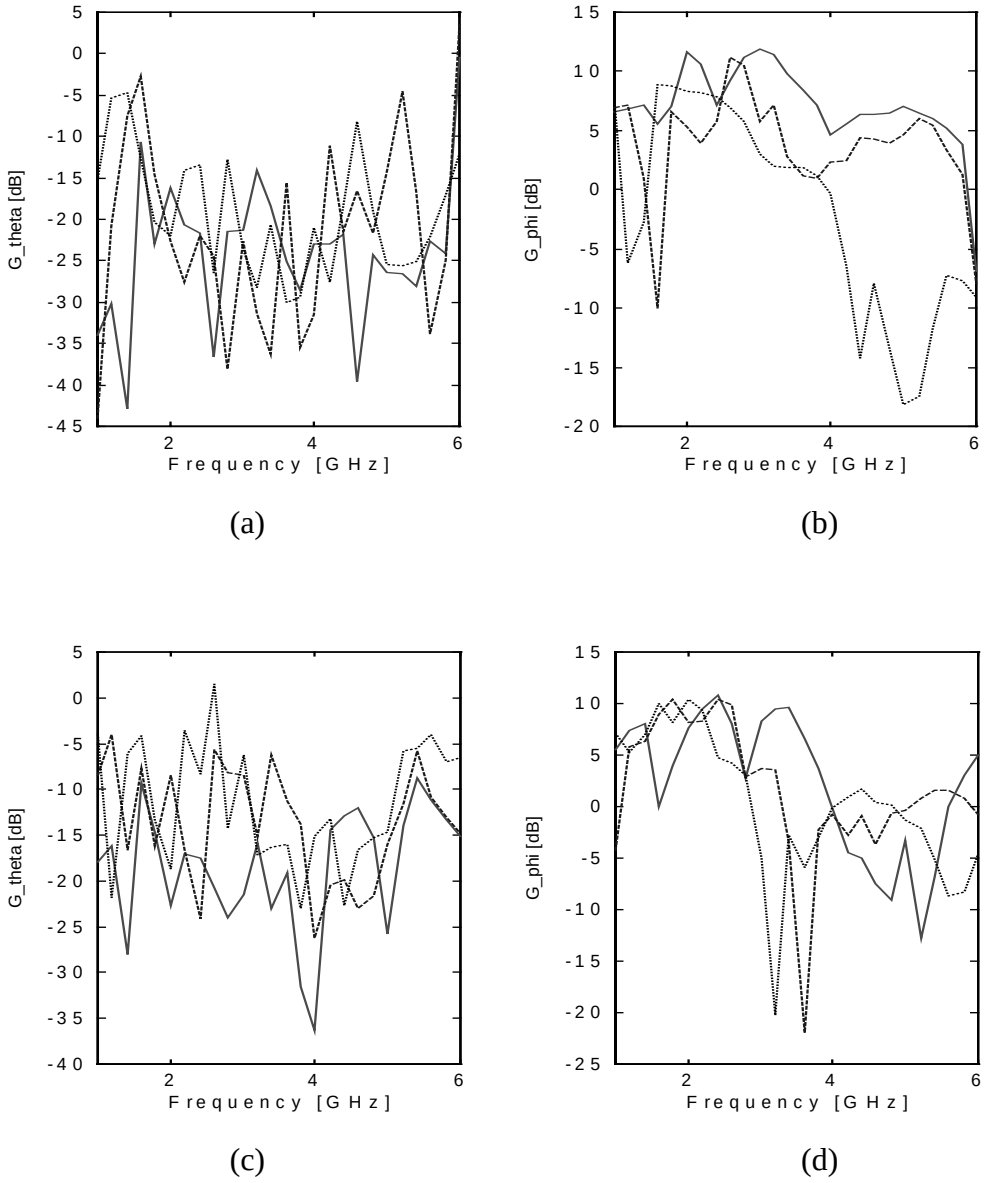

Figure 4.3.1-1 Variations of gain versus frequency for 5-turn (a), (b) LPLA-GR and (c), (d) inverted LPLA-GR with α=30° (solid line), 45° (dashed line), and 60° (dotted line).

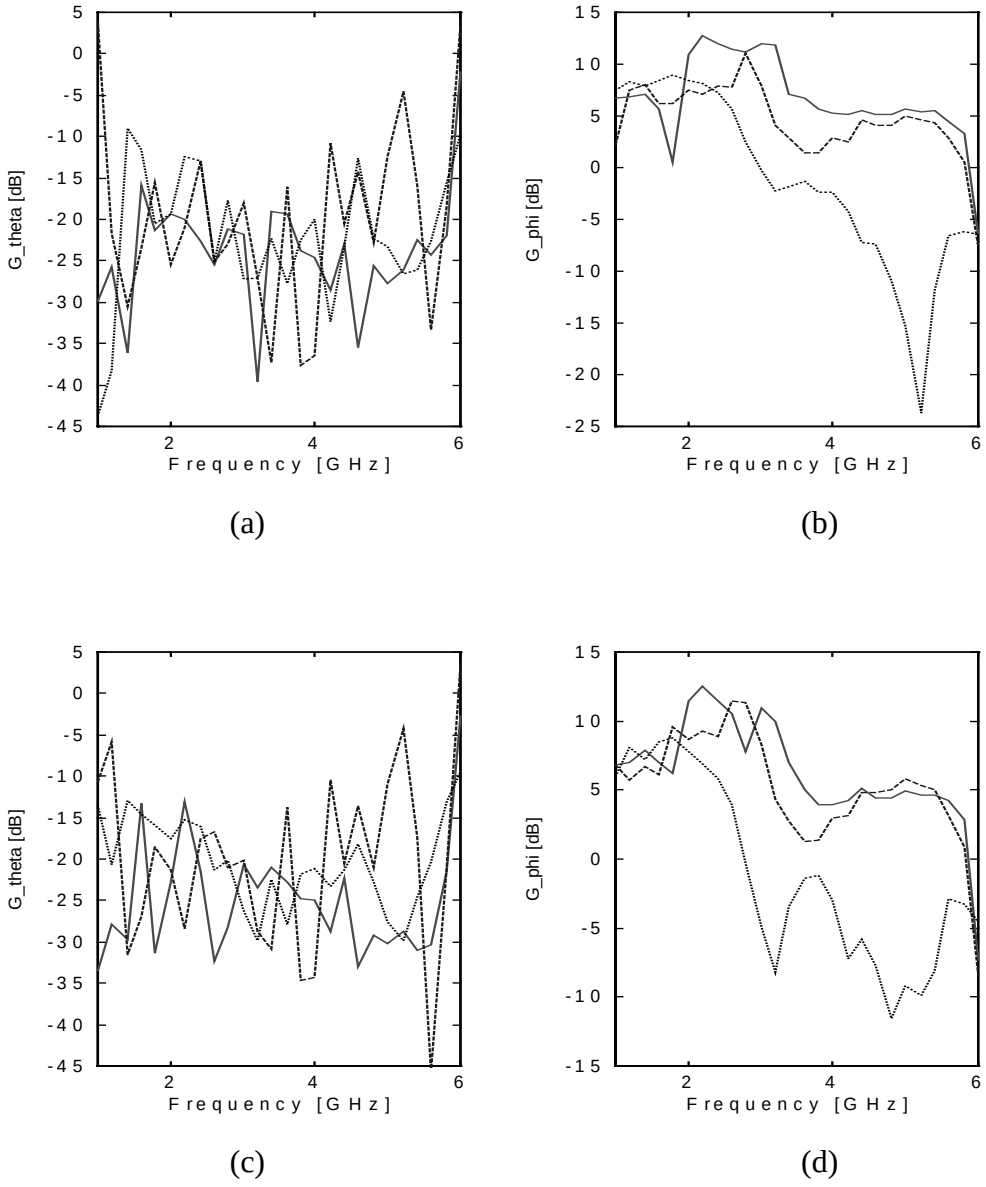

Figure 4.3.1-2 Variations of gain versus frequency for (a), (b) 6-turn LPLA-GR and (c), (d) 7-turn LPLA-GR with α=30° (solid line), 45° (dashed line), and 60° (dotted line).

It is emphasized that the overall bandwidth is influenced by the antenna input impedance. The input impedances of these antennas fluctuate widely over the corresponding frequency ranges, as will be discussed later.

Figure 4.3.1-3 illustrates G_ϕ for the 8-, 9-, and 10-turn LPLAs with GR in the H-plane. As in all previous cases in this section, generally the LPLAs-GR with $\alpha=30^\circ$ provides higher gain than the other two antennas with $\alpha=45^\circ$ and 60°. This is quite natural because the elements of the LPLA-GR with $\alpha=30^\circ$ have closer circumferences than the others.

4.3.2 Far-Field Pattern

As mentioned in the preceding section, the ESP yields the two orthogonal gain components. Referring to (4.3.1-1) and (4.3.1-2), E_θ and E_ϕ far-field patterns are the same as G_θ and G_ϕ gain patterns, respectively, because radiation pattern is a plot of relative power versus angular coordinates. Appendix C contains the computed far-field radiation patterns for a 6-turn LPLA with $\alpha=30^\circ$ and a 7-turn LPLA with $\alpha=45^\circ$. These antennas have ground reflector and the frequency range is 1.55 GHz to 4.4 GHz. Figure 4.3.2-1 shows the typical far-field patterns for 6-turn LPLA-GR with $\alpha=30^\circ$ in the E-plane obtained from ESP, using 28 segments per wavelength for each loop and feed line between two adjacent loops.

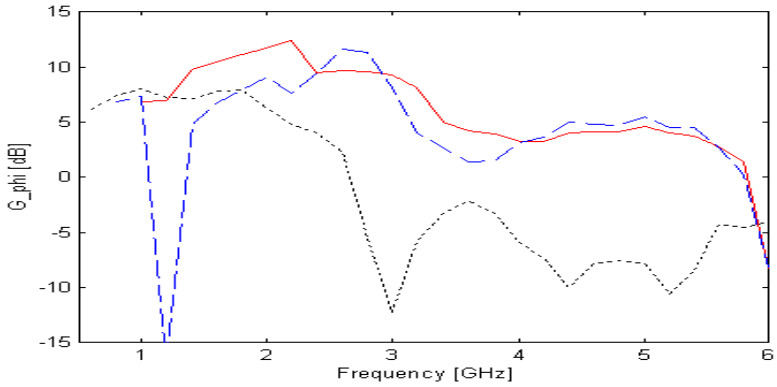

(a)

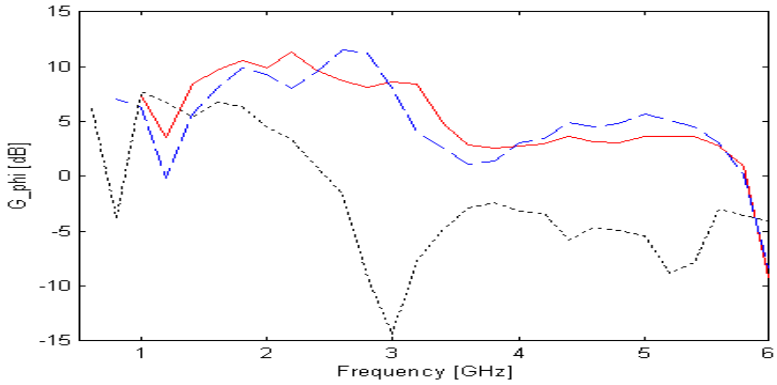

(b)

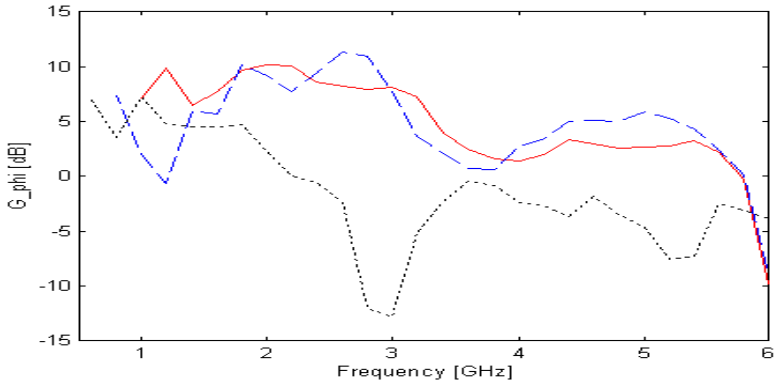

(c)

Figure 4.3.1-3 Variations of G_ϕ versus frequency for (a) 8-turn (b) 9-turn and (c) 10-turn LPLA-GR with $\alpha = 30^\circ$ (solid line), 45° (dashed line), and 60° (dotted line).

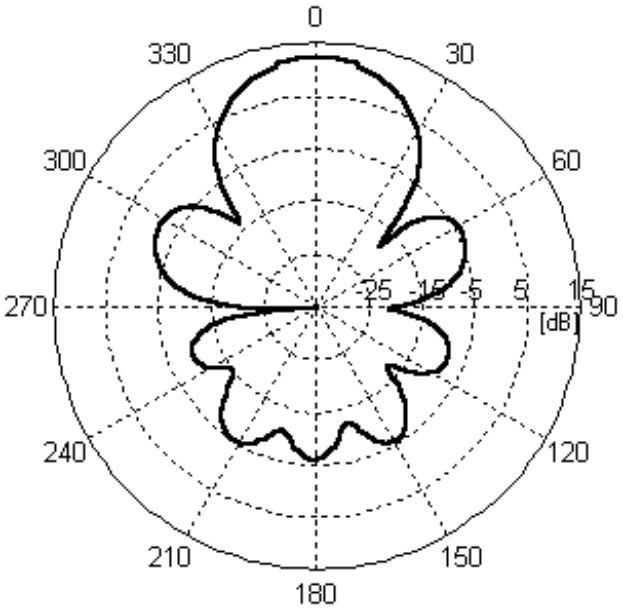

(a)

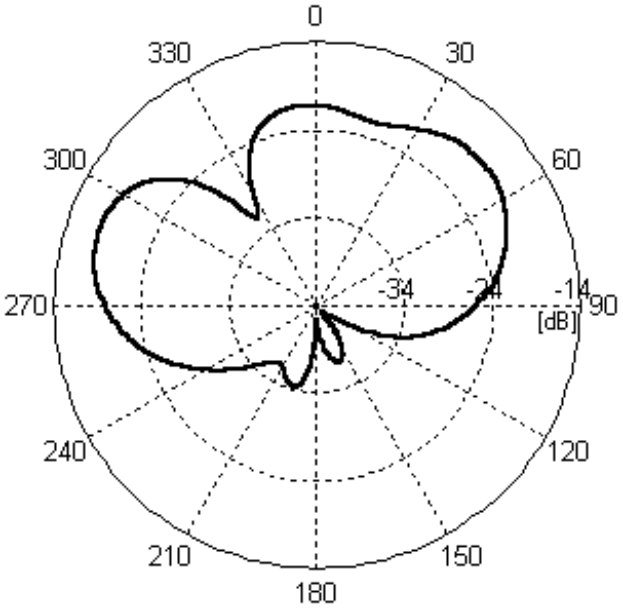

(b)

Figure 4.3.2-1 Radiation patterns for a 6-turn LPLA-GR with $\alpha=30^\circ$ at 2301 MHz in the E-plane: (a) G_θ, (b) G_ϕ.

Referring to Figure 4.3.2-1, the E-plane pattern for G_θ has a relatively broad beamwidth. The 10 dB beamwidth, which is often used to characterize parabolic feeds, may be a more appropriate measure of this antenna's radiation pattern than the 3 dB beamwidth. The 10 dB beamwidth of the 6-turn LPLA-GR with $\alpha = 30^\circ$ is about 63°, while the 3 dB beamwidth is about 36°. The SLL (Side Lobe Level) is about 14.0 dB below the main beam. It is noted that unlike G_ϕ which is dominant in the H-plane as discussed in Section 4.3.1, G_θ is dominant in the E-plane as shown in Figures 4.3.2-1, and C-1 in Appendix C.

It is also noticed that there is small amount of back radiation behind the ground reflector. The back lobe is created from the scattering at the edges of the ground reflector. If the ground reflector is enlarged, the back lobe can be reduced more. In Figure 4.3.2-1 (a), the front-to-back ratio is about 18.787 dB, which indicates that the pattern can be considered as unidirectional.

The broad beamwidth and high front-to-back ratio are also observed in the far-field patterns presented in Appendix C. Furthermore, the patterns in Appendix C confirm the 47.62% bandwidth for the 6-turn LPLA-GR with $\alpha = 30^\circ$ and 21.05% for the 7-turn LPLA-GR with $\alpha = 45^\circ$, which are obtained in Section 4.3.1. Over the bandwidth of each antenna, gain variations are less than 3 dB and the patterns sustain their shapes. The half-power beamwidths (HP) for the 6-turn and 7-turn antennas over their respective bandwiths are summarized below :

- HP for G_θ patterns of 6-turn 30° LPLA-GR in the E-plane $\approx 36^\circ$
- HP for G_ϕ patterns of 6-turn 30° LPLA-GR in the H-plane $\approx 44^\circ$
- HP for G_θ patterns of 7-turn 45° LPLA-GR in the E-plane $\approx 29^\circ$
- HP for G_ϕ patterns of 7-turn 45° LPLA-GR in the H-plane $\approx 37^\circ$

4.3.3 Polarization

In the two preceding sections, it was noted that G_ϕ component of the gain is dominant in the H-plane, while it is negligible in the E-plane. This indicates that the LPLA-GR is a linearly polarized antenna [24]. These characteristics are also those of a single-loop antenna that constitutes the element for the LPLA.

In the same way, the LPLA-GR provides linear polarization in the $\phi=45^\circ$ plane, which lies between the E- and H-planes, similar to the single loop antenna. Figure 4.3.3-1 illustrates this characteristic in the 45° plane. G_θ and G_ϕ are nearly equal to 6.75dB. Besides, the phase difference between these two gain components is close to zero in the $\theta=0^\circ$ direction, ensuring the linear polarization. It is also confirmed in Figures in Appendix C over all frequency range that LPLA provides the linear polarization.

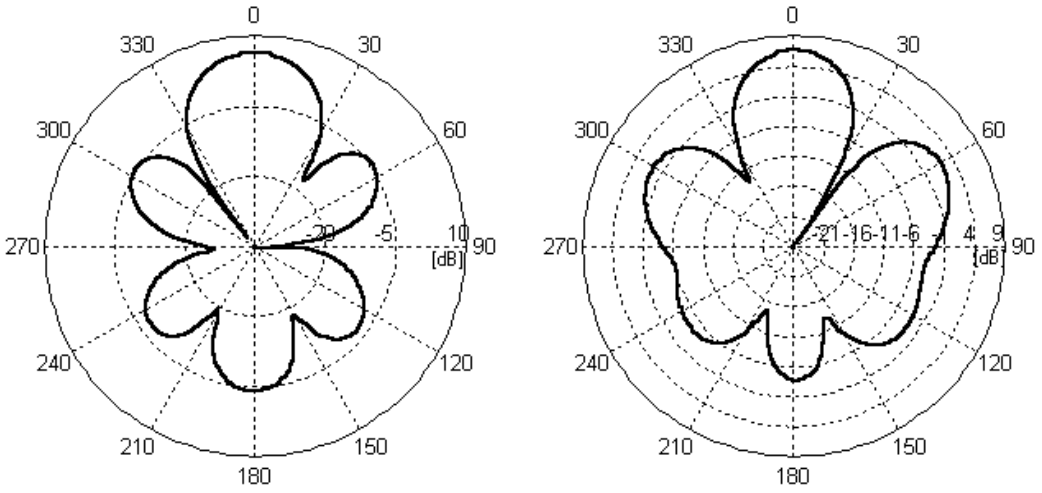

(a) (b)

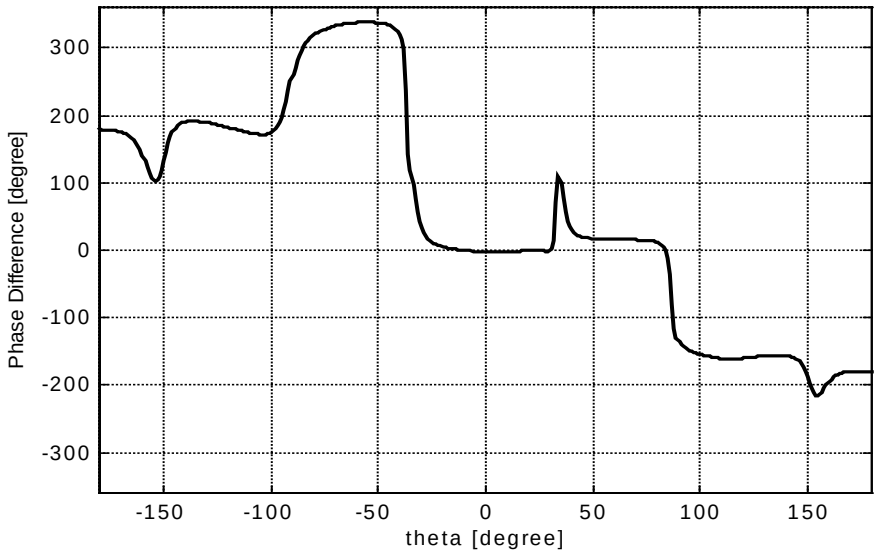

(c)

Figure 4.3.3-1 Radiation characteristics for the 6-turn LPLA-GR with α=30° at 2001 MHz in the 45° plane : (a) G_θ pattern plot, (b) G_ϕ pattern plot, and (c) the phase difference between E_θ and E_ϕ.

4.3.4 Input Impedance

Input impedance is one of the most important characteristics of an antenna. To avoid signal distortions, constant input impedance over a wide bandwidth is desirable. The ESP calculates the antenna input impedance by using the following formula:

$$[I_n] = [Z_{mn}]^{-1}[V_m] \qquad (4.3.4\text{-}1)$$

where $[V_m]$ represents a delta gap voltage source. Once $[Z_{mn}]$ is found from the EFIE, the approximate current distribution in discrete form on an antenna can be computed and then the antenna input impedance Z_A found by inverting antenna current I_A at the unit voltage feed point.

Even though the ESP calculations of gain and pattern converge rapidly with coarse segmentation as shown in Appendix D, it is not the case in input impedance calculation of complicated geometries like the 6-turn LPLA-GR. The input impedance is very sensitive to the number of segments used in the simulation of antennas and fluctuates widely over the gain bandwidth. Figure 4.3.4-1 shows the input impedance versus frequency (real and imaginary parts) for a 6-turn LPLA-GR with $\alpha=30^\circ$ in two cases corresponding to about 12 and 28 segments per wavelength. We believe that input impedance results from ESP are not reliable enough to make conclusive and unambiguous assessment. For this reason, input impedance measurement is indispensable in practice and the measured results will be presented in Section 5.3.

However, it can be inferred that the LPLA-GR has resonance characteristic because the impedance contains significant reactance part over the operation frequency. This phenomenon is well observed in measured results.

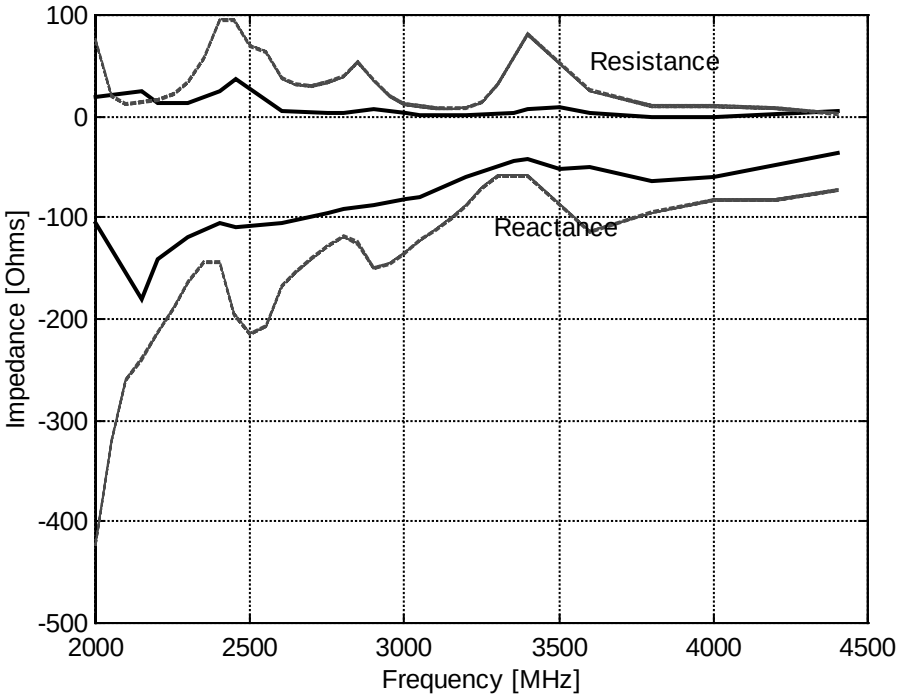

Figure 4.3.4-1 Input impedance versus frequency for a 6-turn LPLA-GR with α=30° when about 12 segments (dashed lines) and 28 segments (solid lines) per wavelength are used.

4.4 Comparison of LPDA, LPLA without Ground Reflector and LPLA with Ground Reflector

So far, LPDA, LPLA without ground reflector and LPLA with ground reflector have been investigated in Sections 2.3, 3.2, and 4.3, respectively. All the geometries can be used to achieve high gain, wide bandwidth, and unidirectional far-field radiation pattern. However, a LPLA without ground reflector provides 1.5 to 2 dB higher gain than a LPDA with the same scale and spacing factors, number of elements, and terminal resistance over their respective frequency ranges of operation, as shown in Figure 3.2-4. It was also noticed that the gain calculated by Rojarayanont [18] is about 2 to 4 dB higher than that obtained from ESP. Taking the fact into account, it becomes evident that the 6-turn LPLA-GR with α=30° provides about 5 dB higher gain than the LPLA without GR. As for the antenna input impedance, it seems that Z_{in} for LPLA without GR varies less than that for LPLA with GR over a wide bandwidth.

Furthermore, both of LPLAs with and without GR provide reduced transverse dimensions by a factor of $2/\pi$ as compared to the LPDA at their respective resonant frequencies. It can be understood by

$$\frac{transverse\ length\ of\ LPLA}{transverse\ length\ of\ LPDA} = \frac{\lambda_{rl}/\pi}{\lambda_{rd}/2} = \frac{2}{\pi} \qquad (4.4\text{-}1)$$

where λ_{rl} (wavelength at the resonance of loop element) = λ_{rd} (wavelength at the resonance of dipole element). They also have the advantage that the loop elements may be circular, square, or rectangular and hence an added degree of flexibility.

4.5 Expected Applications of the LPLA

Because of smaller transverse dimensions than LPDA, both LPLAs with and without GR can be useful in situations where size is important, as in aircraft, spacecraft, and satellites. They can be mounted on cars for the mobile communications. They are also expected to be useful as receive antennas in EMC (ElectroMagnetic Compatibility) scattering range as shown in Figure 4.5-1 [25].

Another important potential application of LPLAs is as feeds for parabolic reflector antennas [26, 27]. If the LPLA-GR is used for the feed, the whole system can be considered as dual reflector antenna. It is well known that these features are very useful in the area of satellite communications, which demand very high directivity. Figure 4.5-2 illustrates an application of the log-periodic antenna as a feed for the reflector. To be precise, the feed is a log-periodic toothed trapezoidal wedge antenna discussed in Section 2.2.2.

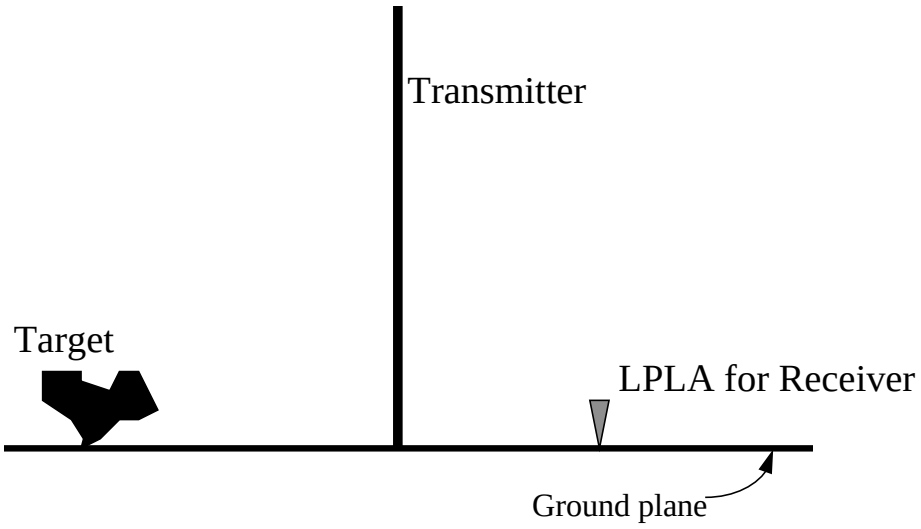

Figure 4.5-1 Schematics of time-domain scattering range

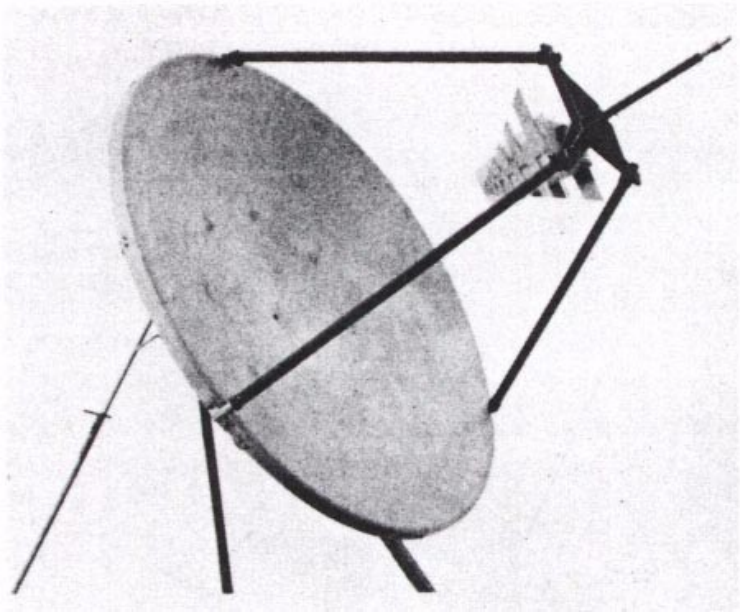

Figure 4.5-2 Four-foot dish with the log-periodic feed [26].

Chapter 5. Measurements of LPLA with Ground Reflector

In order to confirm the results of the numerical analysis, three LPLAs with GR were built and tested for far-field pattern and antenna input impedance. The far-field measurements were taken on the Virginia Tech antenna range and the input impedance measurements by using a network analyzer over a wide range of frequencies. These results are presented in this chapter and compared to those generated numerically by the ESP in Chapter 4. Section 5.1 will describe the construction of antennas, while Sections 5.2 and 5.3 discuss measurements of far-field pattern and input impedance, respectively.

5.1 Antenna Construction

Three prototype LPLAs with GR were constructed for experimental study. The choice of antenna parameters were made based on simulation results presented in Section 4.3. The names referred to the three constructed prototype LPLAs with GR are listed in Table 5-1. Figure 5.1-1 illustrates the photograph of LP2.

Table 5-1 Parameters for constructed LPLAs with GR

Antennas	Design Parameters			
	N	Scale Factor (τ)	Subtended Angle (α)	Spacing Factor (σ)
LP1	6	0.84	30°	0.149
LP2	6	0.84	30°	0.149
LP3	7	0.84	45°	0.097

The LP1 and LP2 antennas, which have gain operating bands from 2 to 3.25 GHz, are intended for operation in a higher frequency range, while LP3 has been designed for operation in a lower frequency range from 1.7 to 2.1 GHz. Also, the feed points are located on two parallel lines having 10 mm spacing for LP1 and 14 mm spacing for LP3. The LP2 is identical to the LP1 except that the feed points are located on two lines with an angle of 10° and intersecting at the apex of antenna cone. Measurements in these frequency ranges can be performed conveniently at the Virginia Tech Antenna Laboratory.

The construction of antennas began with drawing the two-dimensional body shapes of LP1, LP2, and LP3 on a two-ply vellum bristol board (a kind of paper). Then, the conical surfaces, on which the loop elements and their feeds are mounted, were formed.

A copper wire with a diameter of 1 mm (0.99 mm by measure) was used for the construction of each loop element with two crossed arms for feeding. The loop elements were placed on the conical surface and were secured by gluing the copper wire to the paper. Each element was then connected to the neighboring element by soldering the crossed arms, as illustrated in Figure 5.1-1.

Finally, each LPLA was mounted above a circular ground reflector with a diameter of 30.4 cm as shown in Figures 1-2 and 5.1-1. The antenna is fed with two coaxial cables by means of two ‘RF rear-panel-mount gold connectors’. The inner conductors of the coaxial cables are connected to feed terminals of the antenna near the apex, while the outer conductors of the cables are attached to the ground plane, as indicated in Figure 5.2-1.

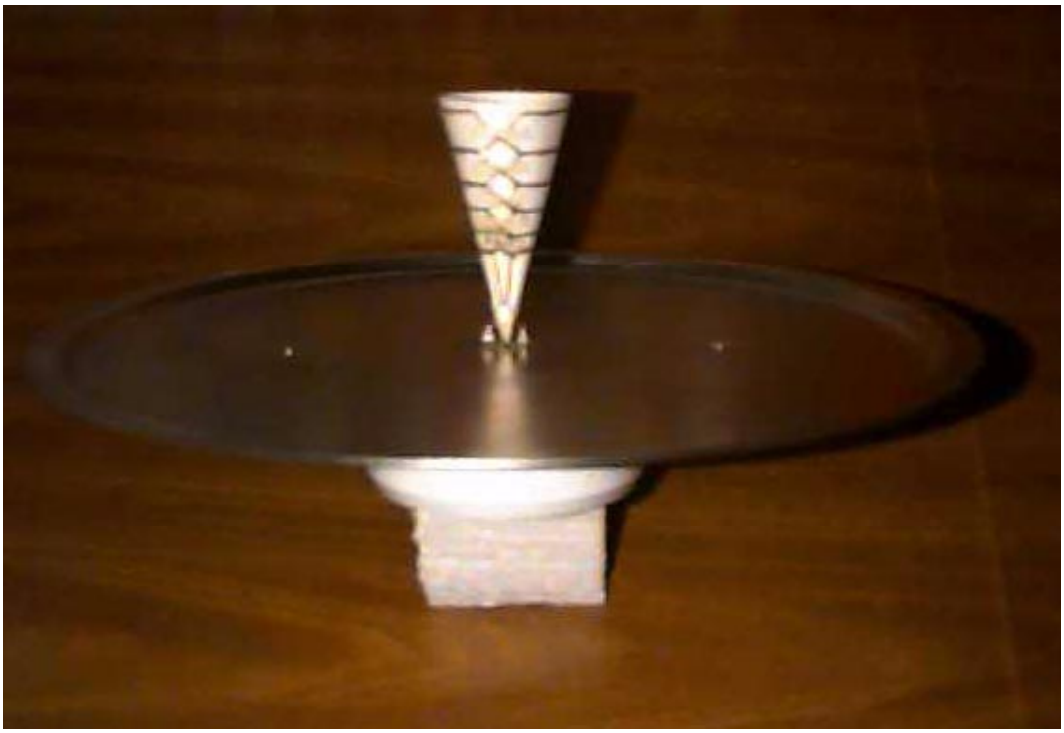

Figure 5.1-1 Photograph of a 6-turn LPLA with $\alpha=30^\circ$ mounted above a ground reflector.

5.2 Far-Field Pattern Measurements

The two feed lines of LPLA form a balanced transmission line which should be connected to a test equipment by means of a coaxial cable. In these measurements, an unbalanced coaxial cable connects the antenna under test to the receiver equipment. In order to connect this unbalanced cable to the balanced line, a balun should be used as shown in Figure 5.2-1. Considering the measurement frequency range for the test antennas, a model 4346 Narda balun was used. This balun has an operating frequency range from 2 to 18 GHz.

For the source antenna, a model SGA-20 horn antenna was used. It has a width of 14.5″ and a height of 10.75″ at the aperture, and is fed by a WR 430 (4.3″×2.15″) waveguide. Generating the TE_{10} dominant mode, the source antenna can rotate in the direction of roll, thus allowing the E field to be vertically or horizontally polarized. Actually, the source antenna is a standard gain horn antenna. Its gain characteristic, however, is not necessary because only radiation patterns are of interest in this experiment.

Once the source horn was fixed vertically or horizontally, the test antenna was rotated about the test tower for copolarized or cross-polarized radiation pattern. This kind of polarization measurement should be in the E- and H-planes for at least 4 cut tests. An attempt was also made to take pattern cuts in the 45° plane between the E- and H-planes like the numerical analysis in Section 4.3.3. Here, the principal planes are determined by the locations of cross feed line, as discussed in Section 3.1.

Figure 5.2-2 shows measured and calculated far-field patterns of G_θ component for LP1 at 2301 MHz in the E-plane. The measured G_θ pattern has HP of about 37° and SLL of about 9.12 dB. The corresponding calculated pattern shown in Figure 5.2-2 (b) indicates that HP ≈ 36° and SLL ≈ 14.0 dB. There is a good agreement between the measured and calculated patterns as noted by comparing Figures 5.2-2 (a) and (b).

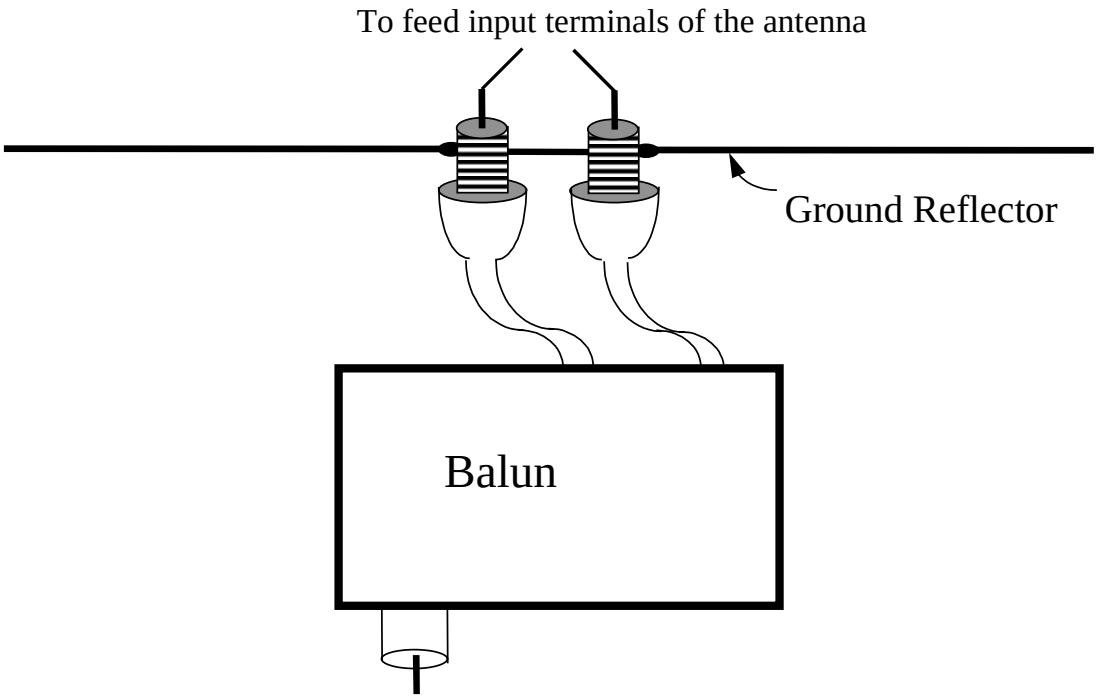

Figure 5.2-1 Feed arrangement for LPLA with GR

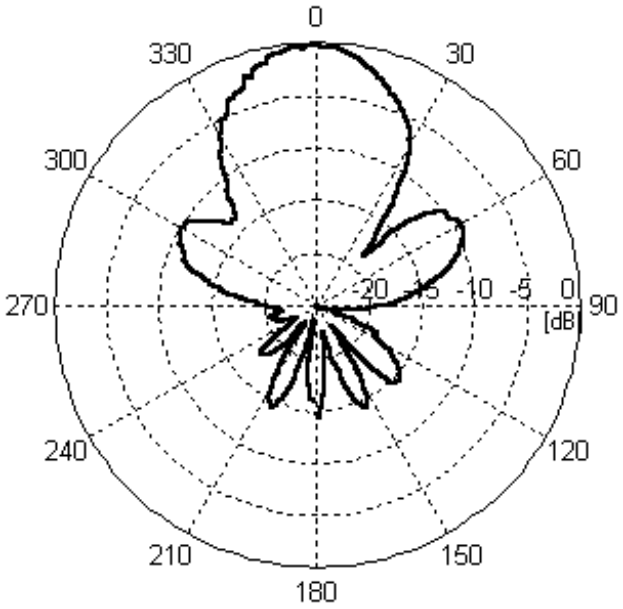

(a)

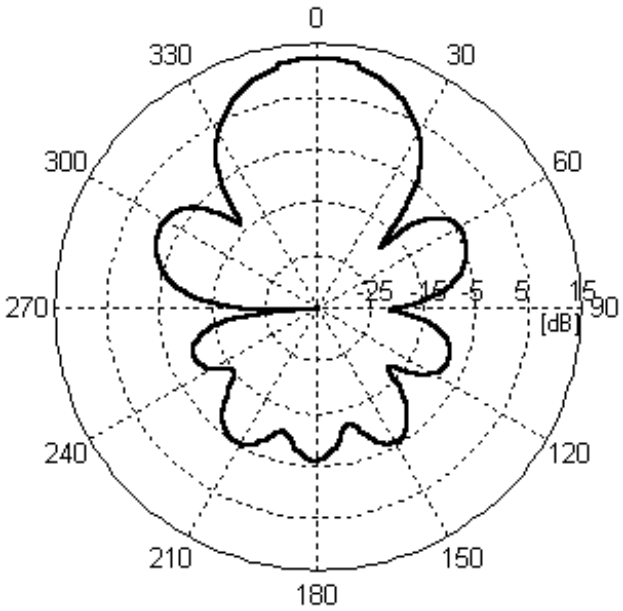

(b)

Figure 5.2-2 (a) Measured G_θ pattern and (b) Calculated G_θ pattern for LP1 at 2301 MHz in the E-plane

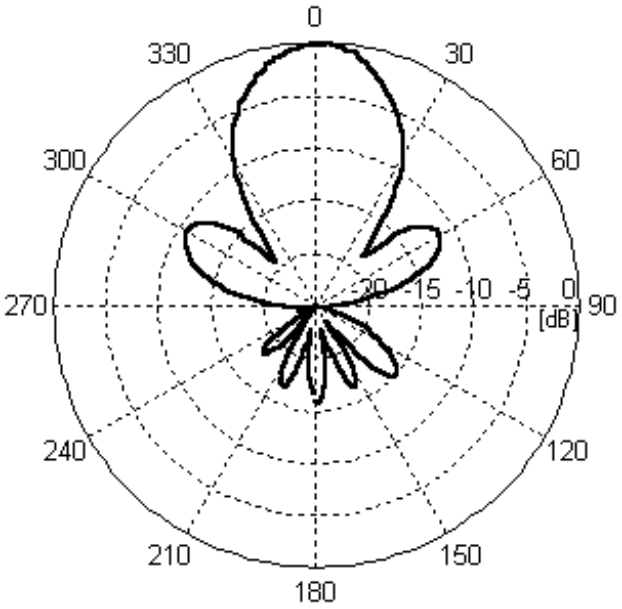

(a)

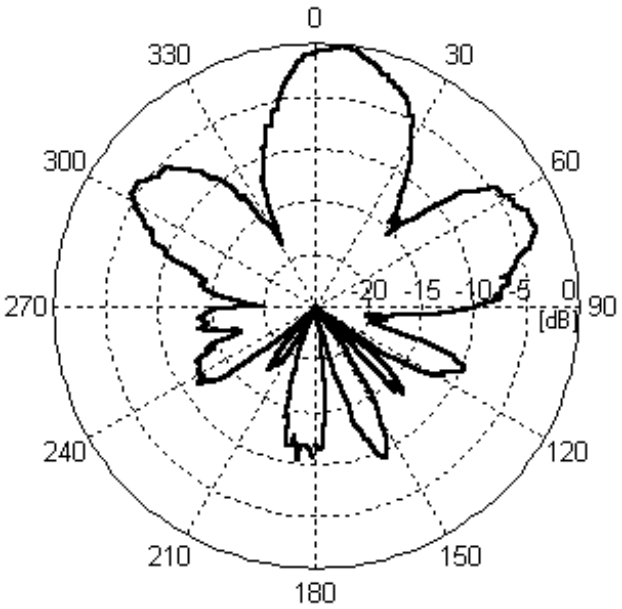

(b)

Figure 5.2-3 Measured far-field patterns for LP2 at 2301 MHz in the E-plane.
(a) G_θ, (b) G_ϕ

Figure 5.2-3 shows measured far-field patterns for LP2 at 2301 MHz in the E-plane. The LP2 yields G_θ pattern with HP ≈ 34° and SLL ≈ 10.72 dB. These values are close to the corresponding simulation results illustrated in Figure 4.3.2-1, of which the dominant G_θ pattern is presented again in Figure 5.2-2 (b).

While the measured G_θ patterns agree well with the calculated pattern, the G_ϕ patterns seem to be different from the computed pattern as shown in Figure 4.3.2-1 (b) in the E-plane. This is due to the fact that the ϕ-component of the electric field is very small and looks like noise. Thus, the G_ϕ pattern in the E-plane can be ignored as investigated in Section 4.3.

Figure 5.2-4 illustrates measured and calculated G_θ patterns at 1.8 GHz in the E-plane for LP3. The measured G_θ pattern has HP of about 29° and SLL of about 4.04 dB. Similarly, the calculated G_θ pattern has HP of about 32° and SLL of about 4.72 dB. Therefore, comparison of Figure 5.2-4 (a) and (b) indicates that the overall agreement between the measured and calculated patterns is good.

Appendix E contains the measured patterns for both far-field components, E_θ and E_ϕ. Tables E-1, 2 and 3 are useful for easy and valuable comparison with G_θ and G_ϕ patterns from the ESP in Appendix C.

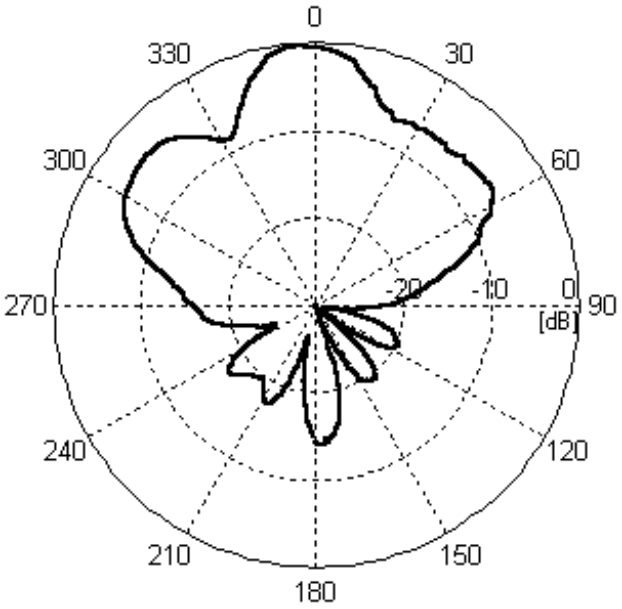

(a)

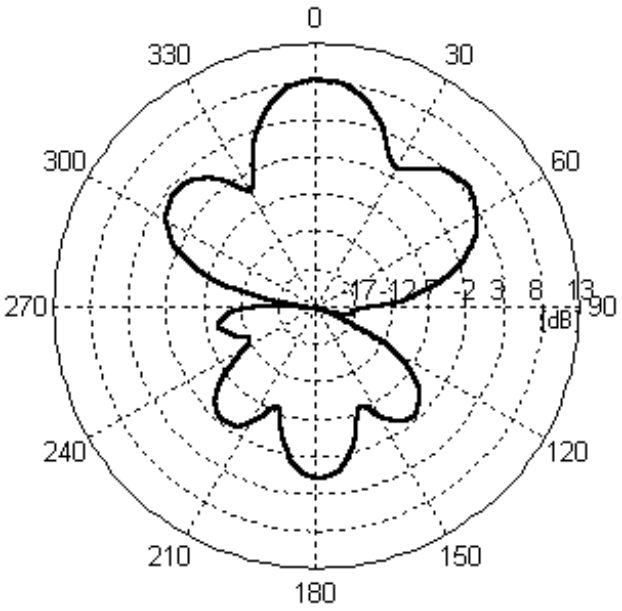

(b)

Figure 5.2-4 (a) Measured G_θ pattern and (b) Calculated G_θ pattern for LP3 at 1.8 GHz in the E-plane

5.3 Input Impedance Measurement

As discussed in Section 4.2.4, the antenna input impedance is a very important issue. The ESP simulation result of LPLA with GR for input impedance, however, is not reliable.

Fortunately, there is a good method to test the impedance of wideband balanced antennas, such as LPLA with GR [28]. If a balanced antenna is treated as a two port network, the scattering parameters of the antenna can be measured by a network analyzer. Here, a balun as in Figure 5.2-1 (b) is not necessary, which makes the measurement easier. The antenna impedance can be calculated using the following formula [28]:

$$Z_{Antenna} = 2Z_0 \frac{1 + s_{11} - s_{21}}{1 - s_{11} + s_{21}} \qquad (5.3\text{-}1)$$

An HP 8720C network analyzer was used for measuring the scattering parameters, s_{11} and s_{21}, after calibration. The network analyzer referenced at the ends of the two port coaxial cables, which have the characteristic impedance (Z_0) of 50Ω. A total of 1601 sampling points covered a frequency range from 800 MHz to 8 GHz. Consequently, a step frequency of 5 MHz was set up for antenna input impedance measurements.

Figures 5.3-1, 2, and 3 show the normalized input impedance measured for LP1, LP2, and LP3, respectively. Small resistance values close to zero and significant reactance are noticed as expected in the simulation results of Section 4.3.4. However, the exact values from the measurement do not agree with those from the simulation. The reason is that the ESP code is not reliable in the input impedance calculation for the complicated geometries like LPLA.

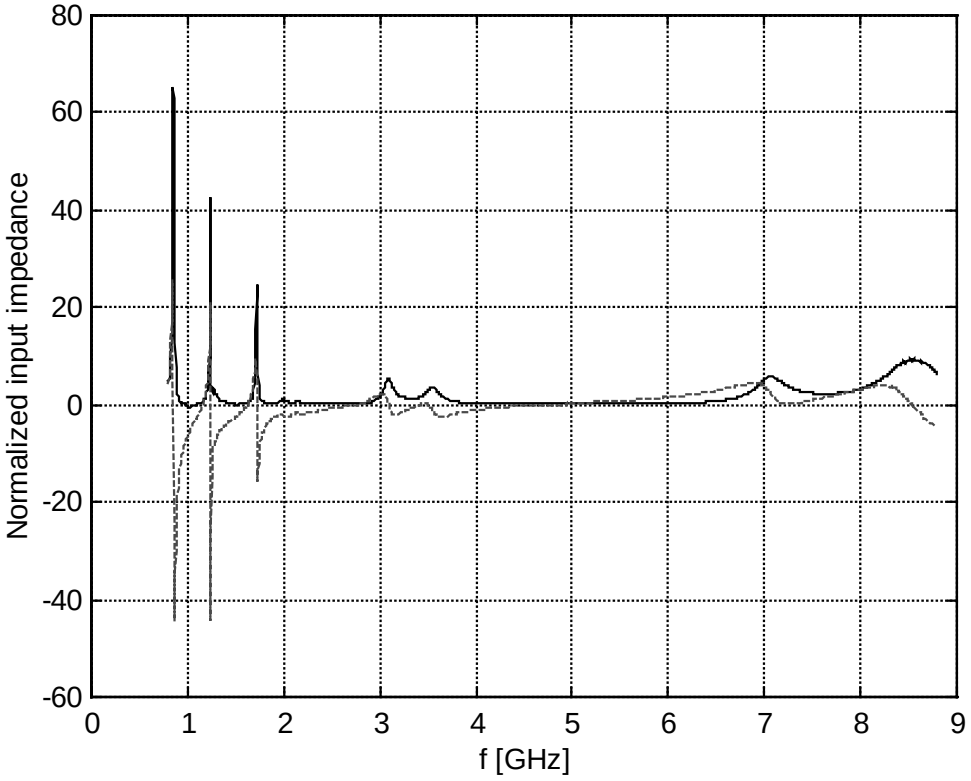

Figure 5.3-1. Normalized input impedance to Z_0=50Ω for LP1 :
Resistance (solid line) and Reactance (dashed line).

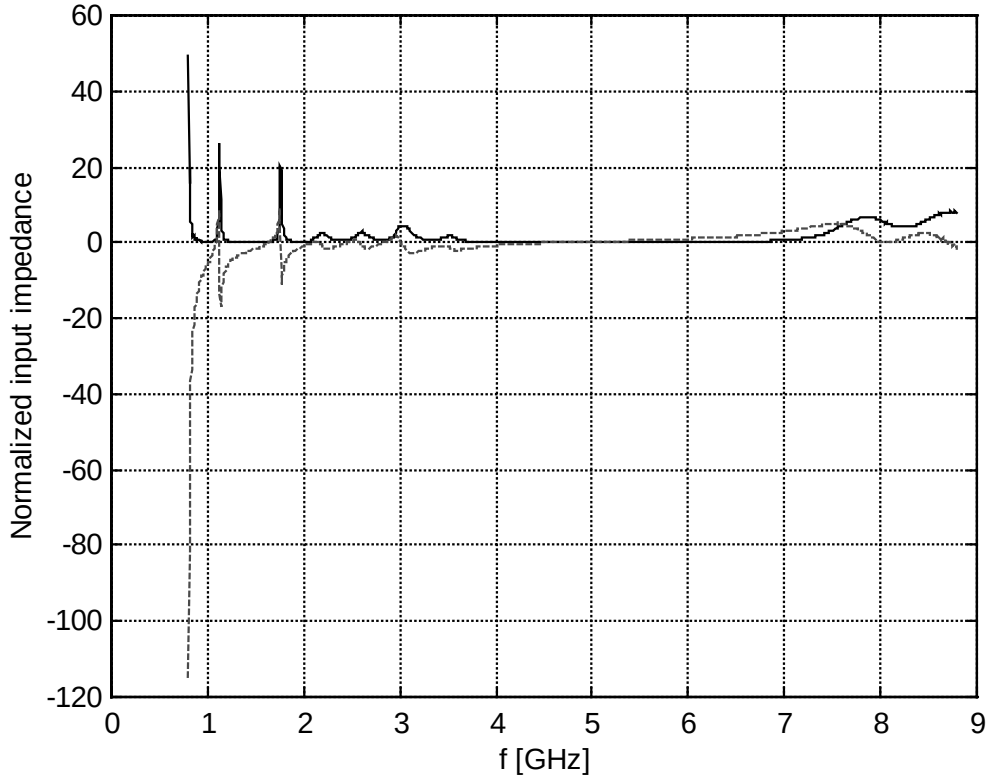

Figure 5.3-2. Normalized input impedance to Z_0=50Ω for LP2 :
Resistance (solid line) and Reactance (dashed line).

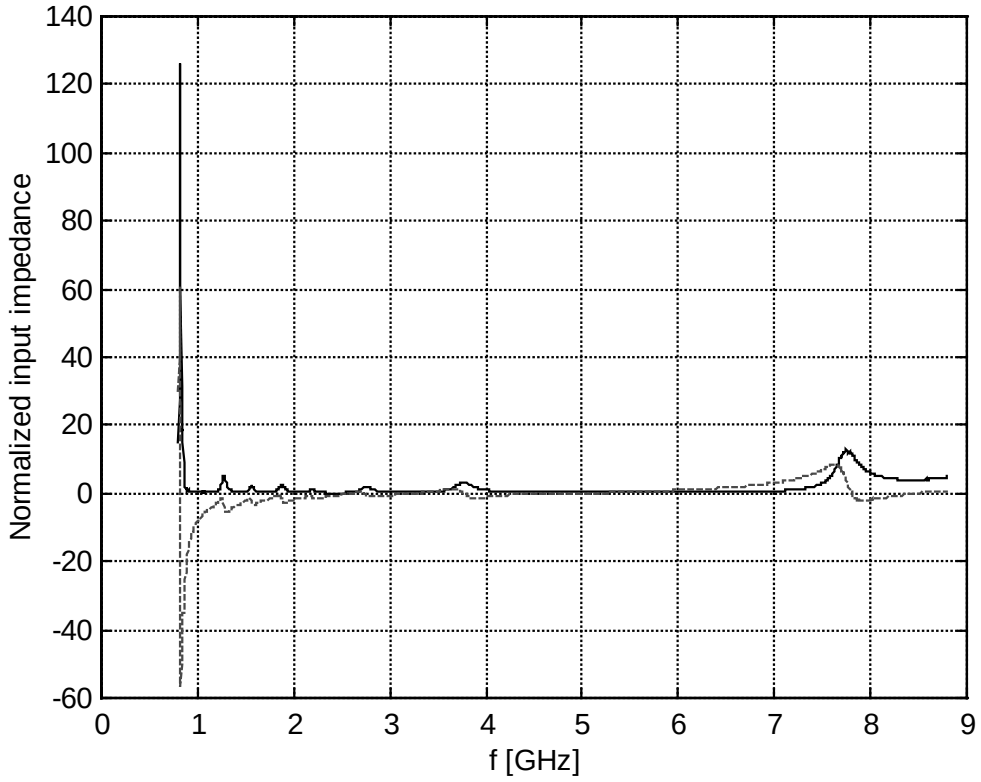

Figure 5.3-3. Normalized input impedance to Z_0=50Ω for LP3 :
Resistance (solid line) and Reactance (dashed line).

In a small region, there is a little negative resistance, which seems to be an error from the test. Also, sometimes s_{11} is different from s_{22}, which should be the same ideally. After correcting the slight negative resistance by replacing it with 0.05Ω and averaging s_{11} and s_{22}, actual resistance and VSWR (Voltage Standing Wave Ratio) were computed using MATLAB. Here, the VSWR can be calculated from the following formula [29]:

$$VSWR = \frac{1+|\Gamma|}{1-|\Gamma|} \tag{5.3-2}$$

where Γ is the reflection coefficient defined by

$$\Gamma = \frac{Z_A - Z_0}{Z_A + Z_0} \tag{5.3-3}$$

Figures 5.3-4, 5, and 6 illustrate the resistance and VSWR for LP1, LP2 and LP3. It is worth noting that LP2 provides promising VSWR values from 2460 to 2930 MHz, which belongs to gain bandwidth. The input impedance bandwidth is 17.44%. From this result, it can be implied that the feed lines, also, should follow the angle dependence concept, which was discussed in Section 2.1.1.

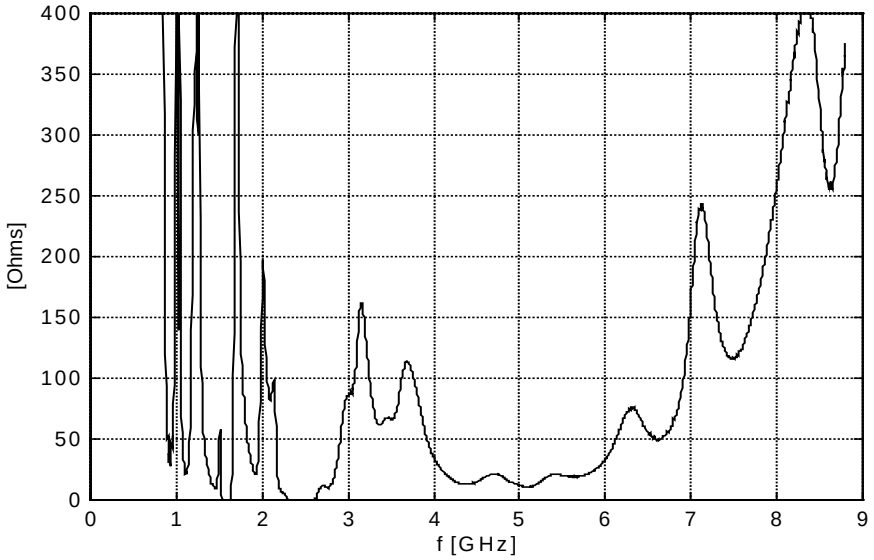

(a)

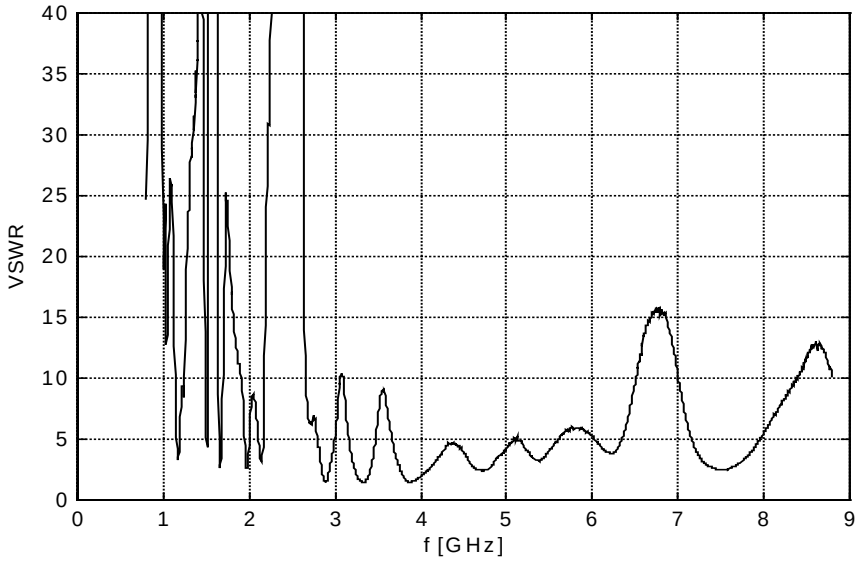

(b)

Figure 5.3-4 (a) Input resistance and (b) VSWR for LP1 with correction of negative resistance and averaging of s_{11} and s_{21}

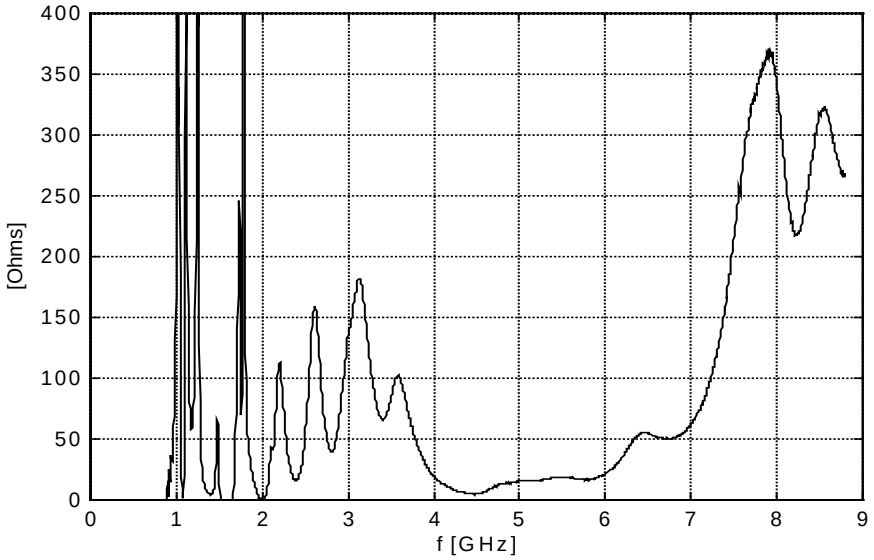

(a)

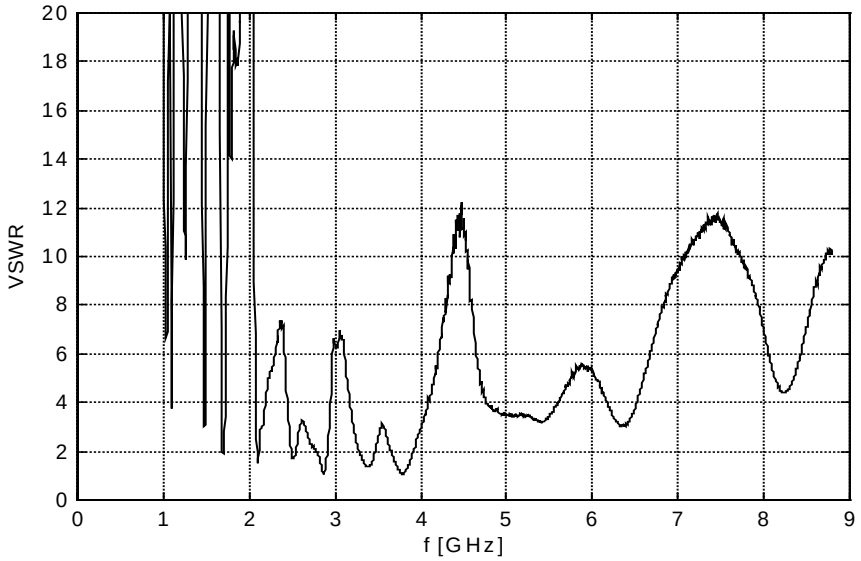

(b)

Figure 5.3-5 (a) Input resistance and (b) VSWR for LP2 with correction of negative resistance and averaging of s_{11} and s_{21}

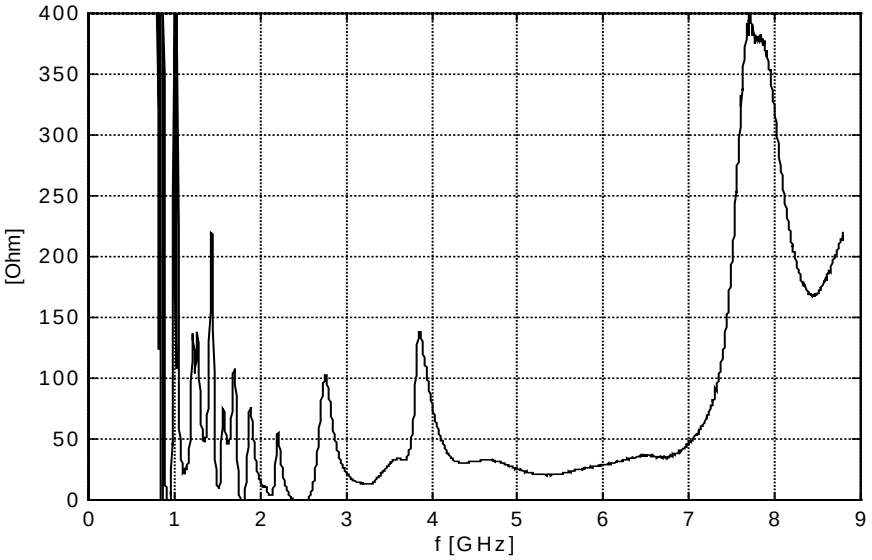

(a)

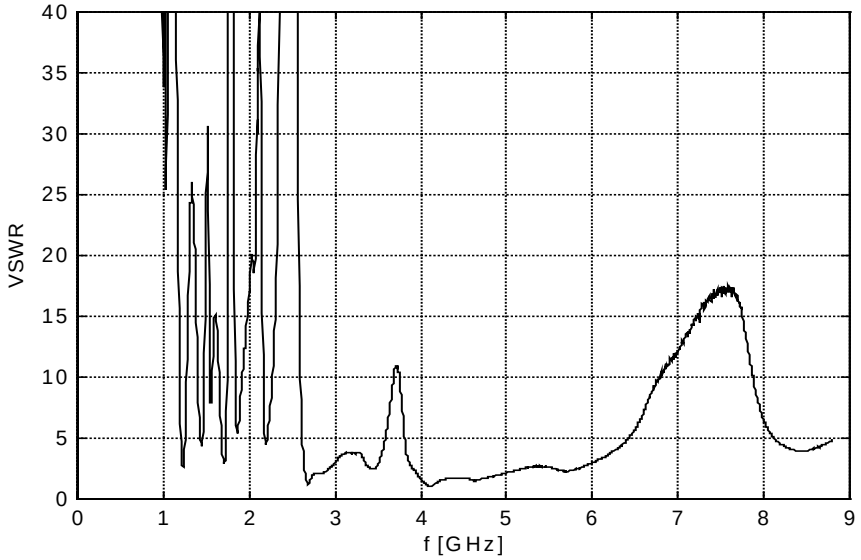

(b)

Figure 5.3-6 (a) Input resistance and (b) VSWR for LP3 with correction of negative resistance and averaging of s_{11} and s_{21}

Chapter 6. Conclusions and Recommendations for Future Work

The log-periodic loop antenna with ground reflector has been presented as a new type of wideband antenna. Compared to existing log-periodic antennas such as LPDA and LPLA without GR, the LPLA with GR provides higher gain and wider gain bandwidth. The numerical analysis of the LPLA with GR was carried out using the ESP program, which is a code based on the piecewise sinusoidal Galerkin's method–a kind of method of moments.

Three prototype LPLAs-GR were built and tested in the Virginia Tech Antenna Laboratory for radiation pattern and input impedance. The important results and conclusions of this investigation are summarized in Section 6.1 and recommendations for future work are presented in Section 6.2.

6.1 Summary of Results

- Compared to the LPDAs, the LPLAs provide the advantage of size reduction in transverse dimensions by a factor of $2/\pi$.
- The radiation characteristics of the loop element in the axial direction are preserved in both LPLAs with and without GR, whose fields in the broadside direction are cancelled due to 180° alternating phase shift between the adjacent loop elements. The G_θ far-field pattern is dominant in the E-plane, while the G_ϕ pattern is dominant in the H-plane. Hence, the LPLAs have linear polarization and unidirectional patterns.
- Improvement of several decibels in gain can be achieved by using ground reflectors in the apex region of LPLAs. For example, the gain (or directivity) of a 6-turn 30° LPLA-GR can be about 12 dBi. Also, the smaller is the subtended angle (α) and the closer to unity is the scale factor (τ), the larger will be the directivity of the antenna.
- The ground reflector seems to increase the bandwidth. For example, the 6-turn 30° LPLA with GR yields 47.62 % gain bandwidth.
- LPLAs with GR are expected to find applications as feeds for reflector antennas, as mobile communication antennas, and as detectors in EMC scattering range.

6.2 Recommendations for Future Work

- **Planar LPLA.** If the spacing factor (σ) goes to zero, the 3-dimensional LPLA becomes 2-dimensional LPLA. This planar LPLA is also an interesting geometry and is suggested to be analyzed, using the subroutine WGEOM in Appendix B or by another method.
- **Optimization of LPLA design.** LPLA with good performance from the point of view of gain, bandwidth, beamwidth, etc., can be designed by optimizing its geometry. If the optimization is made by controlling τ (scale factor), σ (spacing factor), α (subtended angle), zero offset, etc., higher gain, wider polarization or input

impedance bandwidth are likely to be achieved.

- **Input impedance bandwidth.** The input impedance of LPLAs with or without GR needs to be more carefully studied. Ways of increasing input impedance bandwidth need to be explored. For example, terminal resistance can be included for impedance matching.
- **Gain Measurement.** A horn antenna was used as source in the far-field pattern measurements. By using the gain characteristic of the standard gain horn antenna, gain measurement and comparison with simulation results can be made.
- **Parabolic Reflector for satellite communications.** Construction and test of dual reflector antennas using the LPLAs with GR are suggested. These will provide a very high directivity, which is a required characteristic for satellite communications.

REFERENCES

1. V. H. Rumsey, “Frequency Independent Antennas”, IRE national convention record, Part I, pp. 114-118, 1957.

2. D. G. Berry and F. R. Ore, “Log Periodic Monopole Array ”, IRE Int. Conv. Rec., Vol. 9, pp. 76-85, 1961.

3. M. N. Roy and J. S. Chatterjee, “Helical Log-Periodic Array”, IEEE Trans. on Antennas and Propag., Vol. AP-16, pp. 592-593, September 1968.

4. D. F. Kelley and W. L. Stutzman, “Array Antenna Pattern Modeling Methods That Include Mutual Coupling Effects”, IEEE Trans. on Antennas and Propag., Vol. AP-41, pp. 1625-1632, December 1993.

5. A. Safaai-Jazi and J. C. Cardoso, “Radiation Characteristics of a Spherical Helical Antenna”, IEE Proc.-Microw. Antennas Propag., Vol. 143, pp. 7-12, February 1996.

6. E. H. Newman and R. L. Dilsavor, *A User’s Manual for the Electromagnetic Surface Patch Code: ESP Version III*, The Ohio State University, ElectroScience Laboratory, NASA Technical Report No. 716148-19, May 1987.

7. R. H. DuHamel and D. E. IsBell, “Broadband Logarithmically Periodic Antenna Structures”, IRE national convention record, Part I, pp. 119-128, 1957.

8. D. E. IsBell, “Log Periodic Dipole Arrays”, IRE Trans. on Antennas and Propag., Vol. AP-8, pp. 260-267, May 1960.

9. R. L. Carrel, “Analysis and Design of the Log-Periodic Dipole Antenna”, Ph.D. Dissertation, Elec. Eng. Dept., University of Illinois, 1961.

10. C. E. Smith, *Log Periodic Antenna Design Handbook*, 1st Ed., Ohio, 1966.

11. V. H. Rumsey, *Frequency Independent Antennas*, Academic Press, New York, 1996.

12. R. S. Elliott, “A View of Frequency Independent Antennas”, The Microwave Journal, Vol. 5, pp. 61-68, December 1962.

13. Y. Mushiake, *Self-Complementary Antennas*, Springer-Verlag, Berlin, 1996.

14. R. L. Carrel, “The Design of Log-Periodic Dipole Antennas”, IRE Int. Conv. Rec., Part I, pp. 61-75, 1961.

15. W. L. Stutzman and G. A. Thiele, *Antenna Theory and Design*, 2nd Ed., John Wiley and Sons, New York, 1998.

16. D. F. DiFonzo, “Reduced Size Log Periodic Antennas”, The Microwave Journal, Vol. 7, pp. 37-42, December 1964.

17. M. D. Singh, S. P. Kosta and A. Singh, “Log Periodic Antenna with Loop Elements”, International Journal of Electronics, Vol. 32, pp. 81-84, January 1972.

18. B. Rojarayanont and T. Sekiguchi, “A Study on Log-Periodic Loop Antennas”, The Trans. of IECE of Japan, Vol. J60-B, pp. 583-589, August 1977.

19. D. H. Werner, “An Exact Integration Procedure for Vector Potentials of Thin Circular Loop Antennas”, IEEE Trans. on Antennas and Propag., Vol. AP-44, pp. 157-165, February 1996.

20. R. G. Brown, R. A. Sharpe, W. L. Hughes, and R. E. Post, *Lines, Waves, and Antennas*, 2nd Ed., John Wiley and Sons, New York, 1973.

21. H. Jasik and R. C. Johnson, *Antenna Engineering Handbook*, 3rd Ed., McGraw-Hill, New York, p.5-13 1993.

22. S. Ito, N. Inagaki, and T. Sekiguchi, “An Investigation of the Array of Circular-Loop Antennas”, IEEE Trans. on Antennas and Propag., Vol. AP-19, pp. 469-476, July 1971.

23. J. H. Richmond and N. Wang, “Sinusoidal Reaction Formulation for Radiation and Scattering from Conducting Surfaces”, NASA Contractor Report, NASA CR-2398, Washington D. C., June 1974.

24. W. L. Stutzman, *Polarization in Electromagnetic Systems*, Artech House, Boston, MA, 1993.

25. C. L. Bennett and G. F. Ross, “Time-Domain Electromagnetics and Its Applications”, Proceedings of the IEEE, Vol. 66, pp. 299-318, March 1978.

26. R. H. DuHamel and F. R. Ore, “Log Periodic Feeds for Lens and Reflectors”, IRE national convention record, Vol 7, pp. 128-137, 1959.

27. D. E. IsBell, “A Log-Periodic Reflector Feed”, Proceedings of the IRE, Vol. 47, pp.1152-1153, June 1959.

28. W. A. Davis, J. R. Nealy, G. F. Ricciardi, and W. L. Stutzman, ‘Techniques for the Measurement of the Impedance of Wideband Balanced Antennas’, Electromagnetics Seminar, Virginia Tech, February 11, 1999.

29. E. C. Jordan and K. G. Balmain, *Electromagnetic Waves and Radiating Systems*, 2nd Ed., Prentice-Hall, N. J., 1968.

30. The Mathworks Inc., *The Student Edition of MATLAB, Version 4 User’s Guide*, Prentice-Hall, N. J., 1995.

Appendix A. Matlab program for the calculation of far-field patterns

Based on the concept of Section 3.1 and Werner's paper [19], the following programs were coded by using MATLAB ver 4.2 b [30]. These two codes, A.1 and A.2, calculate E_θ pattern in the E-plane and the E_ϕ pattern in the H-plane, respectively.

A.1 slet.m

```
%To get radiation pattern from (106) of Werner
clear;

freq=2.0e9;   %operation frequency
lambda=300e6/freq;
r=100*lambda;   %far-field region
b=0.023873;   %radius of the circular loop antenna

theta=[0.1:0.1:360]*pi/180;
beta=2*pi/lambda;

w=beta*b*sin(theta);

E_theta=-60*pi*i*cot(theta)*sin(pi/2)*exp(-i*beta*r) ...
      .*besselj(1,abs(w))/r;

net = abs(E_theta)/max(abs(E_theta));   %normalized in the linear scale

polarwt(theta,net)   %function to plot the pattern in wanted polar form
```

A.2 slep.m

```
%To get radiation pattern from (106) of Werner
clear;

freq=2.0e9;   %operation frequency
lambda=300e6/freq;
r=100*lambda;   %far-field region
b=0.023873;   %radius of the circular loop antenna

theta=[0.1:0.1:360]*pi/180;
beta=2*pi/lambda;

w=beta*b*sin(theta);

E_theta=-60*pi*i*cot(theta)*sin(pi/2)*exp(-i*beta*r) ...
      .*besselj(1,abs(w))/r;

net = abs(E_theta)/max(abs(E_theta));   %normalized in the linear scale

polarwt(theta,net)   %function to plot the pattern in wanted polar form
```

Appendix B. Subroutine WGEOM for LPLA

The Fortran source code is presented for the ESP subroutine, WGEOM, which was used to generate input data for the geometry of the log-periodic loop antenna as described in Section 3.2 and 4.1. WGEOM should be very useful because it allows the user to change the parameters of the wire structure without having to recompile the program. The ESP User's Manual [6] contains a full explanation of how to define the geometry of a wire antenna with a subroutine and integrate it with the main program.

The three input parameters for the LPLA can be accepted in the subroutine by the following READ statements:

- NLP - Total number of loop elements that the LPLA would have.
- RADI - Data of radius which each element would have in meters. This parameter includes the data of NPL numbers with a space between two radius data. The unit is in meters.
- GAP - Spacing between the two adjacent loops, except that the first datum is the spacing between the apex and the first loop. This parameter also includes the data of

NPL numbers with a space between two radius data. The unit is in meters.

As an example, the input file for the computation of the 10-turn LPLA without ground reflector in Section 3.2 is given below (See [6] for detail).

```
1  2  1  1  1  0  4  6  18  1  0  0
1  1  2  0.0
0  0  2  90.0
0  0  0  0  0  0
0  0  0  0
1000.0  -1.0  0.0034
0
0  0
10
.04699 .05221 .05801 .06446 .07162 .07958 .08842 .09824 .10912 .12129
.001 .059049 .06561 .0729 .081 .09 .1 .111111 .123457 .137174
```

As another example, the input file for the computation of the 7-turn, 45° LPLA with ground reflector in Section 4 is given below.

```
1  2  1  1  1  0  4  6  18  1  0  0
1  1  2  90.0
0  0  2  90.0
0  0  0  0  0  0
0  0  0  0
2250.0  -1.0  0.0005
1
4  0.20  1  3  0
-0.12  -0.12  0.0
 0.12  -0.12  0.0
 0.12   0.12  0.0
-0.12   0.12  0.0
0  0
7
.01213 .01444 .01719 .02046 .02436 .02899 .03452
.032275 .005576 .006638 .007903 .009408 .0112 .013333
```

The WGEOM subroutine for the 7-turn LPLA is listed below.

```
C***********************************************************************
C                    WGEOM Subroutine for Log-Periodic Loop Antenna
C                      Generates input data for the geometry of a LPLA
C
C                      Programmed by Jeong Il  Kim
C***********************************************************************
C
C234567
      SUBROUTINE WGEOM(IA,IB,X,Y,Z,NM,NP,NAT,NSA,NPLA,VGA,BDSK,
     &ZLDA,NWG,VG,ZLD,WV,NFS1,NFS2,NRUN,A)
      DIMENSION IA(1),IB(1),X(1),Y(1),Z(1),RADI(7),GAP(7),ZOFFSET(8),
     &NMC(7), NMCS(8), NTS(7), XS(6), CIF(7), NS(7), NSS(8),
     &NSA(1), NPLA(1), BDSK(1)
      COMPLEX VGA(1), ZLDA(1), VG(1), ZLD(1)
      REAL  PI
C
C
C ******* The Log-Periodic Loop Antenna geometry is now defined *******
C
C  Number of loops of Log-Periodic Antenna
      READ(5,*)NLP
C  The radii for all the loops
      READ(5,*)RADI
C  The spaces between the adjacent two loops
      READ(5,*)GAP
C
      PI = 3.14159265
```

```
C
C  Define coordinates of wire start-points and end-points of segments
C
C  Calculate the distance from zero point (feed point).
          ZOFFSET(0)=0.0
          DO 10 L=1,NLP
             ZOFFSET(L)=ZOFFSET(L-1)+GAP(L)
             print *,ZOFFSET(L)
       10 CONTINUE
C  Calculate the circumferences for all the loops
          DO 20 L=1,NLP
             CIF(L)=2*PI*RADI(L)
       20 CONTINUE
C
C  Calculate the numbers of segments for all the connection feed lines
C  and loops, and Insure that each NMC & NS is an even number.
          print *,'WV=',WV
          NMCS(0)=0
          NSS(0)=0
          DO 50 L=1,NLP
             NMC(L)=GAP(L)*25/WV + 0.99999999
             NMC(L)=2*((NMC(L)+1)/2)
             NMCS(L)=NMCS(L-1)+NMC(L)
             NS(L)=CIF(L)*20/WV + 0.99999999
             NS(L)=2*((NS(L)+1)/2)
             NSS(L)=NSS(L-1)+NS(L)
             print *,nmc(l),ns(l)
       50 CONTINUE
C
C  Total number of wire segments, NM (definition required by ESP)
```

```
      NM = NSS(NLP) + 2*NMCS(NLP) - 2*NLP
C  Total number of wire points, NP (definition required by ESP)
      NP = NSS(NLP)-NLP + 2*(NMCS(NLP)-NLP) + 1
      print *,'NM=',nm,'  NP=',np
C
C  Apex point
      X(1) = 0.0
      Y(1) = 0.0
      Z(1) = 0.00000001
C
C  Define the first bottom circular loop
      DO 200 K=1,NMC(1)
        X(1+K)=RADI(1)*COS(2*PI/NS(1))*K/NMC(1)
        Y(1+K)=RADI(1)*SIN(2*PI/NS(1))*K/NMC(1)
        Z(1+K)=ZOFFSET(1)*K/NMC(1)
        IA(K)=K
        IB(K)=K+1
  200 CONTINUE
C
C  Define the first feed lines
      DO 250 K=1,NMC(1)
        X(NMC(1)-2+NS(1)+K)=RADI(1)*COS(2*PI/NS(1))*(NMC(1)+1-K)
     &                      /NMC(1)
        Y(NMC(1)-2+NS(1)+K)=-RADI(1)*SIN(2*PI/NS(1))*(NMC(1)+1-K)
     &                      /NMC(1)
        Z(NMC(1)-2+NS(1)+K)=ZOFFSET(1)*(NMC(1)+1-K)/NMC(1)
        IA(NMC(1)-2+NS(1)+K)=NMC(1)-2+NS(1)+K
        IF(K.EQ.NMC(1))GO TO 260
        IB(NMC(1)-2+NS(1)+K)=NMC(1)-1+NS(1)+K
  250 CONTINUE
```

```
  260   IB(NMC(1)-2+NS(1)+NMC(1))=1
C
C  Define the feed lines from the first loop to the last loop element.
        NTS(0)=2
        DO 300 J=1,NLP-1
           NTS(J)=NS(J)-1+2*(NMC(J)-1)+NTS(J-1)
C
           DO 400 K=1,NMC(J+1)
              X(NTS(J)+K-1)=RADI(J)*COS(2*PI/NS(J))+( RADI(J+1)*
     &        COS(2*PI/NS(J+1))-RADI(J)*COS(2*PI/NS(J)) )*K/NMC(J+1)
              Y(NTS(J)+K-1)=-RADI(J)*SIN(2*PI/NS(J))+( RADI(J+1)*
     &        SIN(2*PI/NS(J+1))+RADI(J)*SIN(2*PI/NS(J)) )*K/NMC(J+1)
              Z(NTS(J)+K-1)=ZOFFSET(J)+GAP(J+1)*K/NMC(J+1)
  400      CONTINUE
           IA(NTS(J)+J-1)=NTS(J)-NMC(J)
           DO 410 K=1,NMC(J+1)-1
              IB(NTS(J)+K-1+J-1)=NTS(J)+K-1
              IA(NTS(J)+K+J-1)=NTS(J)+K-1
  410      CONTINUE
           IB(NTS(J)+NMC(J+1)-1+J-1)=NTS(J)+NMC(J+1)-1
C
        XS(J)=X(NTS(J)+NMC(J+1)/2-1)+5*A
        DO 430 L=1,NMC(J+1)/2+1
           IF( XS(J).GT.RADI(J+1)*COS(2*PI/NS(J+1)) ) THEN
              X(NTS(J)+NS(J+1)+NMC(J+1)-4+L)=RADI(J+1)*COS(2*PI/NS(J+1))+
     &                ( XS(J)-RADI(J+1)*COS(2*PI/NS(J+1)) )*(L-1)/(NMC(J+1)/2)
           ELSEIF( XS(J).EQ.RADI(J+1)*COS(2*PI/NS(J+1)) ) THEN
              X(NTS(J)+NS(J+1)+NMC(J+1)-4+L)=RADI(J+1)*COS(2*PI/NS(J+1))
           ELSE
              X(NTS(J)+NS(J+1)+NMC(J+1)-4+L)=RADI(J+1)*COS(2*PI/NS(J+1))-
```

```
     &                    ( RADI(J+1)*COS(2*PI/NS(J+1))-XS(J) )*(L-1)/(NMC(J+1)/2)
          ENDIF
  430  CONTINUE
       IF(NMC(J+1).EQ.2)GO TO 445
       DO 440 L=NMC(J+1)/2+2,NMC(J+1)
          X(NTS(J)+NS(J+1)+NMC(J+1)-4+L)=XS(J)-( XS(J)-RADI(J)*
     &                          COS(2*PI/NS(J)) )*(L-(NMC(J+1)/2+1))/(NMC(J+1)/2)
  440  CONTINUE
  445  DO 450 L=1,NMC(J+1)
          Y(NTS(J)+NS(J+1)+NMC(J+1)-4+L)=-RADI(J+1)*SIN(2*PI/NS(J+1))+
     &                ( RADI(J+1)*SIN(2*PI/NS(J+1))+RADI(J)*SIN(2*PI/NS(J)) )*
     &                (L-1)/NMC(J+1)
           Z(NTS(J)+NS(J+1)+NMC(J+1)-4+L)=ZOFFSET(J+1)-
     &                 GAP(J+1)*(L-1)/NMC(J+1)
  450  CONTINUE
       DO 460 L=1,NMC(J+1)-1
          IA(NTS(J)+NS(J+1)+NMC(J+1)-3+L+J-1)=NTS(J)+NS(J+1)+
     &                                        NMC(J+1)-3+L-1
          IB(NTS(J)+NS(J+1)+NMC(J+1)-3+L+J-1)=NTS(J)+NS(J+1)+
     &                                        NMC(J+1)-3+L
  460  CONTINUE
       IA(NTS(J)+NS(J+1)+2*NMC(J+1)-3+J-1)=NTS(J)+NS(J+1)+
     &                                      2*NMC(J+1)-4
       IB(NTS(J)+NS(J+1)+2*NMC(J+1)-3+J-1)=NTS(J)-NS(J)-(NMC(J)-2)
C
  300  CONTINUE
C
C  Define the second loop element to the last loop element.
       DO 500 J=1,NLP
          DO 600 M=1,NS(J)-3
```

```
            PHI=2*PI*(M+1)/NS(J)
            X(NTS(J-1)+NMC(J)-1+M)=RADI(J)*COS(PHI)
            Y(NTS(J-1)+NMC(J)-1+M)=RADI(J)*SIN(PHI)
            Z(NTS(J-1)+NMC(J)-1+M)=ZOFFSET(J)
            IA(NTS(J-1)+NMC(J)-2+M+J-1)=NTS(J-1)+NMC(J)-2+M
            IB(NTS(J-1)+NMC(J)-2+M+J-1)=NTS(J-1)+NMC(J)-1+M
600       CONTINUE
          IA(NTS(J-1)+NMC(J)-4+NS(J)+J-1)=NTS(J-1)+NS(J)+NMC(J)-4
          IB(NTS(J-1)+NMC(J)-4+NS(J)+J-1)=NTS(J-1)+NS(J)+NMC(J)-3
500   CONTINUE
C
C  Complex voltage generator, VG
          VG(1) = (1.0,0.0)
C  Outer disk radius of disk monopole (should be about .2lambda), BDSK
          BDSK(1) = 0.2*WV
C  Total number of wire attachment points, NAT (LPLA is not attached to the square plate
making the Ground Reflector - definition required by ESP)
          NAT = 0
C  No mutual coupling computations
          NFS1=0
          NFS2=0
C
          RETURN
          END
```

Appendix C. Numerically-Calculated Far-Field Patterns of LPLAs with GR

The far-field radiation patterns are plotted for LPLAs-GR with N=6, $\alpha=30^\circ$, and N=7, $\alpha=45^\circ$ over a frequency range from 1.55 GHz to 4.4 GHz; see Section 4.3. These ESP-calculated patterns may be compared with measured patterns in Appendix E with the help of Tables E-1, 2, and 3. Since G_θ patterns are dominant in the E-plane and G_ϕ patterns in the H-plane, most figures show the dominant patterns. However, a few of non-dominant patterns are included. The gain of each component is defined in (4.3.1-1) and (4.3.1-2) and is related to the electric field component, as mentioned in Section 4.3.2.

Figure C-1 shows calculated patterns for LP1 at 2001 MHz in the E- and H-planes. It is noticed that the G_θ and G_ϕ patterns of Figures C-1 (a) and (d) are dominant in the E- and H-planes, respectively, while the patterns of Figures C-1 (b) and (c) are very small. The rest of calculated patterns are presented in the order of frequency increase in one principal plane per one page. The reason for choice of frequencies such as 2001 MHz, 2301 MHz, 2601 MHz, etc. is that the source generator in the measurement system has a discontinuity at 2000 MHz.

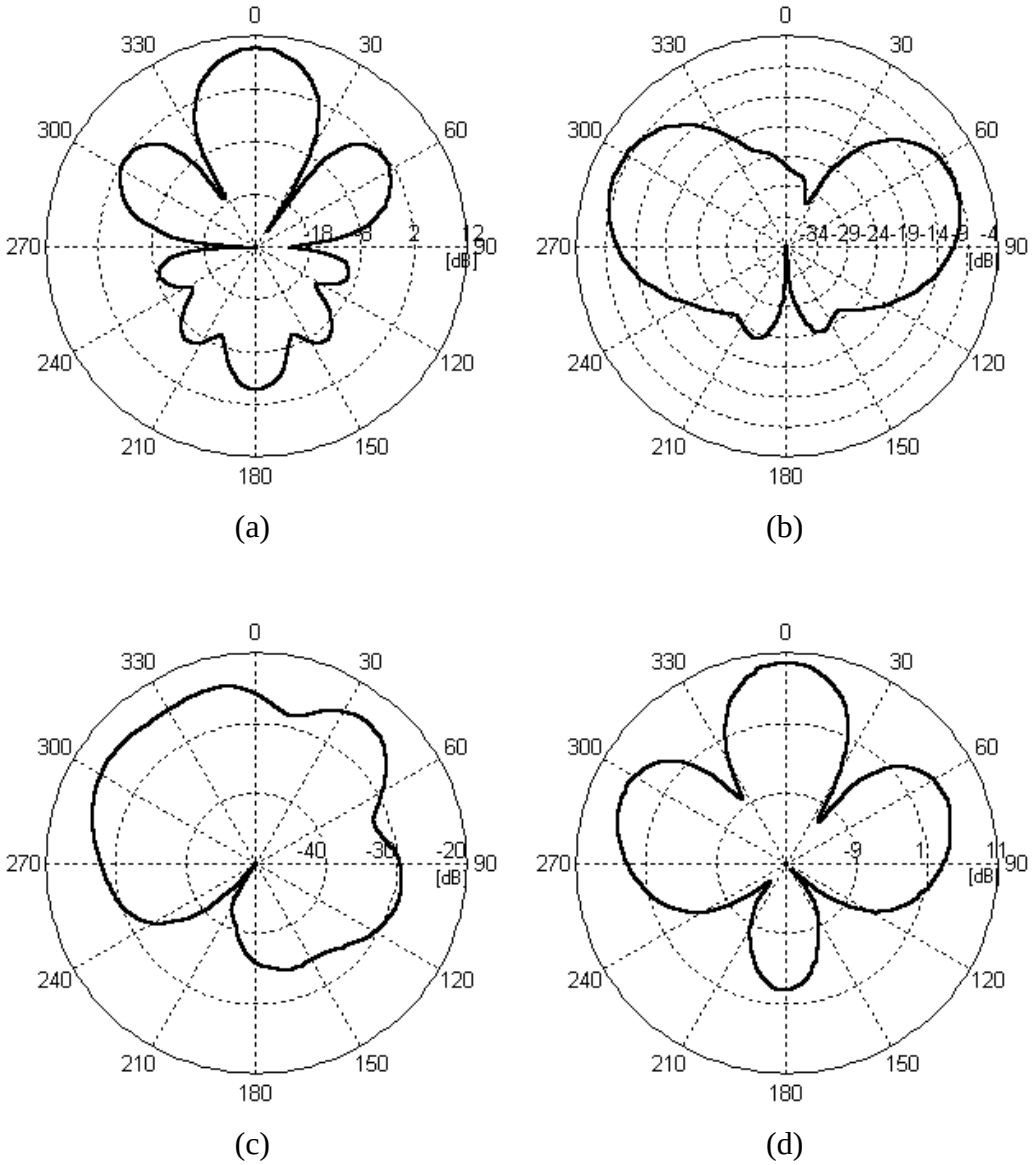

(a) (b)

(c) (d)

Figure C-1 Calculated patterns for LP1 at 2001 MHz : (a) G_θ, (b) G_ϕ in the E-plane
(c) G_θ, (d) G_ϕ in the H-plane

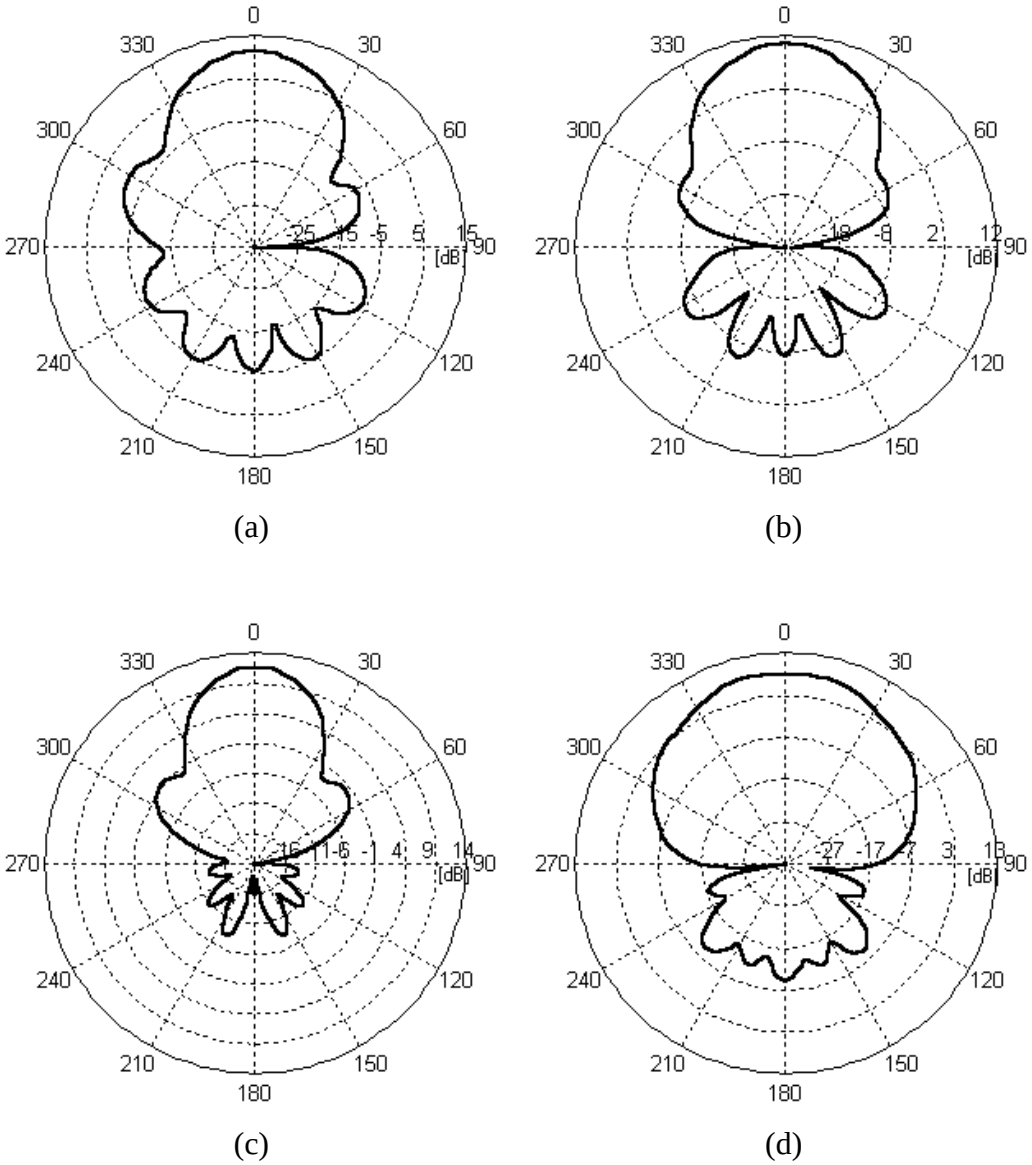

Figure C-2 Calculated G_θ patterns for LP1 in the E-plane at (a) 2601 MHz, (b) 2901 MHz, (c) 3201 MHz, and (d) 3501 MHz

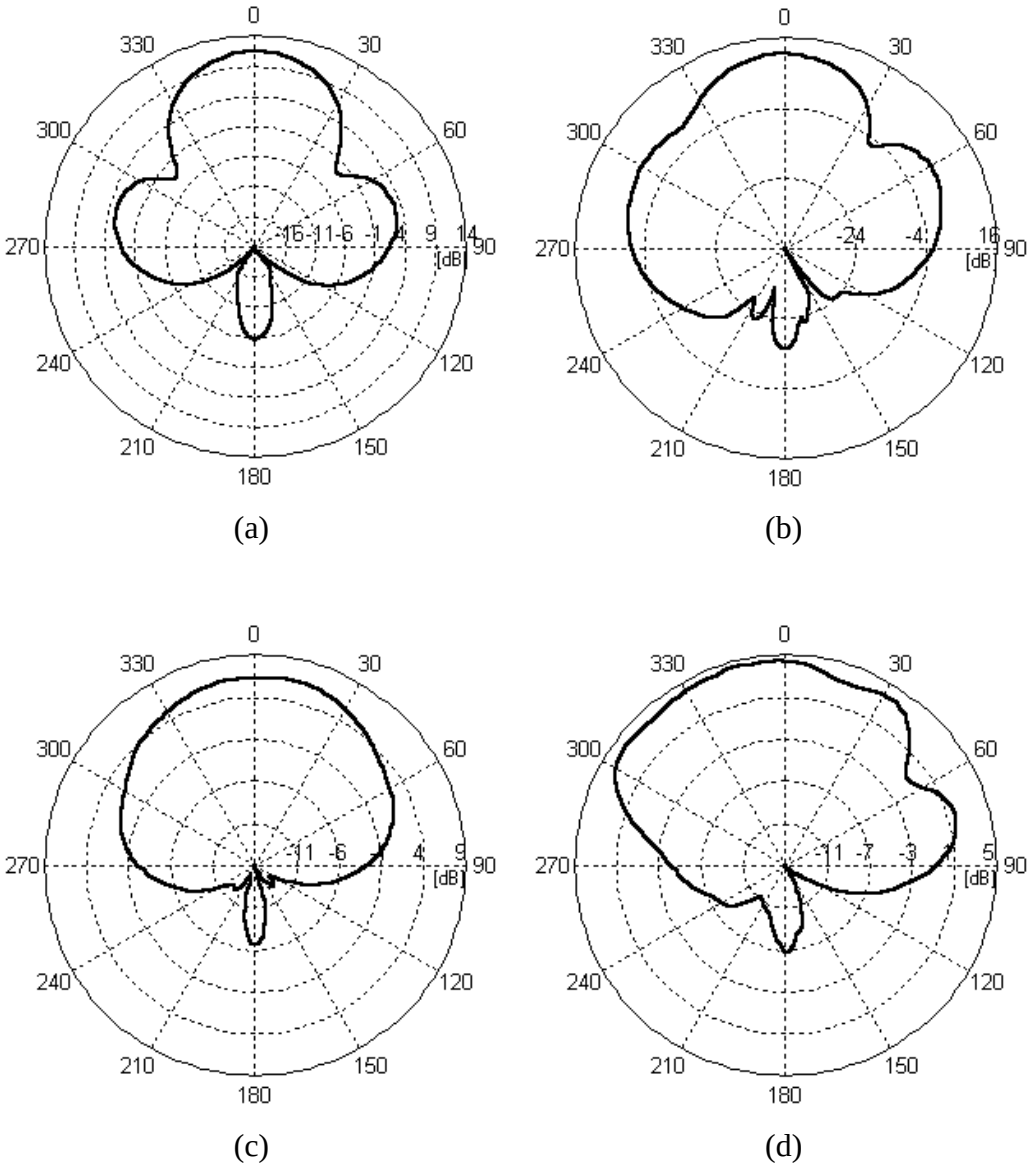

(a) (b)

(c) (d)

Figure C-3 Calculated G_ϕ patterns for LP1 in the H-plane at (a) 2601 MHz, (b) 3201 MHz, (c) 3801 MHz, and (d) 4401 MHz

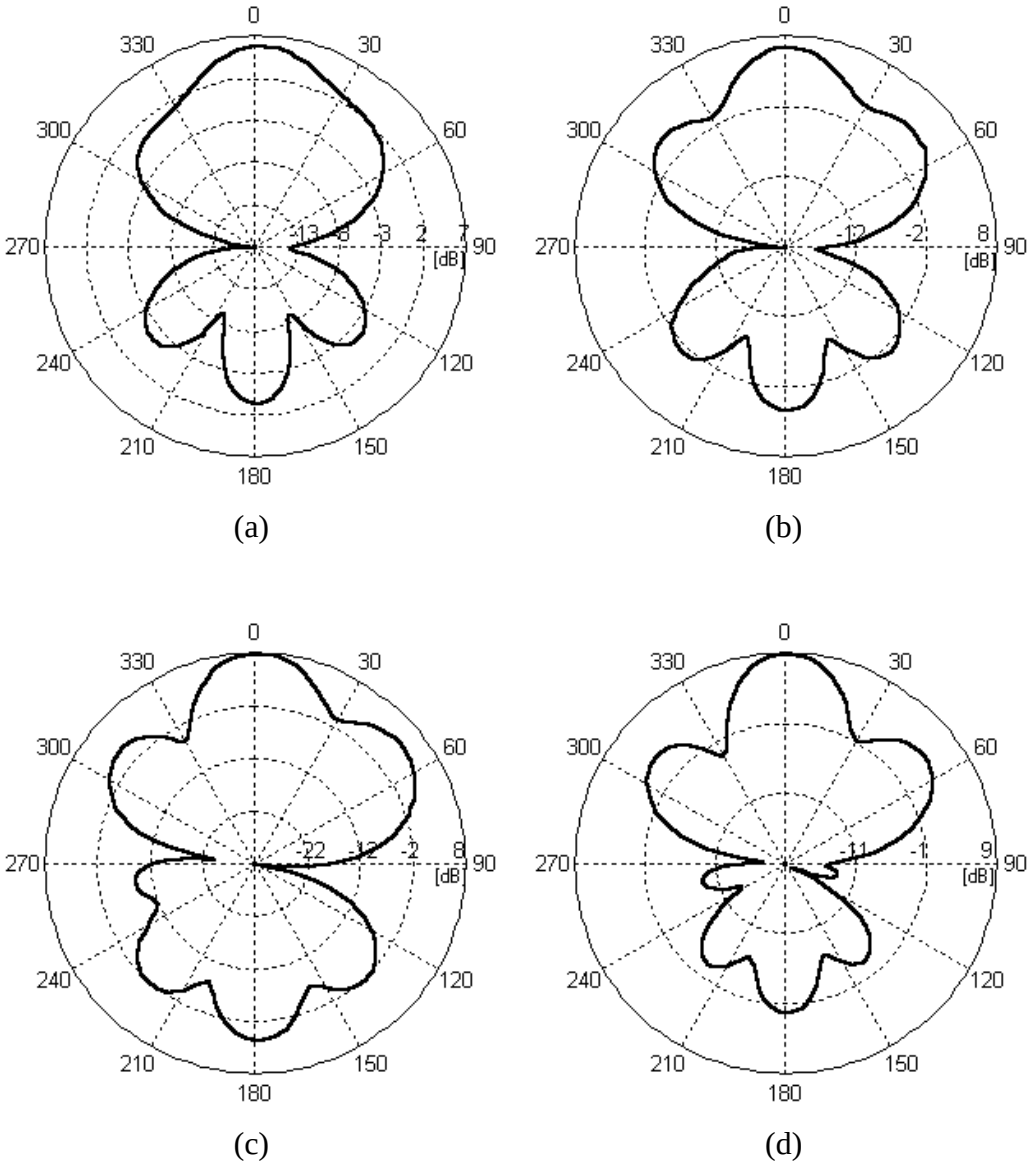

Figure C-4 Calculated G_θ patterns for LP3 in the E-plane at (a) 1.55 GHz, (b) 1.65 GHz, (c) 1.75 GHz, and (d) 1.85 GHz

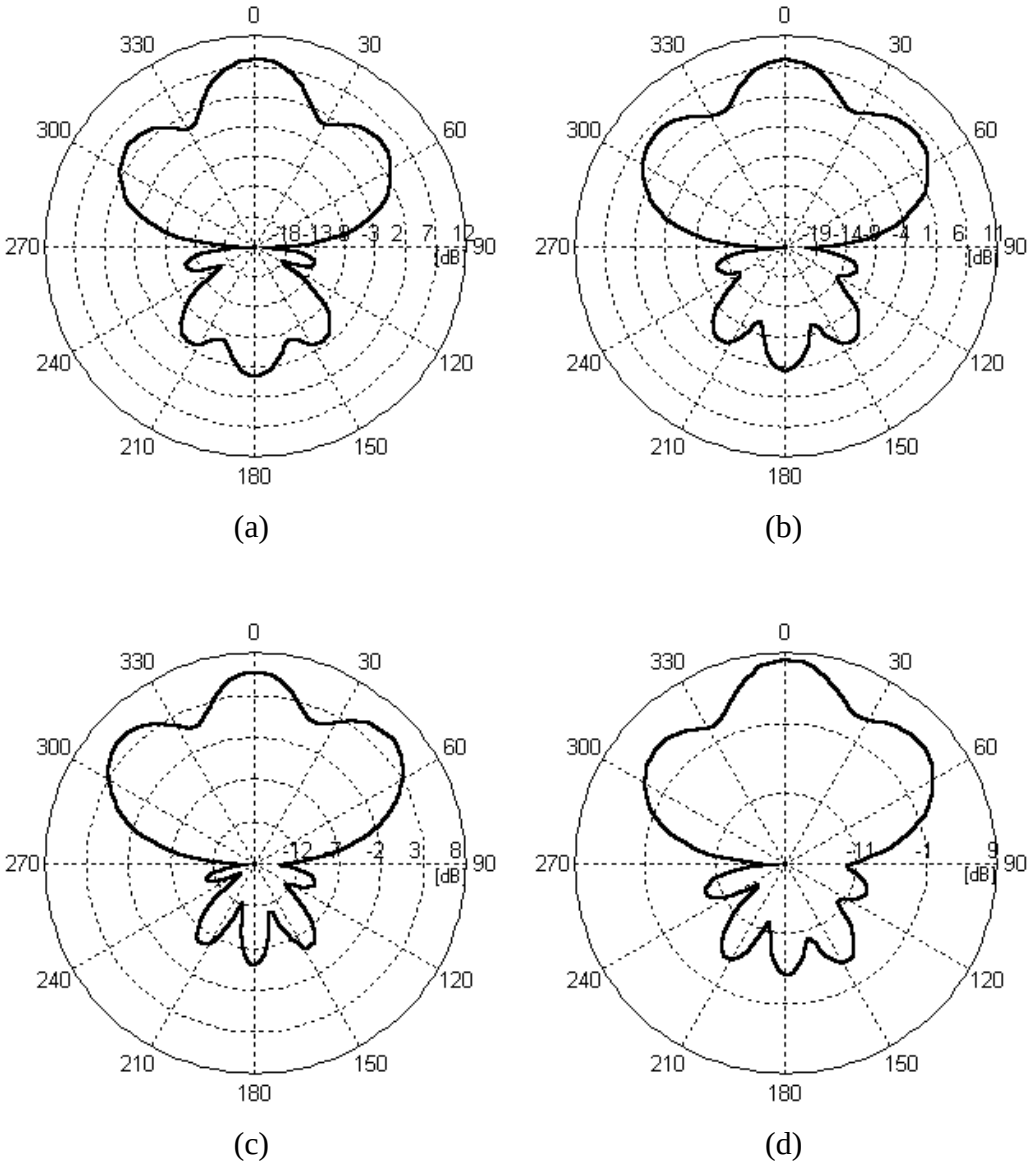

Figure C-5 Calculated G_θ patterns for LP3 in the E-plane at (a) 1.95 GHz, (b) 2.05 GHz, (c) 2.15 GHz, and (d) 2.25 GHz

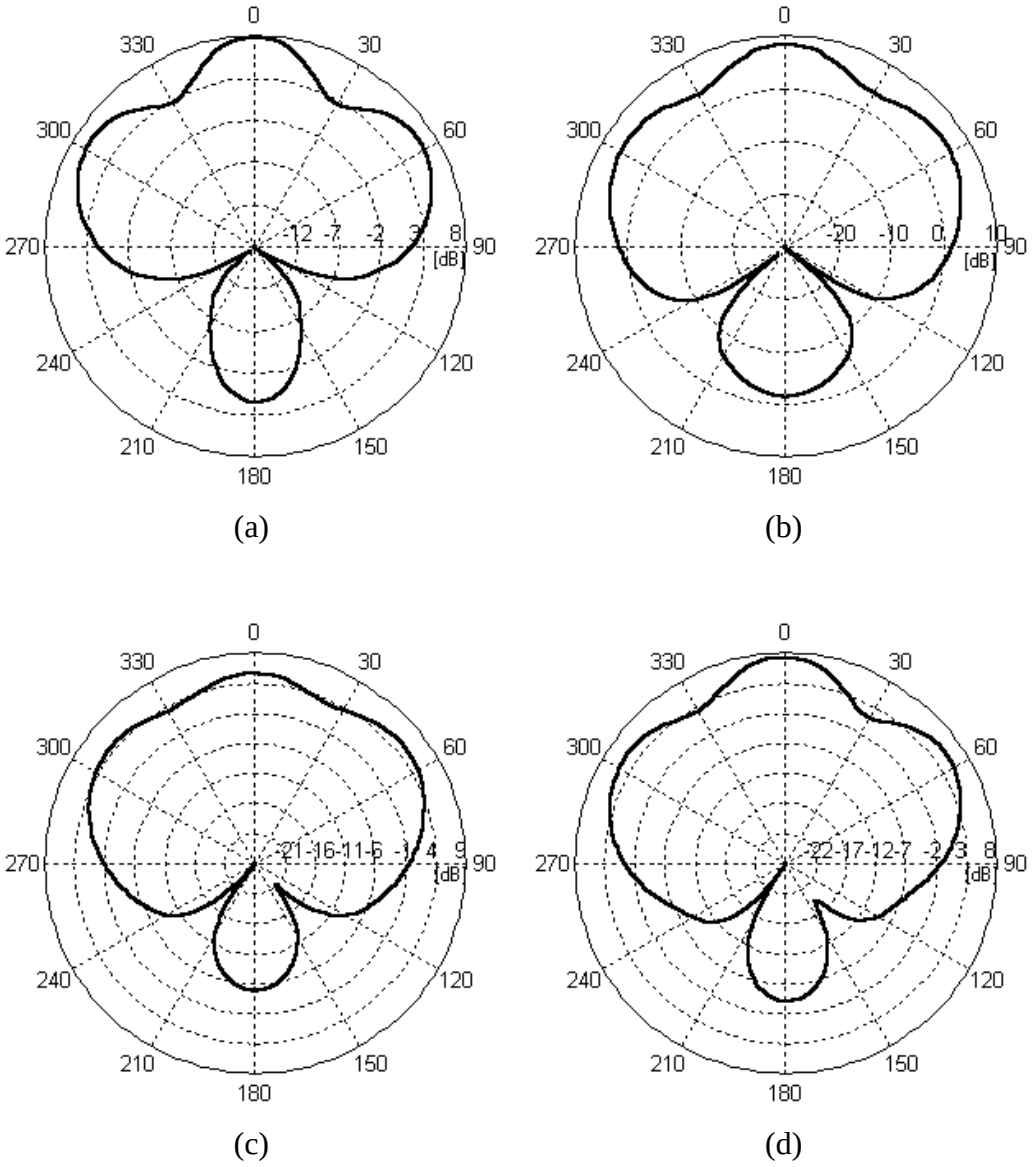

(a) (b)

(c) (d)

Figure C-6 Calculated G_ϕ patterns for LP3 in the H-plane at (a) 1.75 GHz, (b) 1.95 GHz, (c) 2.15 GHz, and (d) 2.35 GHz

Appendix D. Effect of Number of Segments on Radiation Properties Predicted from ESP

In Chapter 4, ESP was used for numerical analysis of LPLAs-GR. It has been reported that ESP converges rapidly for a dipole input impedance [15]. But it does not seem to work for more complex geometries like the LPLAs-GR. Figure 4.3.4-1 illustrates the effect of number of segments on the input impedance.

On the other hand, the ESP provides accurate results for such radiation properties as gain and far-field pattern even with different number of segments. Figure D-1 illustrates gain variations when about 12 segments and 28 segments per wavelength are used for LPLA-GR with N=6, $\alpha=30^{\circ}$. Figures D-2 (a), (b), (c), and (d) show the far-field patterns by using about 12 segments per wavelength. These patterns agree well with Figures C-1 (d), C-3 (a), C-3 (b), and C-3 (c), which were obtained using about 28 segments per wavelength.

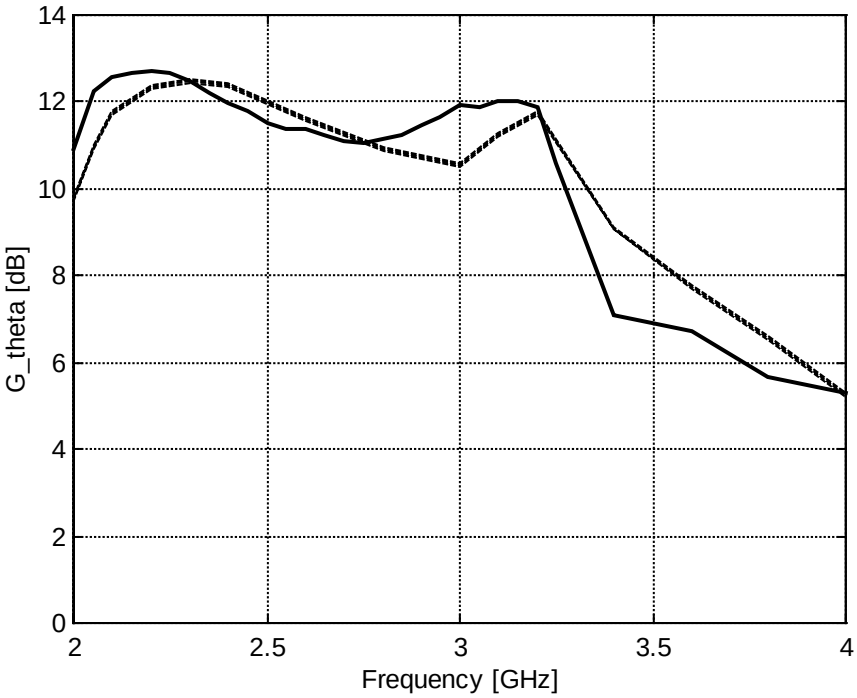

Figure D-1 Gain variations when about 12 segments (solid line) and 28 segments (dashed line) per wavelength are used for LPLA-GR with N=6, $\alpha=30^{\circ}$

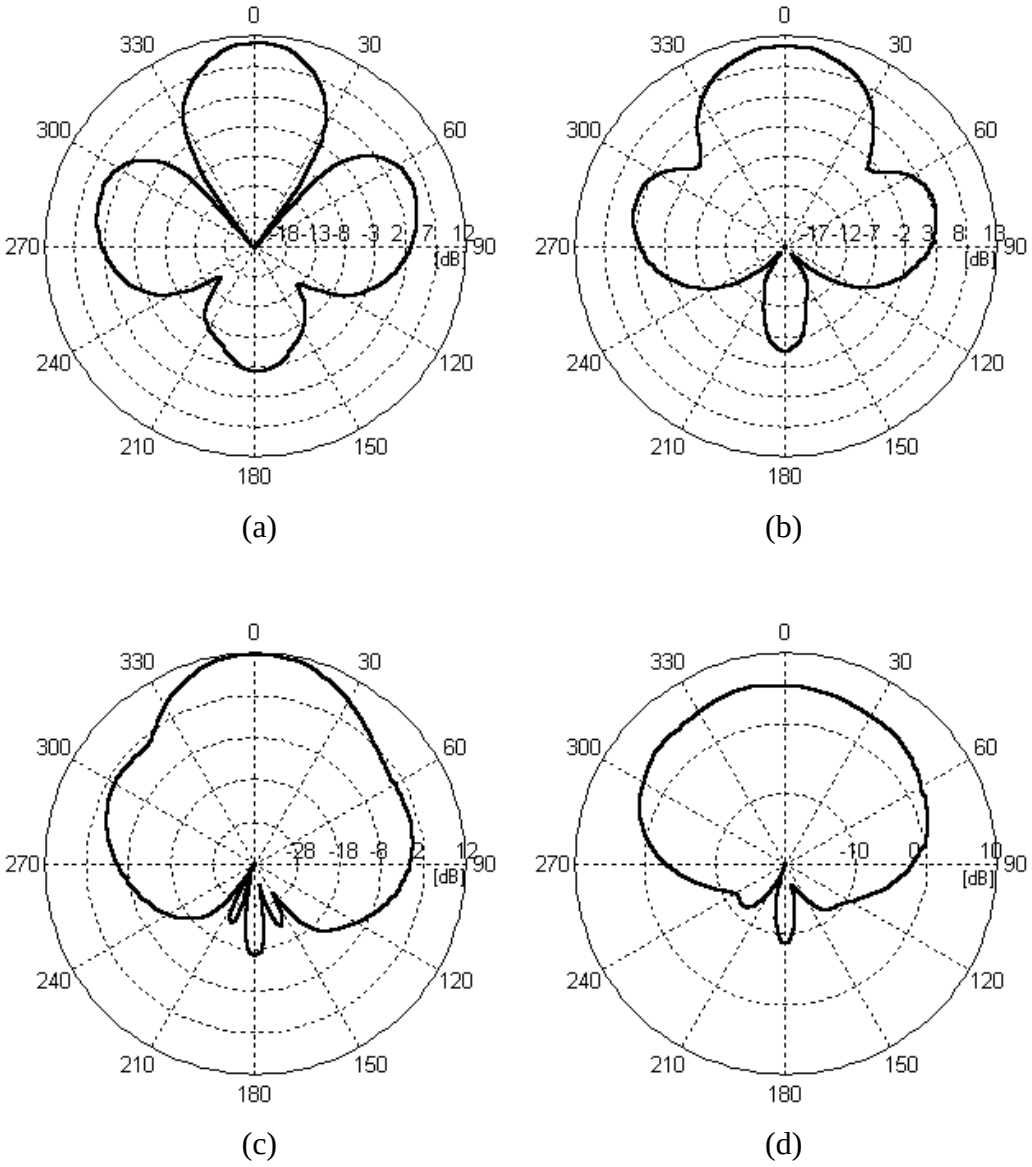

Figures D-2 G_ϕ far-field patterns in the H-plane by using about 12 segments per wavelength at (a) 2001 MHz, (b) 2601 MHz, (c) 3201 MHz, and (d) 3801 MHz

Appendix E. Measured Far-Field Patterns of LPLAs with GR

The measured far-field radiation patterns are presented for LPLAs-GR with N=6, α =30° (LP1 and LP2), and N=7, α=45° (LP3) over a frequency range from 1.55 GHz to 4.4 GHz. Since G_θ patterns are dominant in the E-plane and G_ϕ patterns in the H-plane, most figures show the dominant patterns in each plane. However, a few of non-dominant patterns are included. The normalized magnitudes of both components are plotted in the E-, H-, or 45°-plane in dB scale.

These measured patterns may be compared with numerically-calculated patterns given in Appendix C with the help of Tables E-1, 2, and 3, where C and E are for Figure C and Figure E, respectively. Actually, LP2 antenna was not simulated, but measured. The geometry of the LP2, however, is nearly identical to that of LP1 except the feed line arrangement as mentioned in Section 5.1. Therefore, the calculated patterns for LP1 can be compared with the measured patterns of LP2. The overall agreement between the measured and calculated patterns is very good.

Table 5.2-1 For comparison of simulated and measured patterns for the LP1 antenna

	E plane		45° plane		H plane	
	G_θ	G_ϕ	G_θ	G_ϕ	G_θ	G_ϕ
2001 MHz	C-1 (a), E-1 (a)	C-1 (b), E-1 (b)	Fig. 4.3.3-1 (a), E-6 (a)	Fig. 4.3.3-1 (b), E-6 (b)	C-1 (c), E-1 (c)	C-1 (d), E-1 (d)
2301 MHz	Fig. 4.3.2-1(a), Fig. 5.2-2 (a)	Fig. 4.3. 2-1 (b)				
2601 MHz	C-2 (a), E-2 (a)	E-3 (a)			E-5 (a)	C-3 (a), E-4 (a)
2901 MHz	C-2 (b), E-2 (b)					
3201 MHz	C-2 (c), E-2 (c)	E-3 (b)			E-5 (b)	C-3 (b), E-4 (b)
3501 MHz	C-2 (d), E-2 (d)					
3801 MHz						C-3 (c), E-4 (c)
4401 MHz			E-6 (c)	E-6 (d)		C-3 (d)

Table 5.2-2 For comparison of simulated and measured patterns for the LP2 antenna

	E plane		H plane	
	G_θ	G_ϕ	G_θ	G_ϕ
2001 MHz	C-1 (a), E-7 (a)	C-1 (b), E-7 (b)	C-1 (c), E-7 (c)	C-1 (d), E-7 (d)
2601 MHz	C-2 (a), E-8 (a)	E-8 (b)	E-9 (a)	C-3 (a), E-9 (b)
3201 MHz	C-2 (c), E-8 (c)	E-8 (d)	E-9 (c)	C-3 (b), E-9 (d)

Table 5.2-3 For comparison of simulated and measured patterns for the LP3 antenna

	E plane		H plane	
	G_θ	G_ϕ	G_θ	G_ϕ
1.55 GHz	C-4 (a)			
1.65 GHz	C-4 (b), E-10 (a)			
1.75 GHz	C-4 (c), E-10 (b)	E-12 (a)	E-14 (a)	C-6 (a), E-13 (a)
1.85 GHz	C-4 (d), E-10 (c)	E-12 (b)		
1.95 GHz	C-5 (a), E-10 (d)	E-12 (c)	E-14 (b)	C-6 (b), E-13 (b)
2.05 GHz	C-5 (b), E-11 (a)	E-12 (d)		
2.15 GHz	C-5 (c), E-11 (b)		E-14 (c)	C-6 (c), E-13 (c)
2.25 GHz	C-5 (d)			
2.35 GHz			E-14 (d)	C-6 (d), E-13 (d)

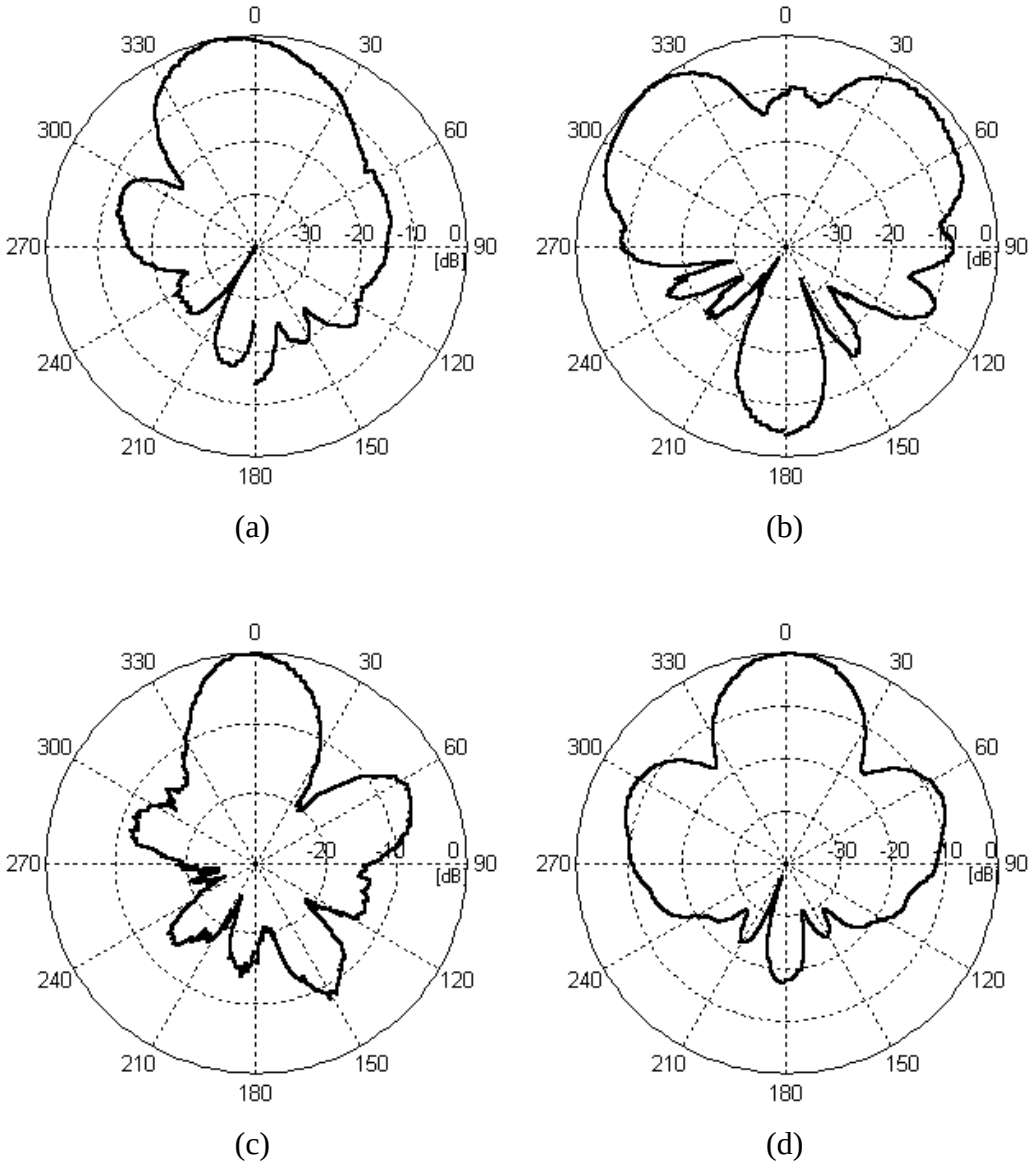

Figure E-1 Measured patterns for LP1 at 2001 MHz : (a) G_θ, (b) G_ϕ in the E-plane (c) G_θ, (d) G_ϕ in the H-plane

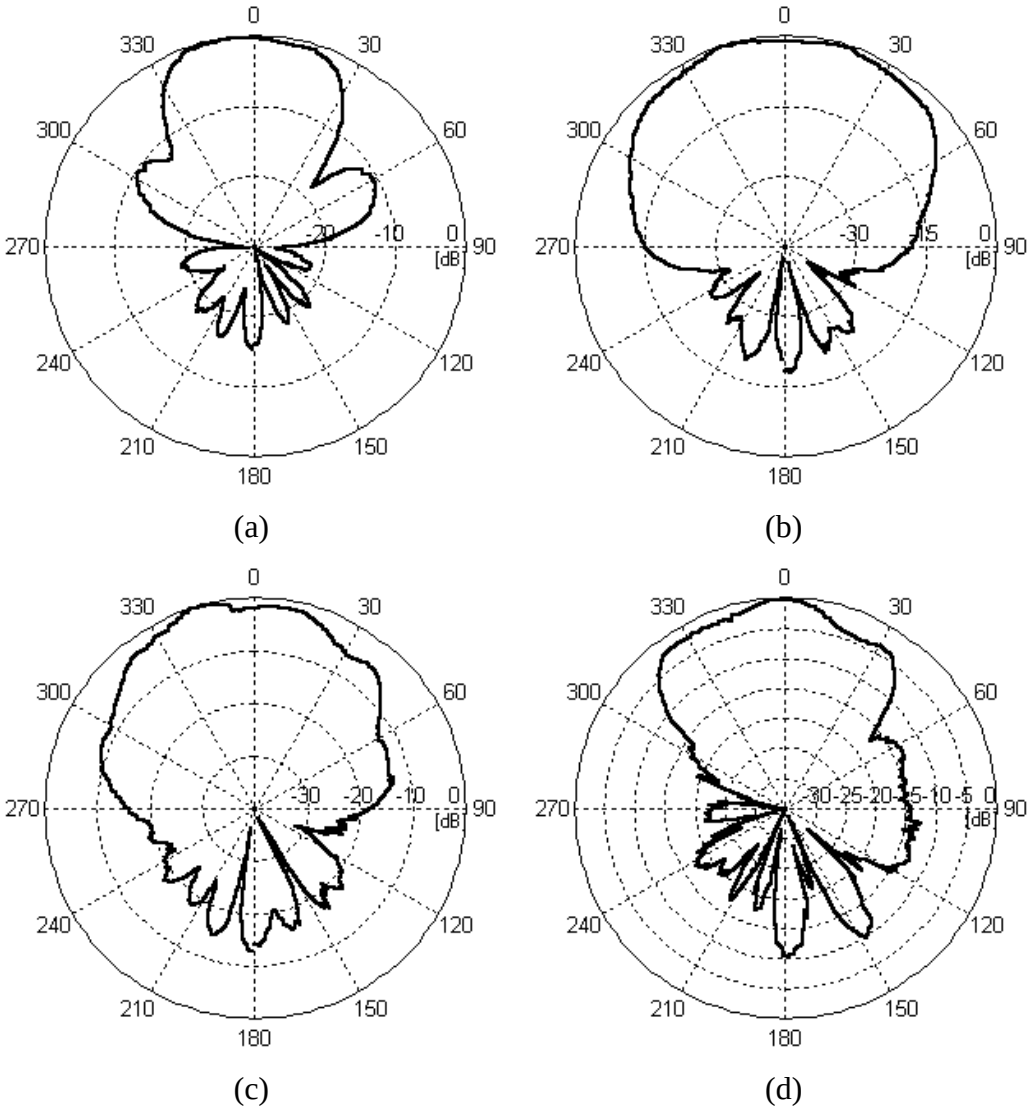

Figure E-2 Measured G_θ patterns for LP1 in the E-plane at (a) 2601 MHz, (b) 2901 MHz, (c) 3201 MHz, and (d) 3501 MHz

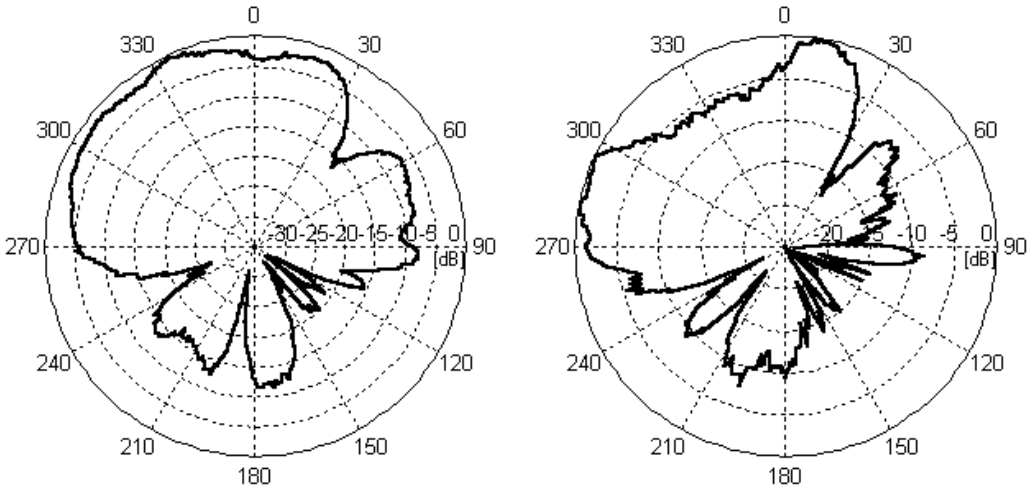

(a) (b)

Figure E-3 Measured G_ϕ patterns for LP1 in the E-plane at (a) 2601 MHz, and (b) 3201 MHz

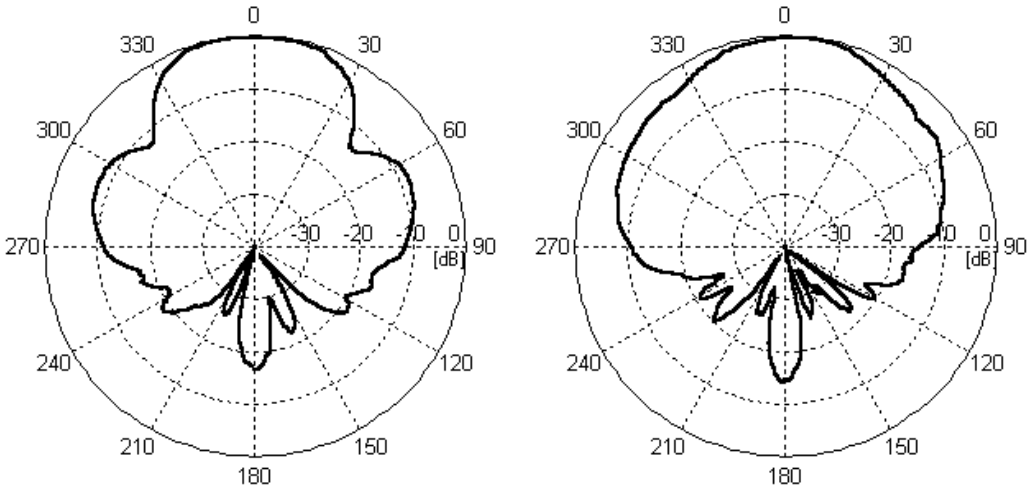

(a) (b)

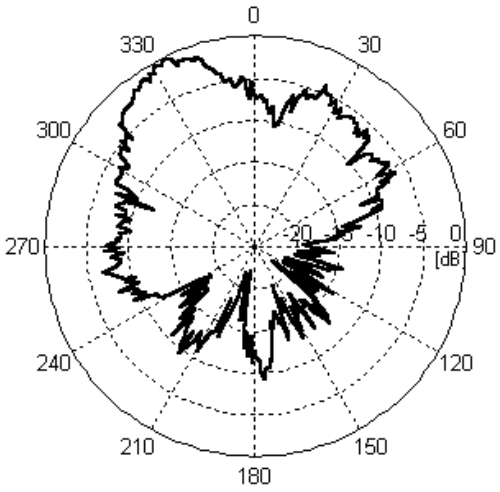

(c)

Figure E-4 Measured G_ϕ patterns for LP1 in the H-plane at (a) 2601 MHz, (b) 3201 MHz, and (c) 3801 MHz

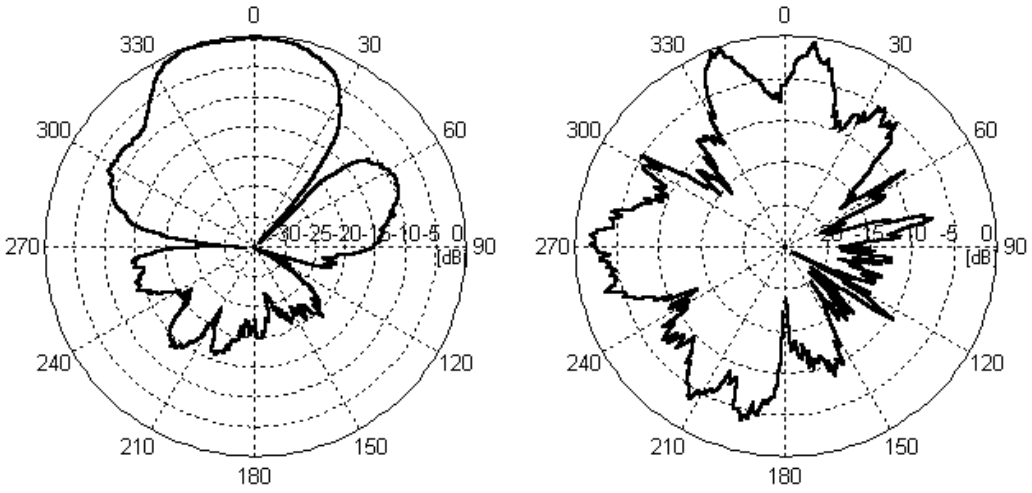

(a) (b)

Figure E-5 Measured G_θ patterns for LP1 in the E-plane at (a) 2601 MHz, and (b) 3201 MHz

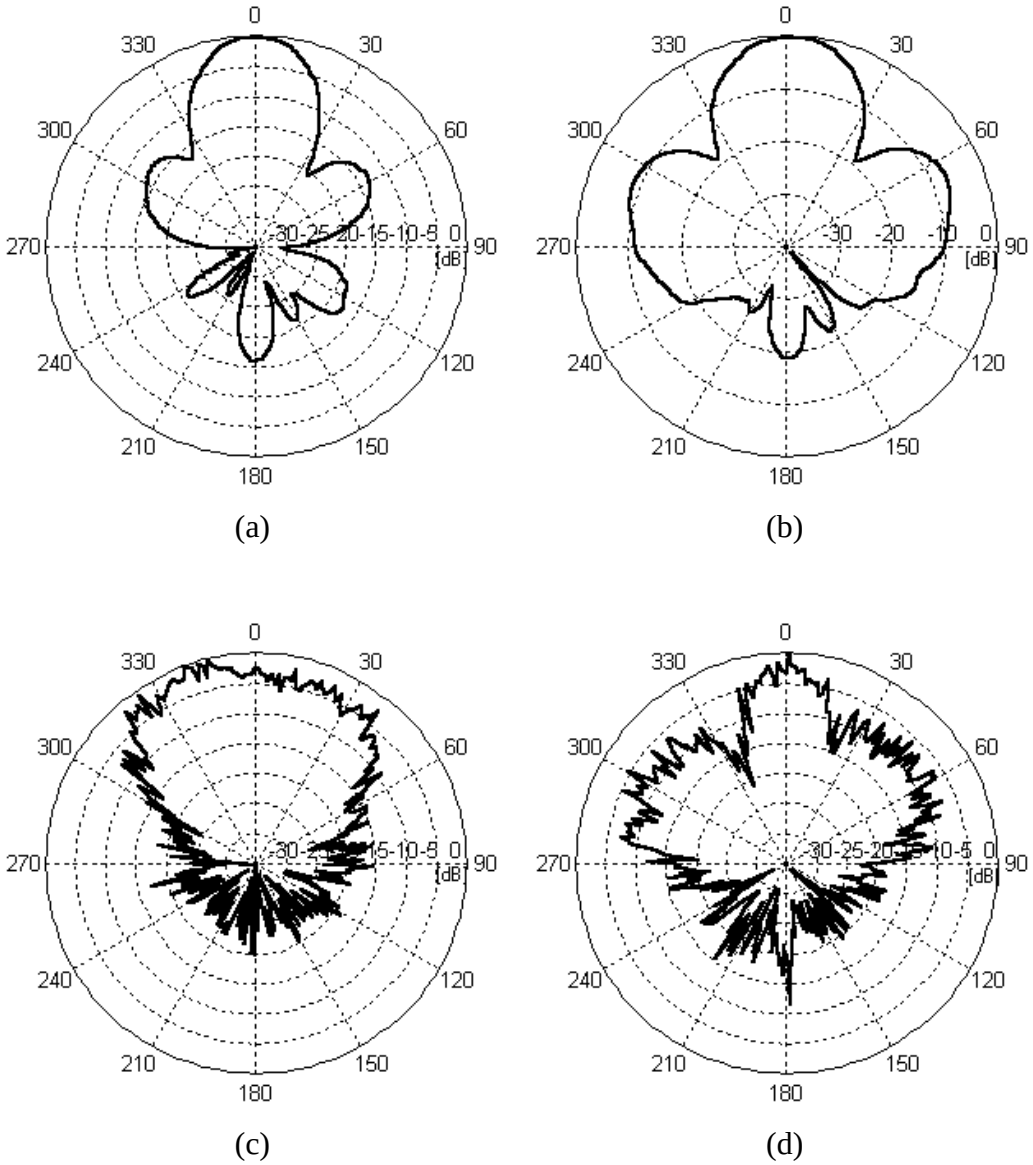

Figure E-6 Measured patterns for LP1 in the 45°-plane at 2001 MHz : (a) G_θ, (b) G_ϕ and at 4401 MHz : (c) G_θ, (d) G_ϕ

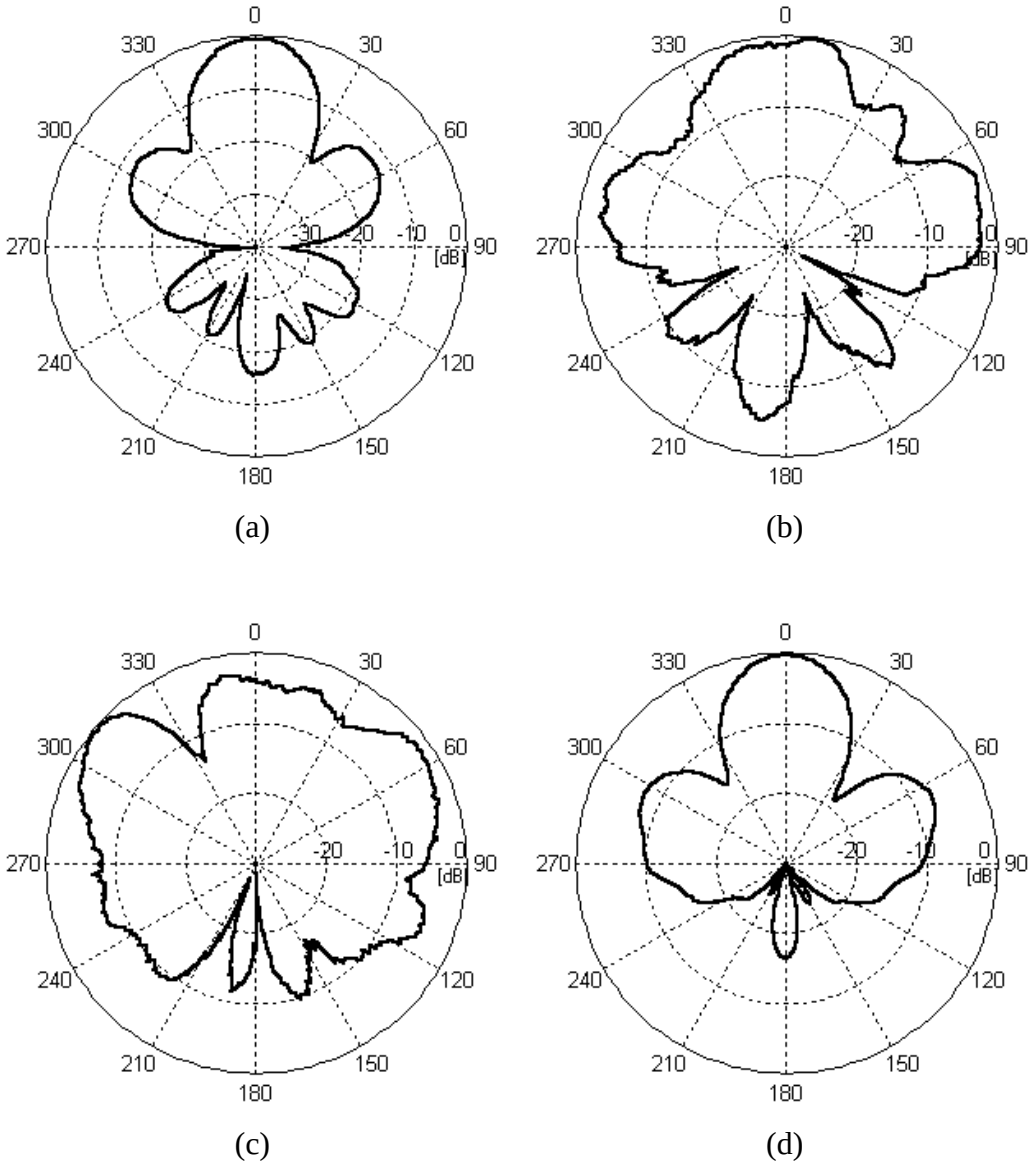

Figure E-7 Measured patterns for LP2 at 2001 MHz : (a) G_θ, (b) G_ϕ in the E-plane
(c) G_θ, (d) G_ϕ in the H-plane

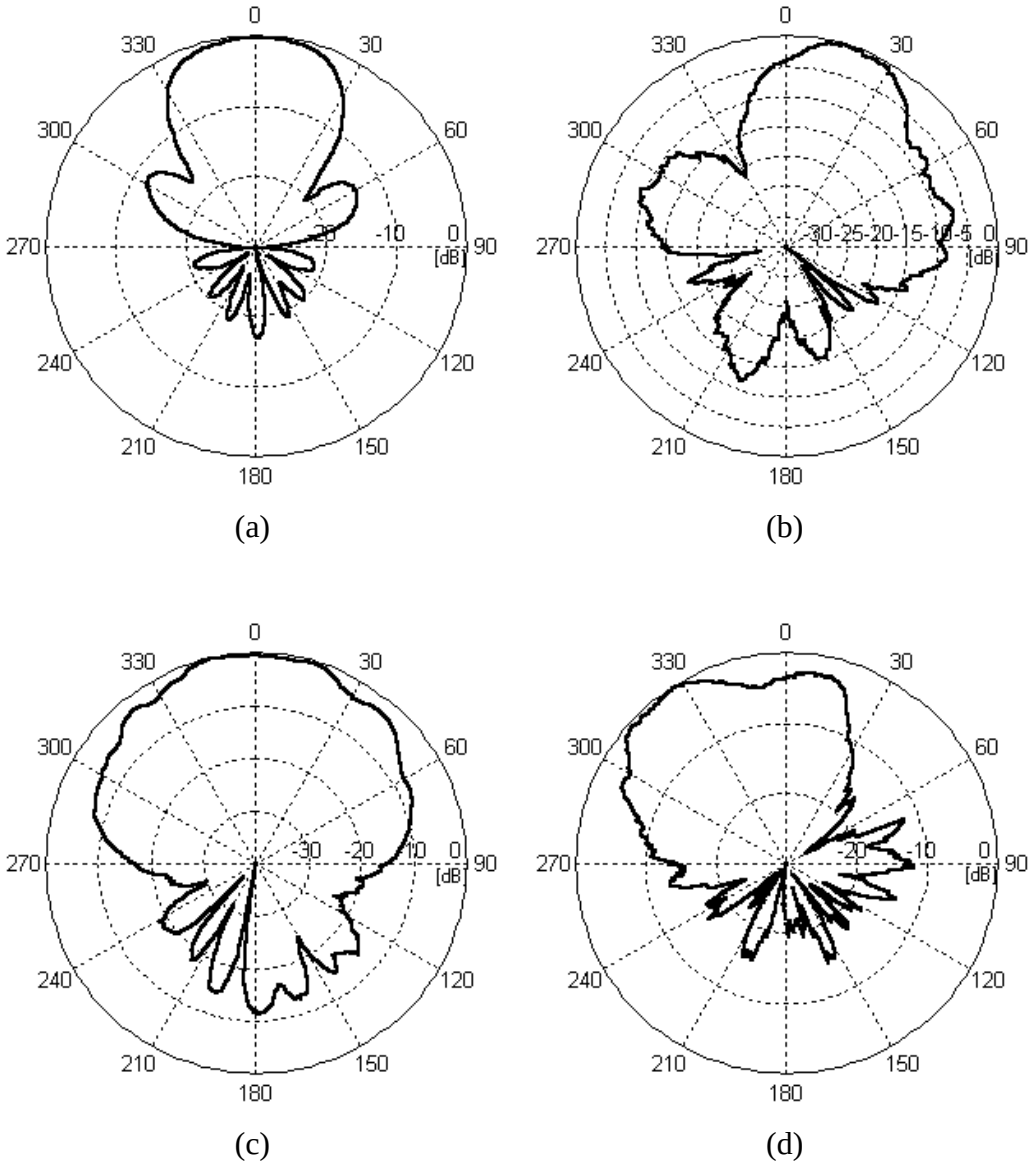

Figure E-8 Measured patterns for LP2 in the E-plane at 2601 MHz : (a) G_θ, (b) G_ϕ and at 3201 MHz : (c) G_θ, (d) G_ϕ

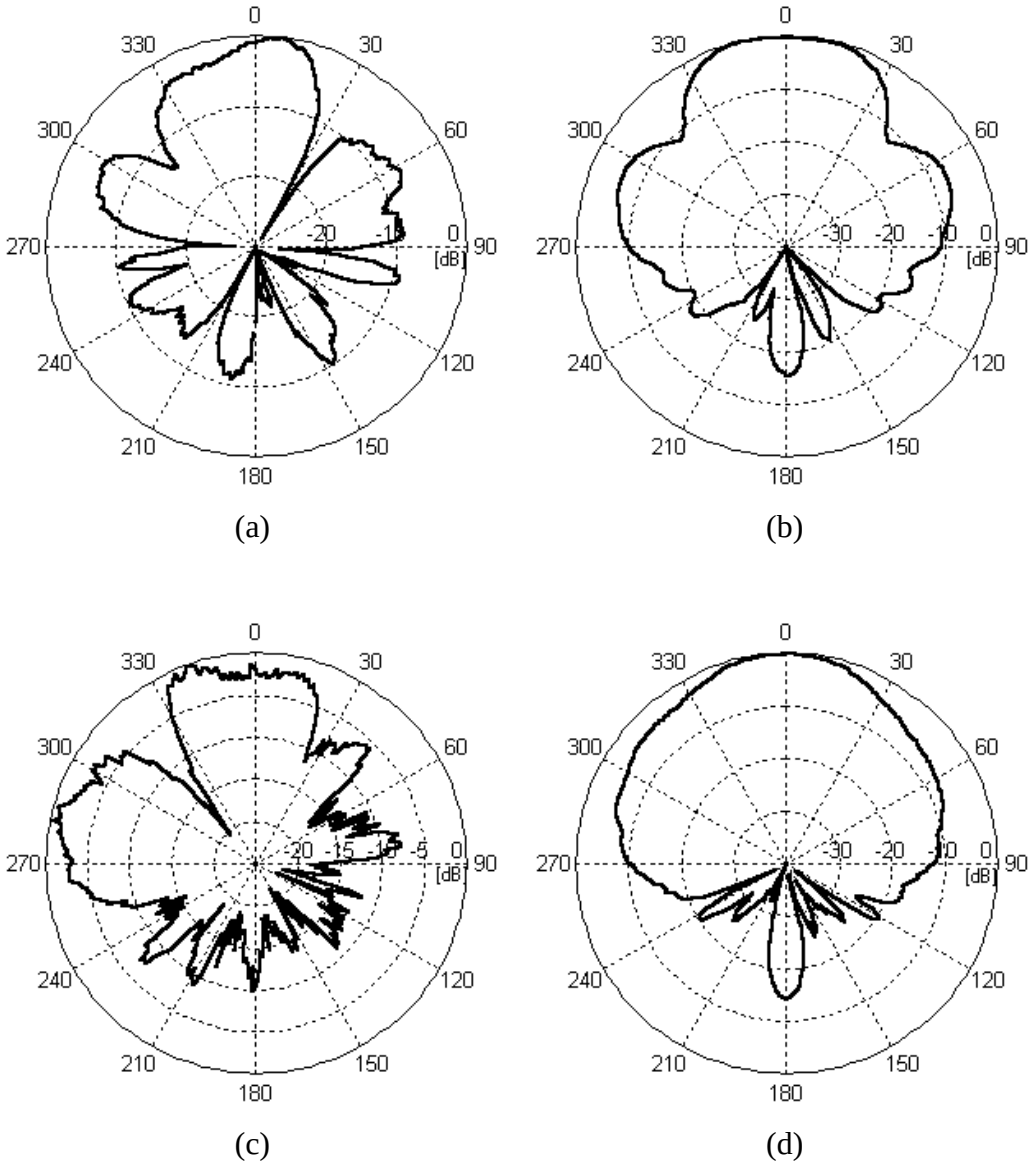

Figure E-9 Measured patterns for LP2 in the H-plane at 2601 MHz : (a) G_θ, (b) G_ϕ and at 3201 MHz : (c) G_θ, (d) G_ϕ

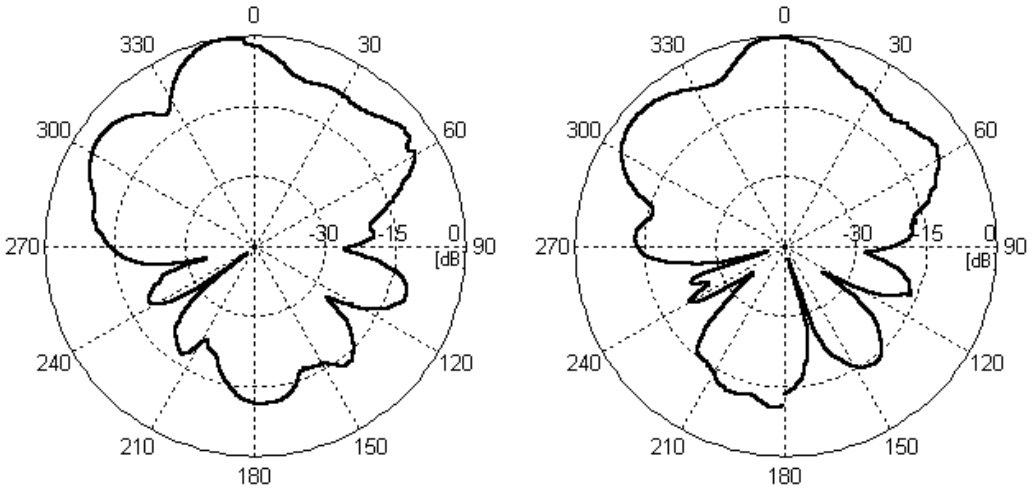

(a) (b)

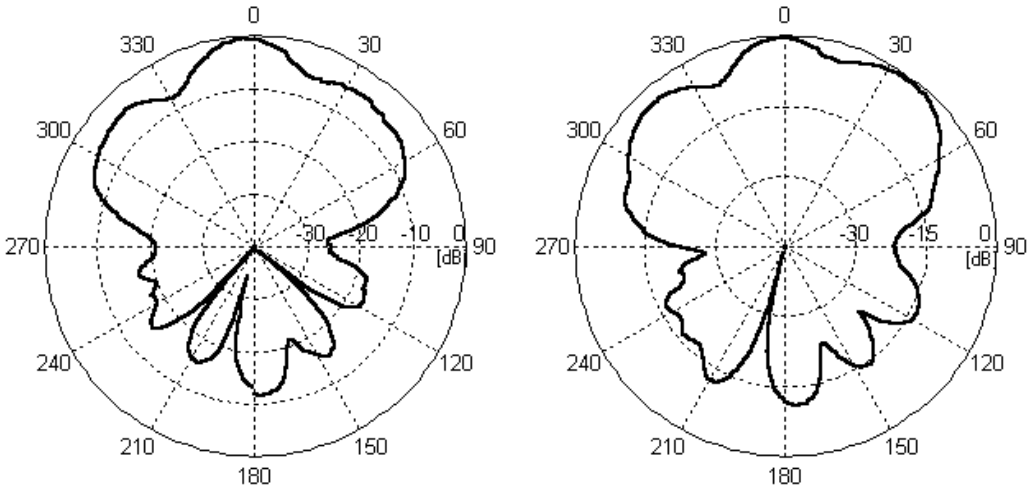

(c) (d)

Figure E-10 Measured G_θ patterns for LP3 in the E-plane at (a) 1650 MHz, (b) 1750 MHz, (c) 1850 MHz, and (d) 1950 MHz

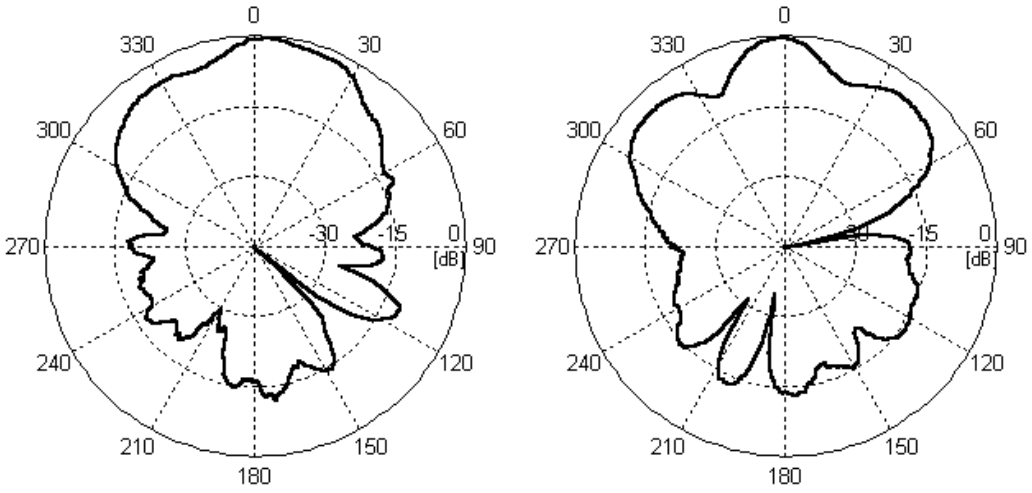

Figure E-11 Measured G_θ patterns for LP3 in the E-plane at (a) 2050 MHz, and (b) 2150 MHz

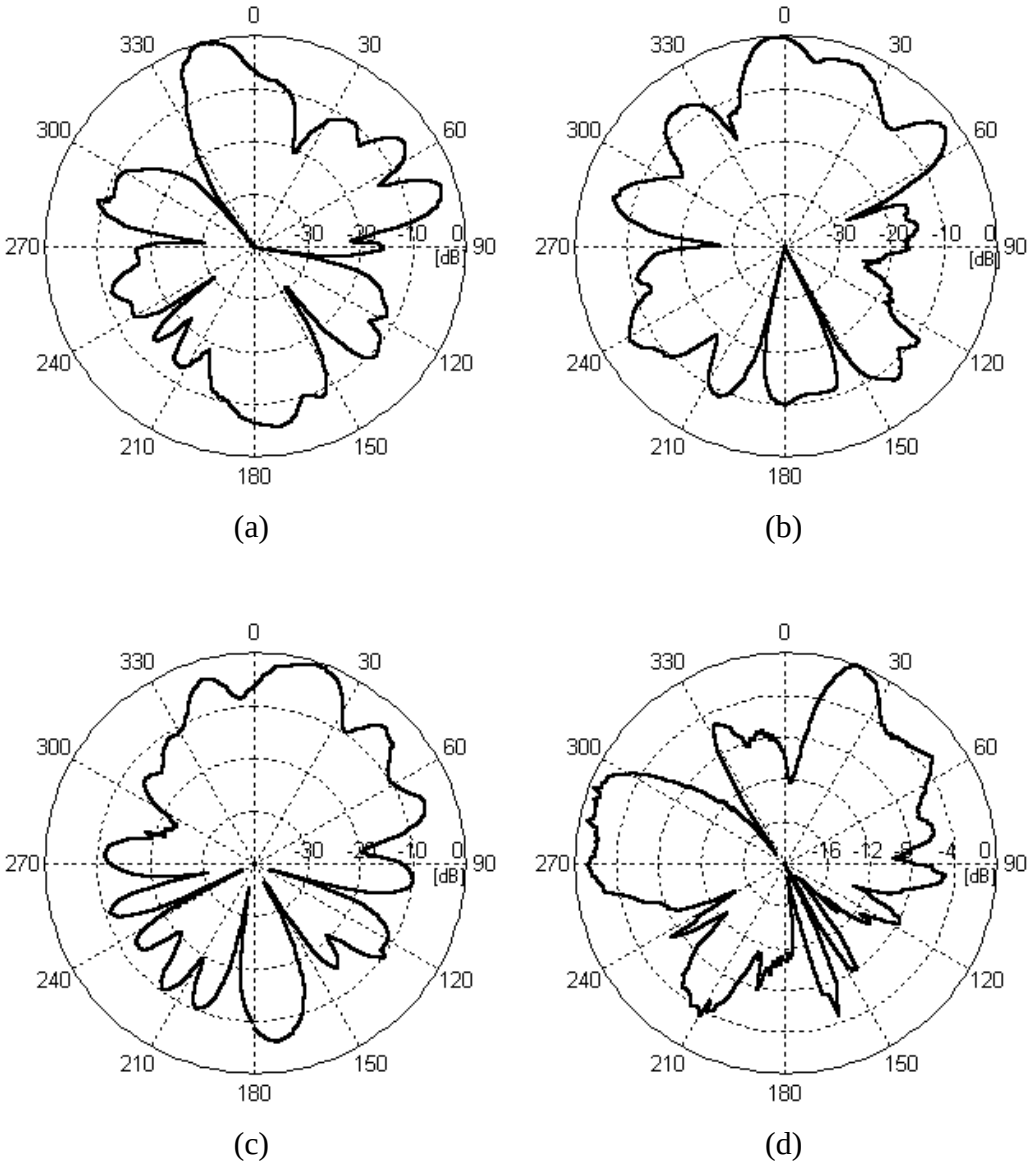

Figure E-12 Measured G_ϕ patterns for LP3 in the E-plane at (a) 1750 MHz, (b) 1850 MHz, (c) 1950 MHz, and (d) 2150 MHz

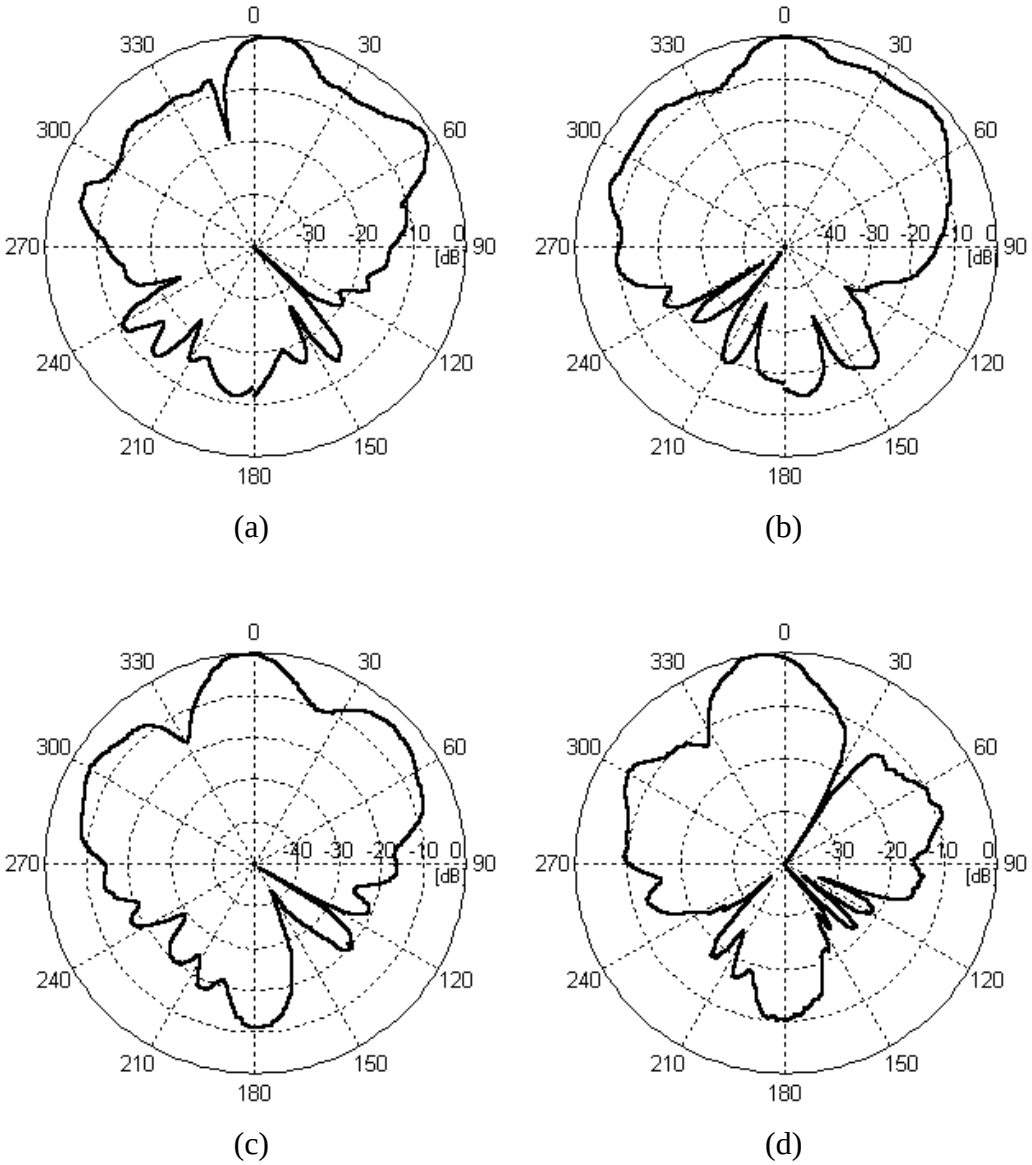

Figure E-13 Measured G_ϕ patterns for LP3 in the H-plane at (a) 1750 MHz, (b) 1950 MHz, (c) 2150 MHz, and (d) 2350 MHz

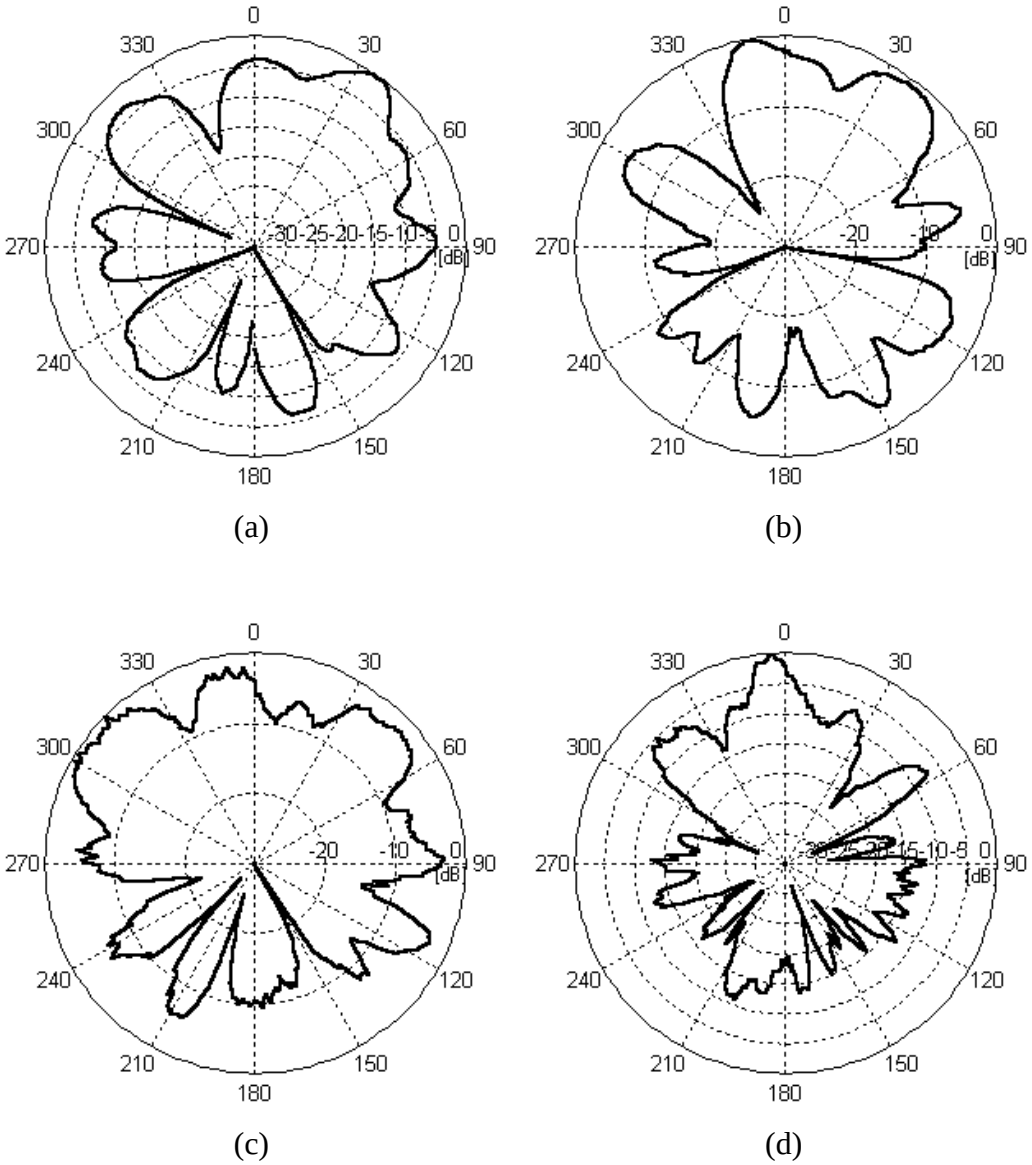

Figure E-14 Measured G_θ patterns for LP3 in the H-plane at (a) 1750 MHz, (b) 1950 MHz, (c) 2150 MHz, and (d) 2350 MHz

Vita

Jeong Il Kim was born to Hong Gil Kim and Jeong Gon Koh in 1971 in Taejon, South Korea. He graduated from Myung Suck High School, Taejon, in 1990 and attended Chungnam National University, where he received the Bachelor of Science degree in electronic engineering in February 1996. He also continued for Master Program in the Chungnam National University and transferred as an exchange student to Virginia Polytechnic Institute and State University, where he received the Master of Science degree in electrical engineering in July 1999.